UNIVERSIDADE D
COIMBRA

Inês Catarina da Fonseca Elias

EVALUATION OF POTENTIAL MARKERS FOR THE DIAGNOSIS AND PROGNOSIS OF CADASIL PATIENTS

Dissertação no âmbito do Mestrado em Biologia Celular e Molecular, orientada pela Doutora Maria do Rosário Almeida, supervisionada pela Professora Doutora Emília Duarte e apresentada ao Departamento de Ciências da Vida da Faculdade de Ciências e Tecnologia da Universidade de Coimbra.

Outubro de 2020

FACULDADE DE CIÊNCIAS E TECNOLOGIA
UNIVERSIDADE D COIMBRA

Evaluation of Potential Markers for the Diagnosis and Prognosis of CADASIL Patients

Inês Catarina da Fonseca Elias

Dissertação de Mestrado na área científica de Biologia Celular e Molecular, orientada pela Doutora Maria do Rosário Almeida (Laboratório de Neurogenética, CNC), supervisionada pela Professora Doutora Emília Duarte (Departamento de Ciências da Vida, FCTUC) e apresentada ao Departamento de Ciências da Vida da Faculdade de Ciências e Tecnologia da Universidade de Coimbra.

Outubro de 2020

Agradecimentos

Gratidão s.f.

(Pop.) Ação de reconhecer ou de prestar reconhecimento a alguém por algo bom; obrigado.

Uma tese de mestrado é um longo caminho, um processo de enriquecimento e crescimento pessoal, em parte solitário. É também um caminho que nunca teria sido percorrido sem muita ajuda, muito apoio e muito incentivo de todos os que me acompanharam neste percurso.

À Doutora Maria do Rosário Almeida, orientadora desta dissertação, quero expressar a minha profunda gratidão pelo privilégio que foi este ano a seu lado, que embora com os percalços que a vida nos foi pondo, nunca me deixou perdida ou desamparada. Obrigada pela paciência, pela confiança e pela esperança que depositou em mim, por todo o incentivo e nunca me deixar esquecer que "o saber não ocupa lugar". Sinto que não podia ter escolhido melhor pessoa para me acompanhar nesta jornada.

À Professora Doutora Emília Duarte, orientadora interna desta tese, por me ter aceite e supervisionado neste percurso.

À Professora Doutora Ana Luísa Carvalho, coordenadora do mestrado de Biologia Celular e Molecular, por ter acreditado no meu potencial, me ter aceite neste mestrado que me fez vir para Coimbra e por me ter dado a conhecer este Laboratório onde vim a realizar a minha tese.

À Ana Santos, a minha companheira de laboratório e de conversa, obrigada pela tua amizade. Obrigada pela confiança, pelas horas e horas de partilha, por me tirares todas as dúvidas, e por seres uma voz positiva e encorajadora ao longo do meu caminho. O que quero dizer é: obrigada por ser quem és, gosto muito de ti.

Às "meninas da neuroquímica", obrigada por me fazerem sentir em casa especialmente com todos os concursos e piqueniques maravilhosos que organizaram. Em especial,

quero agradecer à Doutora Inês Baldeiras, que me ajudou com a minha desorientação nos números e que sem a qual não seria possível concretizar o segundo objetivo desta tese. À Anuschka e Maria João também quero agradecer por todo o positivismo na concretização desta tese. À Ana Rita, que foi essencial para colocar os pontos nos is na área da neuropsicologia dos doentes deste estudo. E à Carolina, nossa vizinha de laboratório, que também sempre foi uma voz de muito incentivo e uma grande ajuda em pequenos detalhes da escrita da tese.

Ao corpo clínico, Dr. Gustavo Santo e Dra. Carolina, pela disponibilidade, pelo interesse e ajuda com o levantamento dos dados clínicos necessários para a realização desta tese.

À Doutora Rachel César, obrigada por me manter quem eu sou e não me deixar desmoronar. Obrigada por me ter ajudado a crescer e evoluir neste tempo que passou.

Às minha amigas, Mónica, Catarina, Rita e Filipa, que acompanharam e aturaram todas as minhas fases, obrigada por estarem cá e se preocuparem, obrigada por existirem na minha vida.

Culmino por fim no início de tudo e núcleo de tudo, que não podia deixar de mencionar, que é a minha família. Um obrigada gigante por todo o apoio e interesse que demonstram mesmo que muitas vezes não façam a mínima ideia sobre o que estou a falar. Mãe, obrigada por tentares entender inglês por mim. Pai, obrigada pela preocupação que demonstras. Aos dois, obrigada por todo o carinho nestes 24 anos, por serem o meu porto seguro e me incentivarem em tudo o que faço e me acompanharem nos caminhos que escolho percorrer. Rita, obrigada pelos carinhos aleatórios que tanto gostas de dar e que às vezes vêm mesmo na altura certa. Pati, obrigada pelo teu *art work* sempre magnífico que me deu duas lindas imagens originais desta tese. Avó, obrigada por todo o teu carinho e toda a tua ajuda que me enche o coração. Maria, a minha tia do coração, obrigada também pela tua energia. E em geral, a todos, obrigada por estarem lá nesta minha montanha-russa que é uma tese de mestrado.

Por fim, o meu profundo e sentido agradecimento a todas as pessoas que contribuíram para a concretização desta dissertação, estimulando-me intelectual e emocionalmente.

"Mas sou sempre eu, assente sobre os mesmos pés. O mesmo sempre, graças ao céu e à terra. E aos meus olhos e ouvidos atentos. E à minha clara..."

Fernando Pessoa

"Daí a deferência que nos merecem as rugas que mapeam o rosto envelhecido, denunciando o atraso com que chegamos, sempre e inevitavelmente, ao encontro de outra pessoa."

Emmanuel Lévinas

"A sabedoria está com os humildes e a humildade com os sábios"

Henrique Li

Index

Page

List of figures

Page

List of tables

Page

List of abbreviations

1000G	1000 Genomes
ACMG	American College of Medical Genetics and Genomics
ADAM	A Disintegrin And Metalloproteinase
ALS	Amyotrophic Lateral Sclerosis
ANKr	Ankyrine repeats
BWA	Burrows-Wheeler Aligner
CADASIL	Cerebral Autosomal Dominant Arteriopathy with Subcortical Infarcts and Leukoencephalopathy
CADD	Combined Annotation Dependent Depletion
CARASAL	Cathepsin A-Related Arteriopathy with Strokes and Leukoencephalopathy
CARASIL	Cerebral Autosomal Recessive Arteriopathy with Subcortical Infarcts and Leukoencephalopathy
CCR	Colorectal Cancer
CMB	Cerebral Microbleeds
CRV	Cerebroretinal Vasculopathy
CSF	Cerebrospinal Fluid
cSVD	Cerebral Small Vessel Disease
ddNTP	Dideoxynucleotides Triphosphates
DNA	Deoxyribonucleic Acid
dNTP	Deoxyribonucleotide Triphosphate
ECD	Extracellular Domain
ECM	Extracellular Matrix

EDTA	Ethylenediamine Tetraacetic Acid
EGFr	Epidermal Growth Factor-Like repeat
EPVS	Enlarged Perivascular Spaces
ER	Endoplasmatic Reticulum
ExAC	Exome Aggregation Consortium
Exo	Exonuclease I
FATHM-MLK	Functional Analysis Through Hidden Markov Models
FD	Anderson-Fabry Disease
FLAIR	Fluid Attenuated Inversion Recovery
FTD	Frontotemporal Dementia
FTLD	Frontotemporal Lobar Degeneration
Gb3	Globotriaosylceramide
gDNA	Genomic DNA
GnomAD	Genome Aggregation Database
GOM	Granular Osmophilic Material
HERNS	Hereditary Endotheliopathy, Retinopathy, Nephropathy and Stroke
HGMD	Human Gene Mutation Database
HS	High Sensetivity
HTRA1	HtrA Serine Peptidase/Protease 1
HVR	Hereditary Vascular Retinopathy
ICD	Intracellular Domain
IGV	Integrative Genomics Viewer
LC3	Light Chain 3
LNr	Notch/Lin-12 repeat
MAF	Minor Allele Frequency
MAML	Mastermind-Like Protein

MMSE	Mini-Mental State Examination
MoCA	Montreal Cognitive Assessment
MRI	Magnetic Resonance Imaging
mRNA	Messenger Ribonucleic Acid
MUTpred	Mutation predictor
NECD	Notch3 Extracellular Domain
NF-H	Neurofilaments Heavy chain
NF-L	Neurofilaments Light chain
NF-M	Neurofilaments Medium chain
NFs	Neurofilaments
NGS	Next Generation Sequencing
NICD	Notch3 Intracelullar Domain
NLS	Nuclear Localizing Signals
NOTCH3	Notch homolog 3
PCR	Polymerase Chain Reaction
PDB	Paget Disease of Bone
PEST	Proline-Glutamine-Serine-Threonine
PolyPhen-2	Polymorphism Phenotyping 2
qPCR	Quantative Polymerase Chain Reaction
RAM	RBP-Jk-Associated Molecule
RBP-Jk	Recombination signal Binding Protein for immunoglobulin κ J region
ROS	Reactive Oxygen Species
RVCL	Autosomal Dominant Retinal Vasculopathy with Cerebral Leukodystrophy
SAP	Shrimp Alkaline Phosphatase
SIFT	Sorting Intolerant From Tolerant

SiMoA	Single Molecule Array
sNF-L	serum Neurofilaments Light chain
SVD	Small Vessel Disease
TGF-β1	Transforming Growth Factor-β1
TIA	Transient Ischemic Attacks
TIMP-3	Tissue Inhibitor of Metalloproteinases 3
UV	Ultraviolet
VSMCs	Vascular Smooth Muscle Cells
VTN	Vitronectin
WMH	White Matter Hyperintensities
WML	White Matter Lesions
α-GAL	Lysosomal α-Galactosidase A

Abstract

Cerebral autosomal dominant arteriopathy with subcortical infarcts and leukoencephalopathy (CADASIL, OMIM #125310) is a fatal and progressive disease caused by mutations in the *NOTCH3* gene which vary in their frequency across populations. Evidence point that multiple pathogenic mechanisms underlie the disease, which is considered the most common inherited cerebral small vessel disease, with a recent new estimated prevalence of 1:300. More than 10 years ago, studies showed exons 4, 11, 18, and 19 to be the most frequently mutated in CADASIL Portuguese patients. However, since then, no further studies have been done on our population. Although the clinical presentation of this disorder, including stroke, migraine with aura, cognitive impairment, and psychiatric disturbances, together with the family history and brain MRI confirms the diagnosis, genetic analysis of *NOTCH3* gene should be used as a final gold standard. Due to the high phenotypic variability both across and within CADASIL families, it is extremely difficult to predict the patients' prognosis and management. Therefore, an early diagnosis and the identification of prognostic markers are essential for preventive care and guiding treatment decisions. Moreover, recent studies have shown a correlation between NF-L serum levels and patients' survival, MRI burden, and cognitive decline.

In line with this, the present study was divided in two main tasks, starting with the genetic and clinical characterization of our CADASIL patients' cohort, followed by the evaluation of the potential of sNF-L values in the prognosis of CADASIL patients. First, the patients with the clinical diagnosis of CADASIL underwent genetic testing, using Sanger and/or NGS sequencing. The identified variants were further evaluated for their pathogenicity using an in-house bioinformatic pipeline. NF-L serum levels of *NOTCH3* mutation carriers and a control group were also determined using SiMoA technology. A total of 53 *NOTCH3* mutation carriers were identified. Of those, 20 were index cases from different families and 33 were relatives. The molecular analysis revealed 12

different heterozygous mutations in which eight were missense cysteine altering mutations (p.R110C, p.R153C, p.G420C, p.R427C, p.C446F, p.R558C, p.R607C, p.C1099Y), three were missense cysteine sparing mutations (p.S497L, p.S978R, p.V1952M) and one was a nonsense mutation (p.R1893*). Although all identified variants had been previously reported in the literature, it was the first time that p.R1893* has been associated with CADASIL phenotype. Interestingly, most *NOTCH3* mutation carriers harbored a variant located in exon 8, 11, 20, or 31 (18,9%, 47,2%, 11,3%, and 9,4% respectively), while the remaining variants were dispersed over the entire *NOTCH3* coding sequence. A further genetic analysis focused on the genes associated with dementia phenotype, performed in patients who developed a particular aggressive cognitive impairment, revealed two siblings with the co-occurrence of a pathogenic variant in *NOTCH3* (p.G420C) and *SQSTM1* (p.S275Ffs*17) genes. Interestingly, double pathogenic variants in both *NOTCH3* and *SQSTM1* genes have never been reported so far in CADASIL patients and suggest a functional interaction between these encoded proteins. Thus, our results support the hypothesis of multiple pathogenic mechanisms underlaying CADASIL, suggesting that sequencing of the entire coding region of the *NOTCH3* gene is relevant for an early and accurate diagnosis of CADASIL patients. Also, the expansion of genetic analysis to other genes associated with the clinical phenotype using NGS-customized gene panel assay might be helpful to provide a better genetic counseling and patient management. Furthermore, our studies concerning the evaluation of the prognostic value of NF-L serum levels revealed a significant correlation between high NF-L serum levels and disease onset, patients' cognitive impairment, and disease severity. Although future studies to a better notion of the true prognostic value of this marker are needed, our results suggest the ability of NF-L serum levels to predict patients' prognosis and also to monitor therapeutic efficiency.

Keywords: CADASIL; Neurofilaments; *NOTCH3*; Next Generation Sequencing; SiMoA

Resumo

A Arteriopatia Cerebral Autossómica Dominante com Enfartes Subcorticais e Leucoencefalopatia (CADASIL, OMIM #125310) é uma doença progressiva e fatal causada por mutações no gene *NOTCH3,* cuja frequência varia entre populações. Evidências mostram que vários mecanismos patogénicos podem estar na base desta doença que é considerada a doença hereditária de pequenos vasos cerebrais mais comum, com uma nova prevalência recentemente estimada de 1:300. Estudos feitos há mais de 10 anos mostraram que os exões 4, 11, 18 e 19 seriam os mais frequentemente afetados em doentes portugueses com CADASIL. No entanto, nenhum outro estudo foi feito na nossa população de doentes desde então. Contudo, apesar do diagnóstico desta doença ser feito tendo por base o quadro clínico do doente, que inclui AVCs, enxaqueca com aura, deficiências cognitivas e distúrbios psiquiátricos, a sua história familiar e o resultado da ressonância magnética cerebral, a análise genética do gene *NOTCH3* deve ser considerada o *gold standard* do diagnóstico. Devido à grande variabilidade fenotípica observada entre e dentro de famílias CADASIL, torna-se extremamente difícil fazer o prognóstico dos doentes e o tratamento dos mesmos. Por isso, o diagnóstico precoce e a identificação de marcadores com valor prognóstico tornam-se essenciais para possibilitar cuidados preventivos e orientar as decisões de tratamento de doentes. Estudos recentes mostram uma correlação dos níveis de NF-L no soro com a sobrevida, a carga lesional na ressonância e o declínio cognitivo de doentes CADASIL.

Neste sentido, o presente estudo foi dividido em duas tarefas principais, começando com a caracterização genética e clínica do nosso *cohort* de doentes CADASIL, seguida pela avaliação do valor prognóstico dos níveis de NF-L no soro de doentes. Em primeiro lugar, os doentes com diagnóstico clínico de CADASIL foram estudados através de sequenciação por *Sanger* e/ou NGS. A patogenicidade das variantes identificadas foi posteriormente avaliada usando uma *pipeline* bioinformática interna. Os níveis de NF-L no soro de doentes CADASIL foram também obtidos usando a tecnologia SiMoA. Foi identificado um total de 53 portadores de uma variante patogénica no gene *NOTCH3*.

dos quais, 20 casos índex, de famílias diferentes, e 33 familiares. A análise molecular revelou 12 mutações diferentes em heterozigotia, das quais oito mutações *missense* com alteração de um resíduo de cisteína (p.R110C, p.R153C, p.G420C, p.R427C, p.C446F, p.R558C, p.R607C, p.C1099Y), três mutações *missense* que não afetam resíduos de cisteína (p.S497L, p.S978R, p.V1952M) e uma mutação *nonsense* (p.R1893*). Embora todas as variantes tenham sido previamente descritas na literatura, foi a primeira vez que a variante p.R1893* foi associada ao fenótipo de CADASIL. É interessante notar que a maior parte dos portadores de uma variante patogénica no gene *NOTCH3* eram portadores de variantes localizadas nos exões 8, 11, 20 ou 31 (18,9%, 47,2%, 11,3% e 9,4%, respetivamente), enquanto as demais se encontravam dispersas ao longo de toda a região codificante do gene *NOTCH3*. Uma análise genética posterior focada em genes associados a um fenótipo de demência, em doentes com um défice cognitivo particularmente severo, revelou dois irmãos com a coocorrência de uma variante patogénica nos genes *NOTCH3* (p.G420C) e *SQSTM1* (p.S275Ffs*17). Curiosamente, a coocorrência de duas variantes patogénicas nos genes *NOTCH3* e *SQSTM1* em doentes CADASIL nunca tinha sido reportada antes e sugere uma interação funcional entre as proteínas codificadas por estes genes. Assim sendo, os nossos resultados suportam a hipótese de que múltiplos mecanismos patogénicos possam estar na base desta doença, sugerindo que a análise de toda a região codificante do gene *NOTCH3* é relevante para um diagnóstico precoce e preciso de doentes CADASIL. Para mais, a expansão da análise genética a outros genes relacionados com fénotipo dos doentes através do uso de painéis NGS personalizados, poderá proporcionar um melhor aconselhamento genético e tratamento dos doentes. Adicionalmente, os nossos estudos acerca da avaliação do valor prognóstico dos níveis de NF-L no soro revelaram uma correlação significativa entre níveis elevados de NF-L no soro e o aparecimento de sintomas, o défice cognitivo dos doentes e a severidade da doença. Embora estudos futuros sejam necessários para uma melhor compreensão do verdadeiro valor prognóstico deste marcador, os nossos resultados revelam a possibilidade da monotorização da eficácia terapêutica e do prognóstico de doentes através da medição dos níveis de NF-L no soro.

Palavras-chave: CADASIL; Neurofilamentos; *NOTCH3*; Sequenciação de nova geração; SiMoA

1. Introduction

With the advances in Medicine over the years, lifespan has increased, accompanied by a change in the top causes of mortality worldwide. With aging, there is a tendency towards cell dysfunction and cellular senescence that together lead to the systemic decline of the individual, representing a risk factor for the development of several diseases. Cognitive decline is one of the most common features observed in the elderly population that can easily aggravate to dementia. Also, blood vessels weak over the years leaving older people more predisposed to vascular problems like strokes and transient ischemic attacks (TIA). Thus, dementia and stroke are a major cause of mortality and severe disability worldwide. It is estimated that until 2060 there will be nearly 14 million people over 65 years old diagnosed with dementia. Also, the majority of strokes (75%) occurs on the elderly. Over the years, knowledge about the mechanisms under these two conditions has been expanded and it is known now that the cardiovascular and neuronal systems are deeply interconnected, with a large net of vessels responsible for the supply of nutrients and oxygen to the brain and neurons. Also, it has been estimated that almost every neuron is supplied by its own capillary. This close relationship between the neuronal and vascular components is crucial to understand the link between stroke and dementia.

Cerebral small vessel diseases (cSVDs) is a recognized cause of dementia among the elderly and the underlying cause of up to 26% of ischemic strokes in Europe (Giau et al., 2019). Moreover, cSVDs is a heterogeneous group of disorders that affects the structure and function of cerebral microcirculation (small arteries, arterioles, capillaries, small veins, and venules of the brain), resulting in tissue damage and reduction of blood supply into grey and deep white matter of the brain (Pantoni et al., 2010). Anatomically, the walls of small arteries and arterioles are formed by three concentric layers (Figure 1.1): the *tunica intima*, formed by a single layer of endothelial cells; the *tunica media*, composed by vascular smooth muscle cells (VSMCs) and some elastin and collagen fibers in the extracellular matrix (ECM); and the *tunica adventitia*, consisting mainly by ECM

with collagen and elastin fibers, some fibroblasts, pericytes and nerve endings (Cipolla, 2009).

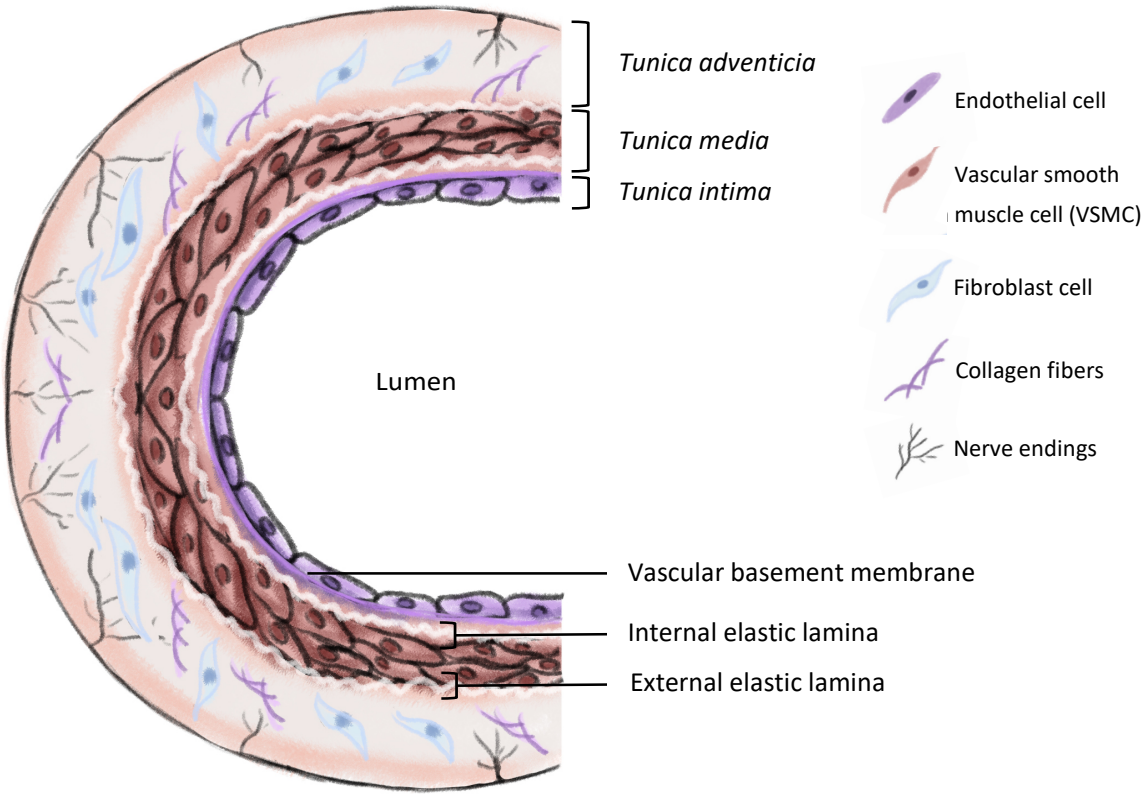

Figure 1.1. Schematic representation of small vessels walls.

Although most cases of cSVD are sporadic, several monogenic cSVDs have been reported in adult patients, the majority with dominant inheritance and each affecting a specific component of the small vessel walls. These include cerebral autosomal dominant arteriopathy with subcortical infarcts and leukoencephalopathy (CADASIL), that will be addressed in detail in further sections, cerebral autosomal recessive arteriopathy with subcortical infarcts and leukoencephalopathy (CARASIL), cathepsin A-related arteriopathy with strokes and leukoencephalopathy (CARASAL), autosomal dominant retinal vasculopathy with cerebral leukodystrophy (RVCL), *COL4A1/A2*-related angiopathies, and Anderson-Fabry disease (FD, Table 1.1).

Table 1.1. Summary of inherited cSVDs main characteristics

	CADASIL	CARASIL	CARASAL	RVCL	*COL4A1/A2*	FD
OMIM	#125310	#600142	-	#192315	#175780 #614483 #611773 #614519	#301500
Trait of inheritance	AD	AR	AD	AD	AD	X-linked
Locus	19q12	10q	20q13.12	3p21	13q34	Xq22
Gene	*NOTCH3*	*HTRA1*	*CTSA*	*TREX1*	*COL4A1* and *COL4A2*	*GLA*
Protein	Notch3 receptor	HtrA serine peptidase/protease 1	Cathepsin-A	DNA-specific 3'-5' exonuclease	Collagen chains α1(IV) and α2(IV)	Lysosomal α-galactosidase A
Affected vessel layer	*Tunica media*	Internal elastic lamina	*Tunica intima*	*Tunica Intima*	Vascular basement membrane	*Tunica media + intima*

CADASIL, Cerebral autosomal dominant arteriopathy with subcortical infarcts and leucoencephalopathy; CARASIL, Cerebral autosomal recessive arteriopathy with subcortical infarcts and leucoencephalopathy; CARASAL, Cathepsin-A-related arteriopathy with strokes and leukoencephalopathy; RVCL, autosomal dominant retinal vasculopathy with cerebral leukodystrophy; FD, Anderson-Fabry disease; AD, autosomal dominant; AR, autosomal recessive

Summarizing, CARASIL is a disorder with autosomal recessive inheritance caused by mutations in the *HTRA1* gene, which encodes for HtrA serine peptidase/protease 1 (Hara et al., 2009). This protein is responsible for the degradation of many substrates mostly situated in the ECM and interacts with transforming growth factor-β 1 (TGF-β1), a cytokine that has an important role in the differentiation and integrity of VSMCs (Nozaki et al., 2015). Impairment of *HTRA1* gene leads to hyaline degeneration and thickening and splitting of the internal elastic lamina of small vessels. Of contrast, CARASAL is a disorder with autosomal dominant inheritance, due to mutations in the *CTSA* gene, which encodes for cathepsin A, an enzyme involved in endothelin-1 degradation and found in association with β-galactosidase and neuraminidase (Bugiani et al., 2016). Its impairment leads to overexpression of endothelin-1 and consequentially affects vascular endothelial cells of small vessels and myalination of axons. Furthermore, RVCL groups cerebroretinal vasculopathy (CRV), hereditary vascular retinopathy (HVR), and hereditary endotheliopathy, retinopathy, nephropathy and stroke (HERNS) initially considered three independent autosomal dominant disorders (Grand et al., 1988; Jen et al., 1997; Ophoff et al., 2001; Storimans et al., 1991). It results from frameshift mutations the C-terminal of *TREX1* gene resulting in a truncated DNA-specific 3'-5' exonuclease which affects granzyme A-apoptosis weakening the autoimmune system and resulting in calcification and fibrous thickening of small vessel walls (Richards et al., 2007). *COL4A1/A2*-related angiopathies are also of autosomal dominant inheritance and caused by alterations in the *COL4A1* and *COL4A2* genes that encode for procollagen

chains α1(IV) and α2(IV) respectively, elements of type IV collagen, the main component of all basement membranes, and therefore when impaired resulting in defected vascular basement membranes (Cutting et al., 1988; Khoshnoodi et al., 2016; Kuo et al., 2012; Van Agtmael et al., 2005). At last, FD is an X-linked disorder with recessive inheritance caused by mutations in the *GLA* gene that encodes for lysosomal α-galactosidase A (α-GAL), that catalyzes the removal of terminal α-galactose groups from diverse substrates and when defective or absent leads to progressive storage of glycosphingolipids, in particular, globotriaosylceramide (Gb3), within the lysosomes of different tissues, causing cellular dysfunction that might trigger inflammation and/or fibrosis, *p.e.* it affects the lysosomal storage of VSMCs and endothelial cells (Eng et al., 1994; Opitz et al., 1965; Zarate et al., 2008).

1.1. CADASIL (OMIM #125310)

Cerebral autosomal dominant arteriopathy with subcortical infarcts and leukoencephalopathy (CADASIL, OMIM #125310), previously known has hereditary multi-infarct dementia, is the most common monogenic cSVD, possibly first described by Van Bogaert in 1955 as a familiar form of Binswanger's disease (Opherk et al., 2004; Van Bogaert, 1955). In 1977, Sourander and Walinder reported a three-generational family affected by multi-infarct dementia with evidences that suggest an autosomal dominant pattern of inheritance (Sourander and Walinder, 1977). Although, was only in 1993 that Tournier-Lasserve reported CADASIL and correlated the disease with alterations at chromosome 19 (Tournier-Lasserve et al., 1993). Three years later the same authors identified *Notch homolog 3* (*NOTCH3)* has the disease-causing gene. CADASIL affects individuals all around the world with hundreds of families already reported (Joutel et al., 1996). In Europe, the prevalence of CADASIL has been estimated to a minimum of two to five per 100,000 adults (Hack et al., 2019). However recent studies point to a higher frequency of *NOTCH3* pathogenic variants in the general population worldwide, with a new estimated prevalence of 1:300 which is 100-fold higher than previously estimated (Rutten et al., 2016, 2019). These later findings suggest not only that CADASIL is underdiagnosed but also that probably, given the highly heterogenous nature of the clinical spectrum of CADASIL, more pathogenic variants are associated with a milder phenotype or may even be non-penetrant in some cases.

1.2. Clinical features associated with CADASIL

CADASIL clinical presentation is very heterogenous among patients and families, however it is essentially characterized by recurrent cerebral ischemic episodes, as a stroke or a TIA, cognitive decline, migraine with aura, and psychiatric symptoms (Chabriat et al., 1995; Di Donato et al., 2017; Kalimo et al., 1999). Ischemic stroke and TIA are the most frequent manifestations of the disease, occurring in 60–85% of symptomatic individuals, usually starting at 45 years old (Chabriat et al., 1995, 2009; Dichgans et al., 1998; Hack et al., 2019). The majority of CADASIL patients has an elevated probability of recurrence, generally experiencing two to five ischemic episodes during their lifetime, resulting, in time, in gait disturbances, motor and cognitive decline, urinary incontinence, and pseudobulbar palsy (Chabriat et al., 2009; Opherk et al., 2004). Cognitive decline is the second most frequent manifestation of CADASIL affecting 60% of patients (Chabriat and Bousser, 2007). It can begin as early as age of 35 and progressively worsen with aging and recurrent ischemic episodes, leading to memory impairment, alterations in language and reasoning, eventual resulting in subcortical dementia in up to 75% of cases usually accompanied by apathy (Dichigans, 2009). Migraine with aura appears in 20-40% of affected patients which represents a frequency five times higher than in general population (Vahedi et al., 2004). Usually, this is the first symptom of the disease, appearing before 20s in some cases (Verin et al., 1995). Psychiatric symptoms affect more than 25% of CADASIL patients, mostly in the form of mood disorders like depression, bipolar disease, and apathy, panic disorders and schizophrenia, that usually start to develop from 40s (Valenti et al., 2008). Although less common, affecting between 5-10% of patients, epilepsy can develop, in some cases as a consequence of cerebral ischemic episodes (Dichgans et al., 1998). Parkinsonism and acute encephalopathy are also uncommon features of CADASIL and some studies report optic anomalies with lesion of the microvasculature of the eye (Andre, 2010; Martins et al., 2014; Miranda et al., 2006; Wegner et al., 2007).

1.3. MRI features associated with CADASIL

Brain magnetic resonance imaging (MRI) of CADASIL patients can show confluent white matter hyperintensities (WMH), multiple subcortical lacunar infarcts and lacunar

lesions, cerebral microbleeds (CMB), enlarged perivascular spaces (EPVS), and brain atrophy, even in patients in their early 20s (Figure 1.2; Mizuno et al., 2020).

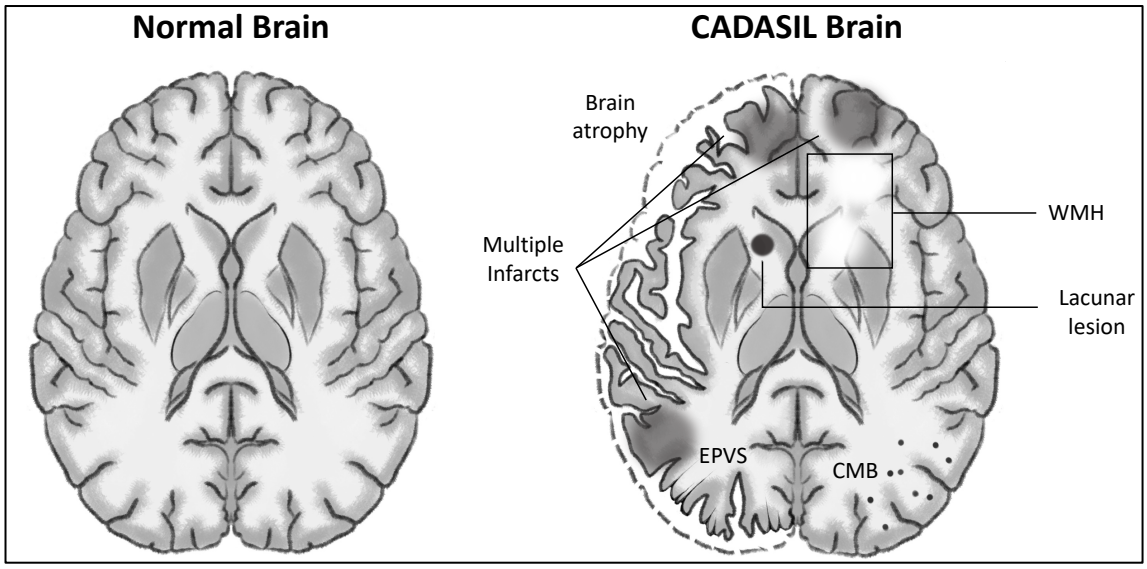

Figure 1.2. Schematic representation of the brain lesions usually present in CADASIL. WMH, white matter hyperintensities; CMB, cerebral microbleeds; EPVS, enlarged perivascular spaces.

It is known that WMH prevalence increases exponentially with age however, WMH are likely to be more common in individuals with family history and/or clinical features of SVD like CADASIL. WMH have a symmetrical brain distribution, and although it affects the whole brain, the involvement of the external capsule and temporal lobes is highly specific in CADASIL affected patients. This type of alterations can be identified even in the subcortical and periventricular white matter of asymptomatic individuals. Multiple subcortical lacunar infarcts and lacunar lesions are parenchymal defects close to the cortex, characteristically localized within the semioval center, thalamus, basal ganglia and pons (Skehan et al., 1995). Notably, MRI lesion load has been shown an important predictor of cognitive impairment in patients with CADASIL (Shi et al., 2018). CMB are present in up to ¼ of the general population and consist in small areas of hemosiderin deposition from silent hemorrhages. CMB are associated with increased risk of ischemic stroke and the risk of associated cognitive decline and dementia are direct correlated with CMB brain affected location. EPVS found in basal ganglia and white matter, which consist in cavities filled with interstitial fluid that surround the small vessels of brain, are also associated with increased risk of dementia. At last, brain atrophy, a consequence

of lacunar lesions and secondary loss of white and grey matter, also seems to correlate with cognitive deficits and is strongly with CADASIL dementia (Viswanathan et al., 2010).

1.4. CADASIL Pathogenesis

1.4.1. Histopathology

Wall thickening of deep penetrating small vessels of the white matter, predominantly duo to marked intimal hyperplasia, is a histopathological hallmark of CADASIL (Dong et al., 2013). Progressive thickening of vessel walls leads to lumen stenosis that ultimately leads to subcortical lacunar infarcts and ischemia. VSMCs apoptosis in CADASIL vessels results in gradual degradation of the *tunica media* with an eventual breakdown of vascular wall integrity, lumen stenosis and vascular insufficiency, that consequentially reduces cerebral blood flow making patient more susceptible to infarcts (Chabriat et al., 2009). Also, there is accumulation of non-amyloid granular osmophilic material (GOM) with around 0.2-2 mm of measure within the *tunica media*. Its exact molecular composition is still unknown, however some studies have revealed that mutant Notch3 extracellular domain and other proteins involved in blood vessel remodeling, like tissue inhibitor of metalloproteinases 3 (TIMP-3), and vitronectin (VTN), are part of GOM composition (Monet-Leprêtre et al., 2013).

A recent study found that large GOM deposits coexist with small and recent ones, both in small vessels of aged mice and *post-mortem* CADASIL brain, indicating that GOM deposits are continuously forming during disease progression (Gravesteijn et al., 2019). Moreover, it has not already been established if GOM deposits form on the cell surface or in the endoplasmatic reticulum (ER) and released into extracellular space after VSMCs apoptosis (Takahashi et al., 2010). To denote that some studies show an impairment of ubiquitination and autophagy in *NOTCH3* mutants, preventing GOM clearance and contributing to toxic protein accumulation (Hanemaaijer et al., 2018; Hase et al., 2018; Lorenzi et al., 2017).

1.4.2. *NOTCH3* gene and signaling

CADASIL is caused by pathogenic mutations in the *NOTCH3* gene located on chromosome 19q12, transmitted with an autosomal dominant pattern (Table 1.1; Joutel et al., 1996; Tournier-Lasserve et al., 1993). The 33 exons of this gene encode for a single-pass

transmembrane receptor protein, composed by 2,321 amino acids, mainly expressed on VSMCs and pericytes (Figure 1; Joutel et al., 2000, 2010; Wang et al, 2008). This receptor is composed of three domains: one large extracellular domain (ECD), responsible for ligand-binding extracellular signaling, one short transmembrane domain, and one intracellular domain (ICD), responsible for intracellular signaling transduction, negative regulation and protein degradation (Figure 1.3A; Coupland et al., 2018). The Notch3 ECD (NECD) is composed of 34 tandem epidermal growth factor-like repeats (EGFr), each with six highly conserved cysteine residues that form disulfide bonds responsible for the correct folding of the receptor and 3 Notch/Lin-12 repeats (LNr) also rich in cysteine residues. The Notch3 ICD (NICD) includes a RBP-Jk-associated molecule (RAM) domain, 7 ankyrine repeats (ANKr) flanked by nuclear localizing signals (NLS), and a C-terminal PEST domain, a sequence that is rich in proline (P), glutamine (E), serine (S), and threonine (T) residues. The first two, are responsible for protein-protein interaction and the last one is involved in protein's stability, negative regulation and protein degradation (Chabriat et al., 2009). In *NOTCH3* signaling pathway, briefly summarized on Figure 1.3B, Notch3 receptor is thought to undergo complex proteolytic processing events starting when the NECD interacts with Delta/Jagged on juxtaposed cells inducing conformational changes in the receptor triggering a proteolytic cleavage of the NECD by ADAM (a disintegrin and metalloproteinase) on the cell surface. Right after, γ-secretase intramembrane proteolysis releases the soluble cytoplasmatic NICD from the membrane. Liberated NICD translocate to the nucleus where interacts with the nuclear RBP-Jk (Recombination signal Binding Protein for immunoglobulin κ J region) repression protein and with the transcriptional co-activator MAML (mastermind-like protein), forming a trimeric complex (Bellavia et al., 2008). Binding of NICD to RBP-Jk depends on a strong interaction between RAM domain and this repression protein and on a weak interaction with the ANKr, specifically able to mediate protein-protein interactions. Indeed, studies show that ANKr are important for the formation of the trimeric complex. Upon these interactions, *NOTCH3* downstream genes transcription is activated and genes involved in VSMCs differentiation, remodeling, and vascular development are expressed. Ultimately, the PEST domain promotes degradation of NICD, since the E3 ubiquitin ligase SCF/Sel-10/FBXW7 ubiquitinates this domain promoting NICD degradation by the proteasome machinery (Luo et al., 2020).

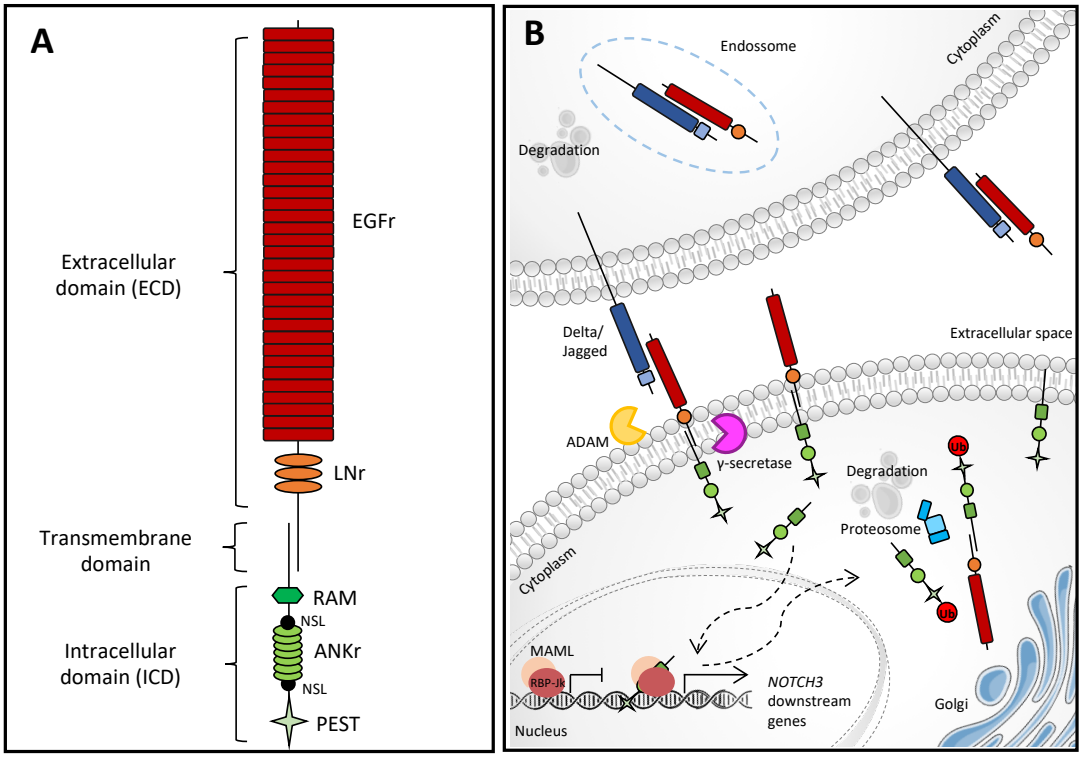

Figure 1.3. Schematic overview of Notch3 receptor structure and signaling. (A) Notch3 receptor structure. EGFr, epidermal growth factor-like repeats; LNr, Notch/Lin-12 repeats; HD, heterodimerization domain; NSL, nuclear localizing signals; ANKr, ankyrine repeats; PEST, sequence that is rich in proline (P), glutamine (E), serine (S), and threonine (T) (B) Notch3 signaling pathway. ADAM, a disintegrin and metalloproteinase; RBP-Jk, Recombination signal Binding Protein for immunoglobulin κ J region; MAML, mastermind-like protein.

Interestingly, most variants involve one of the EGFr-encoding sequences, located in the exons 2 to 24, and results in an odd number of cysteine residues causing disulfide bridges disruption affecting the protein's tertiary structure and resulting in a misfolded receptor. It is known that usually misfolded proteins are retained in the ER to be eliminated. Takahashi et al. demonstrated that defective Notch3 receptors are highly resistant to degradation, therefore being retained in the ER for a long time which causes ER stress with formation of reactive oxygen species (ROS) that impairs cellular growth, proliferation and repairment (Ihalainen et al., 2007; Takahashi et al., 2010). Resuming, mutant *NOTCH3* VSMCs are more sensitive to stress inducers which lead to proteasome dysfunction, activation of apoptotic pathways and cell death (Takahashi et al., 2010). However, why mutant Notch3 receptors are more resistant to degradation is not clear yet. It is possible that the misfolded receptors do not interact properly with chaperones and proteases that normally mediate proteins degradation (Locatelli et al., 2020). In fact, studies using cerebral VSMCs from CADASIL patients have shown a dysfunction in the autophagy-lysosomal pathway, as a consequence of accumulation of intracellular mutated Notch3 receptor (Hanemaaijer et al., 2018).

Further, an autophagy dysfunction or an insufficient autophagy has been linked to lower proliferation rate of VSMCs and to the astrocytes apoptosis in the deep white matter of CADASIL patients (Hase et al., 2018; Panahi et al., 2018).

1.4.3. *NOTCH3* variants associated with CADASIL

Although the vast majority of reported variants in the *NOTCH3* gene are *missense* mutations (95%), there are also some *frameshift*, *nonsense* or *splice-site* mutations identified, resuming a total of more than 200 different mutations reported so far (Di Donato et al., 2017). As already mentioned, most pathogenic variants are cysteine altering variants which involve one of the EGFr-encoding sequences, located in the exons 2 to 24, and result from an alteration of a cysteine encoding triplet. In the literature, it is described a clustering of pathogenic variants in the exons 3 and 4 which encode de EGFr 2-5 (Chabriat et al., 2009). However, the most frequently mutated exons found in CADASIL Portuguese patients are exons 4, 11, 18, and 19 (Guimarães et al., 2010). Less frequently affected, it is known that EGFr 10 and 11 are necessary for Delta/Jagged ligand binding and Joutel et al. found that pathogenic variants affecting those sites, may impair the activity of the Notch3 receptor and alter it physiological function (Joutel et al., 2004). These findings gave rise to the hypothesis that the affected EGFr can influence the pathogenic mechanism responsible for CADASIL and explain heterogenous clinical spectrum observed. Joutel revealed later, through genotype-phenotype correlation analysis in a large cohort of CADASIL patients, that pathogenic variants affecting EGFr 10-11 and EGFr 2-5 are associated with different phenotypes (Joutel, 2011). EGFr 10-11 affected patients presented milder cognitive deficits, a trend for a lower volume of lacunar infarcts, and a significantly higher volume of WMH, when compared with EGFr 2-5 affected patients. Studies demonstrated that lacunar lesion volume and brain atrophy are the strongest MRI markers of global cognitive decline and that extent of WMH does not correlate with the severity of cognitive decline when the other previously MRI markers are taken into account. Moreover, Rutten et al. found that not only mutations affecting EGFr 1-6 were much less prevalent in the general population than pathogenic variants affecting EGFr 7-34, but also that EGFr 1-6 affecting variants predisposed patients to a “classical” CADASIL phenotype while EGFr 7-34 affecting

variants predisposed patients to a milder phenotype, which is in line with the previous studies (Rutten et al., 2016, 2019). They also found that the first group of patients correlated with a decrease in survival, an earlier onset of stroke, and a greater MRI lesion load, which suggested that EGFr pathogenic variant position is a strong indicator of CADASIL severity.

Nevertheless, there are other groups of variants beyond cysteine altering ones that might be also disease causing of CADASIL, however their disease molecular mechanism remains uncertain. Indeed, several studies involving cysteine sparing variants are contradictory in terms of their clinical significance since some authors reported them as causative of CADASIL while others classified them as polymorphisms (Ferreira et al., 2007; Mizuno et al., 2008; Scheid et al., 2008; Ungaro et al., 2009). Thus, when a cysteine sparing variant is detected, the clinical diagnosis should be re-evaluated and, if possible, segregation of the mutation in the affected family members should be performed (Rutten et al., 2014). Furthermore, another group of variants rarely identified in *NOTCH3* gene are the *nonsense* mutations which are variants that generate a premature stop codon. These variants can result in the reduction of *NOTCH3* signaling, *NOTCH3* downstream genes expression impairment or toxic accumulation of NICD in the cytoplasm, which may represent alternative molecular pathogenic mechanisms of CADASIL (Erro et al., 2014; Greisengger et al., 2020; Gripp et al., 2015; Moccia et al., 2014; Parmeggiani et al., 2000; Pippucci et al., 2015; Rutten et al., 2013; Yoon et al., 2015).

Interestingly, biallelic pathogenic variants in *NOTCH3* gene have been reported and they seem not affect the CADASIL patients' phenotype (Abou Al-Shaar et al., 2016; Tuominen et al., 2001). Moreover, some authors have reported the co-occurrence of disease-causing variants affecting *NOTCH3* gene and an additional gene in cases with a slightly more severe phenotype (Soong et al., 2013).

1.5. CADASIL Diagnosis

Currently, CADASIL diagnosis criteria is based in family history of migraine with aura, stroke, mood disorders and/or dementia, magnetic resonance imaging, genetic analysis of *NOTCH3* gene and/or pathological detection of GOM in skin biopsy samples (Mancuso et al., 2020).

1.5.1. Magnetic Resonance Imaging

Small vessels are not easily visualized *in vivo*, therefore brain MRI has a crucial role in the diagnosis and follow up of patients with CADASIL and other cSVDs. Diagnosis is heavily based in the presence of vascular lesions in the subcortical region of the white matter (WML), which can be detected even in asymptomatic individuals. Areas with increased signal are the earliest and more frequent anomalies to appear on T2-weighted and Fluid Attenuated Inversion Recovery (FLAIR) MRI. Almost all CADASIL patients (96%) also present periventricular WMH and diffuse symmetrical alterations in the external capsule and anterior temporal lobes area (Chabriat et al., 1998, 1999). In addition, lacunar infarcts characteristically localize within the semioval center, thalamus, basal ganglia and pons are highly suggestive of CADASIL (Skehan et al., 1995).

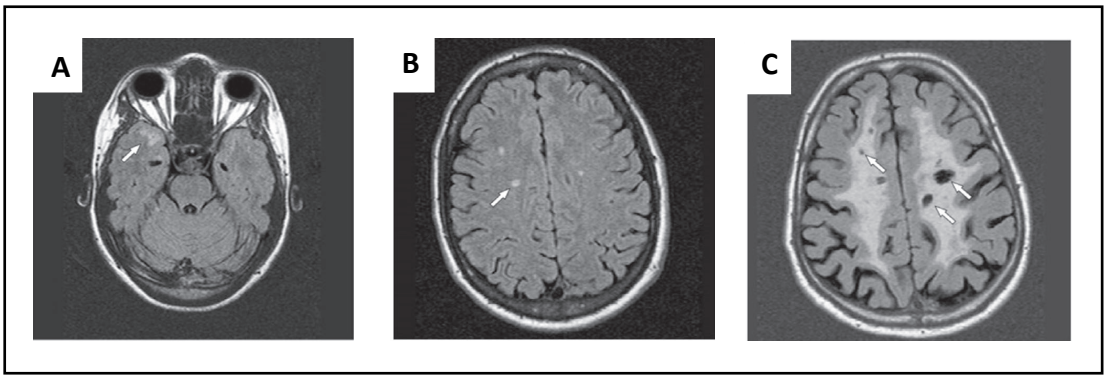

Figure 1.4. Typical pattern of CADASIL abnormalities on MRI. Fluid Attenuated Inversion Recovery (FLAIR) images showing: (A) discrete circumscript areas of white matter hyperintensities (WMH) in the anterior temporal lobes (B) discrete circumscript areas of WMH in the periventricularv semioval center (C) extensive areas of confluent and symmetrical WMH and lacunes (adapted from Mancuso et al., 2020)

1.5.2. Genetic Analysis of *NOTCH3* Gene

For patients with clinical features and/or family history of CADASIL, Sanger sequencing of the most frequently mutated exons of *NOTCH3* gene is performed since it a specificity of 100% and a sensitivity of almost 100% when a cysteine altering variant is detected.

With the advances in sequencing technology, next generation sequencing (NGS) came to increase the capability of identify *NOTCH3* mutations causative of CADASIL as well as other genes which may contribute to or cause CADASIL. Therefore, cases

without a causative variant identified may be screened using a NGS-customized gene panel design to include entire coding region of *NOTCH3* gene and also other genes chosen taking the patient's phenotype into consideration (Dunn et al., 2020).

1.5.3. Pathological Detection of GOM

Although almost all clinical features are connected to the SNC, GOM deposits are not strictly found around VSMCs and pericytes of small vessels of the brain, supporting the theory that CADASIL is a systemic disease (Lewandowska et al., 2011; Morroni et al., 2013). Therefore, in most cases CADASIL can be confirmed by electron ultramicroscopic analysis of small vessels obtained with a skin biopsy. Pathologic evaluation of skin biopsy has been estimated to have a sensitivity of 45% and a specificity of 100% (Markus et al., 2002). However, studies performed later have estimated a higher sensitivity, over 90% (Tikka et al., 2009).

Electron microscopic analysis of CADASIL vessels shows accumulation of GOM within the *tunica media* and fibrosis and thickening of small vessel walls due to VSMCs apoptosis that results in gradual degradation of the *tunica media* with an eventual breakdown of vascular wall integrity and lumen stenosis (Figure 1.5).

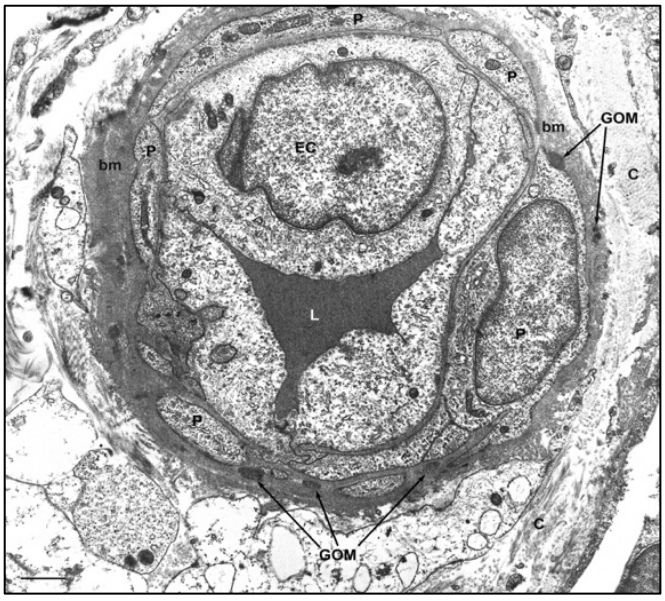

Figure 1.5. Electron ultramicroscopic image of a skin biopsy from a CADASIL patient. Dermal capillary with a thickened basal membrane (bm) and surrounded by pericytes (P), with numerous GOM deposits in the basal membrane. C, collagen; EC, endothelial cell; L, capillary lumen. Scale bar = 0.6 µm. (Morroni et al., 2013)

1.6. CADASIL Prognosis

CADASIL causes major disability and eventually loss of independence as a consequence of recurrent strokes, neuronal loss and vascular cognitive impairment. However, disease severity in CADASIL patients is highly variable both across and within families, even among carriers with the same pathogenic variant, suggesting association with external risk factors. Studies show that some cardiovascular risk factors such as hypertension and smoking can contribute to disease severity, increasing the risk of acute stroke and associating with an earlier onset of stroke in CADASIL patients. Patients can go from mild to severely affected making it highly difficult to make a prognosis for CADASIL patients. Because of this, the identification of prognostic biomarkers is likely to facilitate the elaboration of a more accurate prognosis and eventually be helpful guiding treatment decisions, leading to strategies for disease prevention and personalized therapy in some cases.

1.6.1. Neurofilaments

Neurofilaments (NFs) are intermediate filaments (type IV) consisting of three subunits of 68, 160, and 200 kDa - NF-Light (NF-L), NF-Medium (NF-M), and NF-Heavy (NF-H) respectively – which are part of the composition of the neuronal cytoskeleton, present in perikarya and dendrites but particularly abundant in axons. NFs provide structure to the axons with an essential role in the establishment of the correct diameter of the axon and in the maintenance of the axon caliber. Also, they have a major function in the transmission of electrical impulses down the axon determining the velocity of nerve conduction. These intermediate filaments have a diameter of 10 nm and the central core of the structure is composed by NF-L. In case of axonal damage, NF-L is released into the extracellular space and subsequently into the cerebrospinal fluid (CSF), remaining elevated in circulation for several months according to some studies (Gattringer et al., 2017; Thelin et al., 2017). Therefore, this protein level in the CSF has been used as a biomarker of axonal damage (Jonsson et al., 2010; Sjogren et al., 2001).

Recently, NF-L concentration can be also determined in blood using ultrasensitive immunoassay technology that can detect proteins in blood at sub femtomolar concentrations (10-16 M). According to literature, NF-L serum (sNF-L) levels have

been found to be increased and correlated with disease severity and progression in patients with Frontotemporal Dementia (FTD), Amyotrophic Lateral Sclerosis (ALS), and other neurodegenerative diseases (Lu et al., 2015; Meeter et al., 2016; Rohrer et al., 2016).

Interestingly, Duering et al. showed correlation between sNF-L levels and cSVDs both CADASIL and sporadic cases, which presented elevated levels when compared with controls (Duering et al., 2018). They also correlated sNF-L levels of patients with MRI markers as mean diffusivity and cognitive deficits such as processing speed performance which was the most affected cognitive domain. Moreover, Gravesteijn et al. also showed sNF-L levels elevated in CADASIL patients compared with controls and showed sNF-L levels to be correlated with disease progression, survival, MRI markers and future disability in patients (Gravesteijn et al., 2019). Gravesteijn and colleges showed a decrease in survival, higher lacune count, higher microbleed count and a decline in cognitive and executive functions associated with sNF-L levels in CADASIL patients.

1.7. Objectives

The main aim of this project was to characterize the genetic profile of our CADASIL patients' cohort and also to assess the value of sNF-L values in their prognosis.

As specific objectives it was pretended to:

1) Identify the genetic variants present in patients with clinical features and/or family history of CADASIL and clarify their pathogenic nature;
2) Establish genotype-phenotype correlations;
3) Investigate the usefulness of serum NF-L as a predictive marker of CADASIL patients' prognosis.

2. Methods

2.1. Study population

All participants in this study were recruited at the Coimbra University Hospital, Coimbra. Patients were referred as having clinical features or family history related to cerebral small vessel disease. All patients were subjected to MRI examination and Fazekas scale was applied. Whenever possible, patients were also subjected to a comprehensive neuropsychological assessment protocol, including global cognition and specific cognitive measures.

All patients were screened for the molecular diagnosis of cerebral small vessel disease, and patients with a diagnostic confirmed of CADASIL were recruited for neurofilaments serum study. Further, all identified *NOTCH3* mutation carriers were included in the genetic descriptive study presented in section 3.1. However, only the index cases of the identified CADASIL families were clinical characterized in this study in section 3.1, resuming a total of 20 cases. All studied family members have given previously their written consent in the context of genetic counseling.

2.2. Sample collection

Whole blood samples from each patient were collected: two 3mL tubes with EDTA and one 5mL tube without anticoagulant. The two tubes with EDTA were stored at 4°C for further DNA extraction. The 5mL tube was centrifuged at 1500g at 4°C for 10 minutes and the serum was aliquoted into polypropylene tubes and stored at -20°C until analysis.

2.3. Biochemical techniques

2.3.1. DNA extraction

Extraction of genomic DNA (gDNA) was performed with two different techniques, one simpler and faster using the NZY Blood gDNA Isolation kit, and another that takes longer using the Invisorb® Blood Universal Kit. Briefly, in the first technique, after lysis with Proteinase K, DNA contained in the blood cells was selectively absorbed into silica-based columns and, subsequent washing steps removed contaminants. In the end, gDNA was

eluted in an alkaline elution buffer. The second technique comprises four steps, removal of erythrocytes, lysis of lymphocytes, precipitation of DNA and dissolution of gDNA. It was added Buffer EL to achieve the first step, Lysis Buffer HL and Proteinase K for lysis of lymphocytes, a Precipitation Solution for the third step with discard of supernatant where are the contaminants, ethanol to wash the DNA pellet and at last, Buffer U to elute the DNA. All gDNA samples are properly labeled and stored at 4 to 8°C.

2.3.2. DNA quantification and quality control

DNA concentration and quality control were estimated by spectrophotometry using NanoDrop ND-1000 Spectrophotometer® (Thermo Fisher Scientific) and ND-1000 software v3.5.2. Readings taken at wavelengths of 280 nm and 260 nm allow calculation of the concentration of the amount of protein and nucleic acid (ng/μL) in the sample, respectively. Therefore, the ratio of nucleic acid to protein (260/280) is used as an indicator of purity of DNA samples.

2.3.3. Sanger Sequencing

2.3.3.1. Primer design

As mentioned in Chapter 1, a cluster of missense mutations is observed in exons 3 and 4 of *NOTCH3* gene. Also, although exons 8, 12 and 20 are frequently mutated in patients, exons 4, 11, 18 and 19 are the most frequently affected in CADASIL Portuguese patients. Therefore, sequences of exons 3, 4, 8, 11, 12, 18, 19 and 20 of *NOTCH3* gene were obtained through the ENSEMBL (ensembl.org) database. Primer locations were aimed to flank all coding region of the exons and selected using Primer 3 plus (https://primer3plus.com/) software and OligoCalc (http://biotools.nubic.northwestern.edu/OligoCalc.html) platform, in order to choose the most suitable primers. Resulting primers sequence and respective PCR product length are listed below in Table 2.1.

Table 2.1. *NOTCH3* primers and respective PCR product length

Exon	Sequence (5' - 3')	Product Length (bp)
3F	TGTTGGCTAGGCTGGTCTTG	426
3R	GACCAGGACAGGGTGAGTTT	
4F	GTGAGAGGGGAAGAGTCTGG	501
4R	GAAGGGGGCAAGGATGGTC	
8F	GAGGGGAGCTCCATCGTCT	402
8R	AGTCTCTAAGGGTCCCACTCC	
9F	TGTCGATGAGTAGGAAGGGAAG	298
9R	TCCGCTAACGTGGTTTTACAGG	
11F	CCTCCTGACAGCTTGATGGG	459
11R	AGGAACATGGCATGGAGTGG	
12F	AGAAACAGCACACCTGGAGG	326
12R	AAAGCACGGACAACCTCGTT	
18F	TAAGGGTCAGGGAGTGGGAC	440
18R	AGGGGAAGCACTCAGAGTCA	
19F	TCCTAGGAGGGAGAAGCCAA	415
19R	TGACAGACACACACCATCCC	
20F	GATGGAGTGTGGGTGCGATC	401
20R	GACATACCCATACCAAGCCACA	
31F	CTCACCAATTTCAGGGGTTG	388
31R	CCTGGTTATGTGTGCGTGAG	
32F	CCTCTACCCCTAGGCCACAT	363
32R	GGGGCCCCCAAAAACTTTAG	

Sequence of exons 9, 31 and 32 of *NOTCH3* gene were also obtained and the same tools were used in order to design and choose the best pair of primers flanking all coding region of the exons, since these were found to be affected in some individuals in our cohort.

SQSTM1 gene was sequenced for all patients with a particular aggressive phenotype and therefor sequence of all exons of *SQSTM1* gene were also obtained in order to designed and choose the most suitable primers flanking all coding region of the exons using once more the same tools mentioned above (Table 2.2).

Table 2.2. *SQSTM1* primers and respective PCR product length

Exon	Sequence (5' - 3')	Product Length (bp)
1F	AGACTCCGCCCCTCTCGAG	472
1R	CGAACTGGGGACCCATGCAG	
2F	GCCAGAGCAAGGGGGTAGTC	383
2R	AGCCCTCAAATTGCTGACCCC	
3F	CGACAGAGGGGGAGGACTTTA	470
3R	GTTTCCTGGTGGACCCATTTCC	
4F	CTGCCCAGACTACGACTTGTG	475
4R	GTGTGATTGTAGGGCACCAGG	
5F	GGTCACTGGACAAGATGTCCG	377
5R	CCTTGAGTTGCCCGTGGTCC	
6F	CTTAGCTGCTTGTGGGGACTG	455
6R	CTCCCTCGGGTTTGTAAGTGG	
7F	CGACTGTCTGCCAGGAGCC	403
7R	CTACAGACAGCCCTGCAGTGG	
8F	CCAAGGCAGCAGGGTATGTG	372
8R	TGGCTTCTTGCACCCTAACCC	

2.3.3.2. *NOTCH3* and *SQSTM1* DNA amplification by PCR

Exons 3, 4, 8, 9, 11, 12, 18-20, 31 and 32 of *NOTCH3* gene as well as all exons of *SQSTM1* gene were amplified from the DNA isolated from the blood samples of each patient using polymerase chain reaction (PCR).

The mixture of reagents to amplify the *NOTCH3* and *SQSTM1* exons was prepared for a total volume of 24μL, according to the Table 2.3.

PCR conditions were optimized using a gradient of annealing temperatures to enlarge specificity of the designed primers.

For each reaction, was added 1μL of DNA at 100ng/μL concentration, for a final volume of 25μL of PCR reaction product. The PCR conditions used for each exon of *NOTCH3* and *SQSTM1* genes are discriminated in Tables 2.4, 2.5 and 2.6.

Table 2.3. Reagents used in PCR mix for amplification of *NOTCH3* and *SQSTM1* exons

Reagents	Final Concentration	Reaction Volume (μL)
H_2O	-	14.4
Taq Buffer 5x (Promega)	1x	5
MgCl2 25mM (Promega)	1.5mM	1.5
dNTPs 5mM (Fermentas)	0.2mM	1
Primer Foward 10μM	0.5mM	1
Primer Reverse 10μM	0.5mM	1
DNA polymerase 5U/μL (Promega)	0.5U	0.1

Table 2.4. Thermal cycler conditions for amplification of exons 3 and 4 of *NOTCH3* gene

Cycle step	Temp. (°C)	Time	Cycles
Initial denaturation	96	1min	1
Denaturation	96	10sec	
Anneling	64	10min	35
Extension	72	1min 20sec	
Final Extension	72	5min	1
Storage	4	∞	1

Table 2.5. Thermal cycler conditions for amplification of exon 7 of *SQSTM1* gene

Cycle step	Temp. (°C)	Time	Cycles
Initial denaturation	96	1min	1
Denaturation	96	10sec	
Anneling	66	10min	35
Extension	72	1min 20sec	
Final Extension	72	5min	1
Storage	4	∞	1

Table 2.6. Thermal cycler conditions for amplification of exons 8-9, 11-12, 18-20, and 31-32 of *NOTCH3* gene and exons 1-6 and 8 of *SQSTM1* gene

Cycle step	Temp. (°C)	Time	Cycles
Initial denaturation	94	2min	1
Denaturation	94	30sec	
Anneling	60	30sec	14
Extension	72	30sec	
Denaturation	94	30sec	
Anneling	55	30sec	9
Extension	72	30sec	
Denaturation	94	30sec	
Anneling	50	30sec	9
Extension	72	30sec	
Final Extension	72	10min	1
Storage	4	∞	1

All PCR reactions had a negative control and were performed in Biometra® thermal cyclers.

2.3.3.3. Agarose Gel Electrophoresis

All resulting PCR reaction products were confirmed by agarose gel electrophoresis. Samples were loaded into wells of an 2% weight/weight agarose gel stained with GreenSafe Premium (NZYtech) and exposed to an electric field. Alongside each sample batch respective negative control was loaded. HyperLadder™ IV (Bioline) was used in each run as molecular weight marker for relative size comparison. All resulting bands were visualized and photographed, like in Figure 2.1, using a UV transilluminator, Gel doc_XR® (BIO-RAD) and v4.6.9 of Quantity One® software.

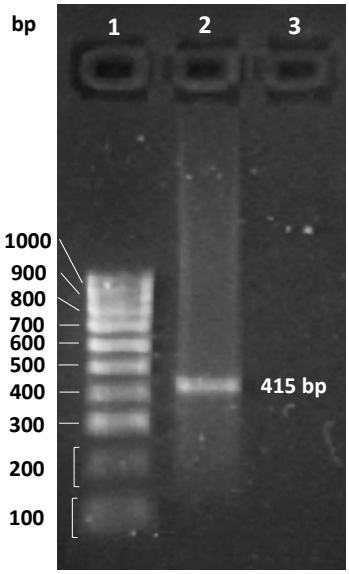

Figure 2.1. Representative agarose gel electrophoresis photograph with HyperLadder™ IV (lane 1), a sample with 415bp (lane 2), and a negative control (lane 3).

2.3.3.4. Purification of PCR Reaction Products

The PCR reaction products were purified using the Exo/SAP Go PCR Purification Kit (Grisp). Based on enzymatic processes, a mix of exonuclease I (Exo) combined with shrimp alkaline phosphatase (SAP) is added to the PCR reaction products to remove excess of primers and dNTPs. Samples were placed into Biometra® thermal cyclers and the selected conditions are listed in Table 2.7.

Table 2.7. Thermal cycler conditions for purification of PCR reaction products using Exo/SAP

Cycle step	Temp. (°C)	Time
Enzymatic activation	37	5min
Enzymatic inactivation	80	10min
Storage	4	∞

2.3.3.5. Sequencing Reaction

The sequencing reactions were performed using the GenomeLab™ Dye Terminator Cycle Sequencing with Quick Start Kit (Beckman Coulter), based on the Sanger sequencing method (Sanger et al., 1977). This technique is based on the incorporation of fluorescently labeled ddNTPs on the 3' end DNA strand by DNA polymerase, leading to termination of the strand elongation due to lack of a 3'-OH functional group. Therefore, in the end, several DNA molecules are obtained with different sizes.

The sequencing reactions were prepared for a total volume of 20μL, according to the Table 2.8, and placed into Biometra® thermal cyclers using the conditions discriminated in Table 2.9.

Table 2.8. Reagents used to prepare the sequencing reactions

Reagents	Reaction Volume (μL)
H_2O	0-9.5*
DNA Template	0.5-10.0**
Sequencing Primer (Foward or Reverse) (10pmol/μL)	1.0
DTCS Quick Start Master Mix	3.0

* To adjust total volume to 20μL
**Volume based on band intensity observed on the agarose gel

Table 2.9. Thermal cycler conditions for sequencing of *NOTCH3* exons

Cycle step	Temp. (°C)	Time	Cycles
Denaturation	96	20sec	30
Anneling	50	20sec	
Extension	60	4min	
Storage	4	∞	1

2.3.3.6. Purification of Sequencing Reaction Products

The sequencing reaction products were purified in order to remove residual salts, excess ddNTPs and other components not incorporated during the reaction that could interfere with the sequencing analysis. The purification was based on ethanol precipitation. A mixture of 62.5μL ethanol (95%), 3μL NaOAc (3M) and 14.5μL ddH_2O was added to each sample, in a 96-well PCR plate, that was sealed with Parafilm and stored at -20°C for 10 min. Three consecutive centrifugations were performed and between them supernatant was discarded and cold ethanol 70% (-20°C) was added to each well. In the end, pellets were resuspended on 25μL of formamide by vortex and one drop of mineral oil was added to each well.

2.3.3.7. *NOTCH3* and *SQSTM1* genes sequence reading and bioinformatic alignment

The sequence reading was performed on a CEQ 8000 Genetic Analysis System automatic sequencer (Beckman Coulter), where the labeled DNA fragments were separated by eight capillary electrophoresis. Base calling was obtained by laser-induced fluorescence in four spectral channels, each one targeting a respective fluorochrome. Sequence read files were exported as electropherograms and further analyzed on the demo version of the SEQUENCHER™ software. The electropherograms were manually analyzed by two independent operators by comparison with the reference *NOTCH3* gene sequence (GenBank accession: NM_000435.2). Whenever a DNA base alteration was identified on the electropherograms, further analysis was performed to rule out its pathogenic nature, according to 2.3.3.8.

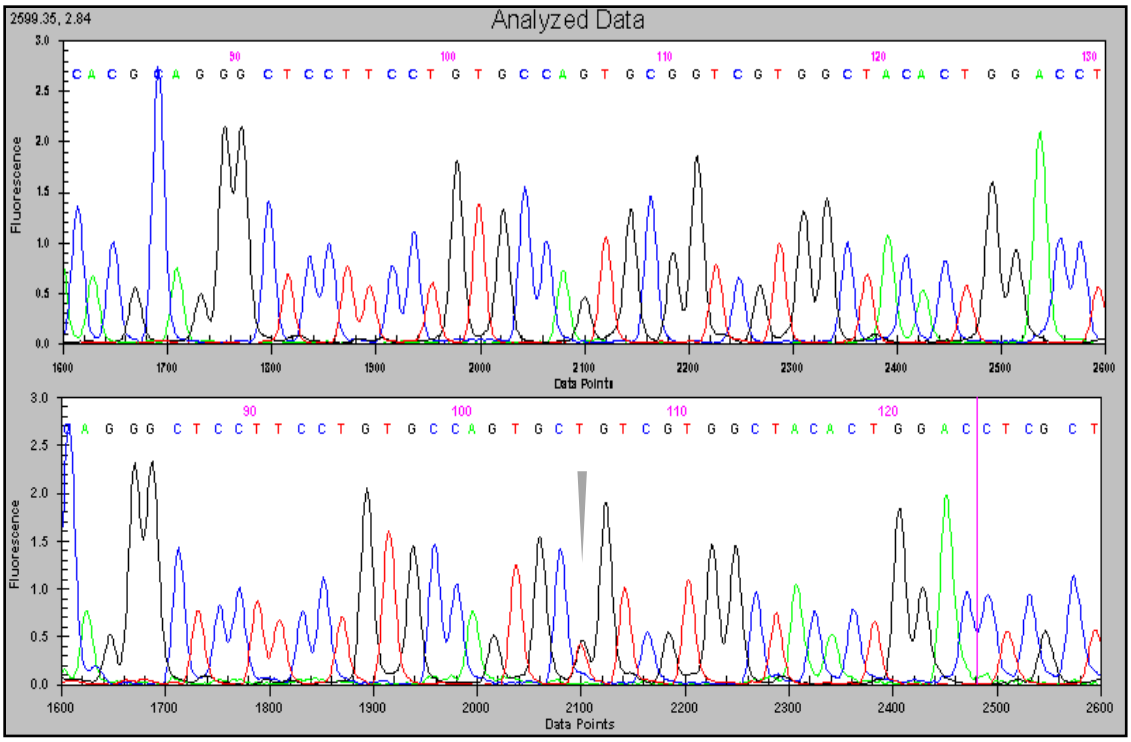

Figure 2.2. Representative electropherograms obtained with Sanger sequencing. Upper panel illustrating the reference sequence and the lower panel showing a heterozygous variant (arrowed).

2.3.3.8. Bioinformatic Analysis and Sequence Variants Interpretation

Any DNA base alteration was evaluated using an in-house bioinformatic pipeline to assess variants pathogenicity, based on population, variant and disease databases and *in silico* tools, following the recommendations of the American College of Medical

Genetics and Genomics (ACMG) and the Association of Molecular Pathology (Richards et al., 2015). Firstly, all variants were search on EMSEMBL and population databases such as: 1000 Genomes (1000G), exome aggregation consortium database (ExAC), genome aggregation database (GnomAD) and dbSNP. Disease databases as HGMD and ClinVar and variant databases as Varsome and UMD-Predictor were also consulted. In order to investigate missense variants effect, a selection of *in silico* tools were also used including SIFT (Kumar et al., 2009), PolyPhen (Adzhubei et al., 2010), Mutation Taster (Schwarz et al., 2010), MUTPred (Pejaver et al., 2017), CADD (Rentzsch et al., 2019), and FATHM-MLK (Shihab et al., 2015).

All identified variants of uncertain significance, probable pathogenic and/or pathogenic were confirmed by a second PCR before being reported.

2.3.4. Next Generation Sequencing

2.3.4.1. Sample preparation

All gDNA samples were diluted in nuclease-free water to a final concentration of 25ng/μL using NanoDrop ND-1000 Spectrophotometer® (Thermo Fisher Scientific) as described in section 2.3.2. Samples concentrations were then confirmed by Qubit® dsDNA HS Assay using Qubit® 4 Fluorometer (Invitrogen).

2.3.4.2. Fragment and adaptor-tagged library preparation (I)

For a total volume of 21μL, the fragmentation reactions were prepared for enzymatic fragmentation and the addition of adaptors at the fragmented ends, was performed using the reagents listed on Table 10 and placed into MyCycler™ thermal cycler (BIO-RAD) with the conditions discriminated in Table 11.

Table 2.10. Reagents for DNA fragmentation and adaptor-tagging

Reagents	Reaction Volume (μL)
SureSelect QXT Buffer (Agilent Technologies)	17
gDNA sample 25ng/μL	2
SureSelect QXT Enzyme Mix, ILM (Agilent Technologies)	2

Table 2.11. Thermal cycler conditions for DNA fragmentation and adaptor-tagging

Cycle step	Temp. (°C)	Time
Step1	45	10min
Step2	4	1min
Step3	4	Hold

To stop fragmentation, it was added 32μL of 1X SureSelect QXT Stop Solution (with 25% ethanol) (Agilent Technologies) to each fragmentation reaction.

2.3.4.3. DNA purification using AMPure XP beads

The adaptor-tagged libraries were then purified using AMPure XP beads (Beckman Coulter). Each library was diluted in 52μL of the homogeneous bead suspension. After incubation for five minutes, tubes were placed in the DynaMag^{TM}-2 magnetic stand (Invitrogene) until the solution cleared and beads were washed with fresh ethanol (70%) in a total of two washes. DNA was further eluted in 11μL of nuclease-free water, and each cleared supernatant was kept on ice.

2.3.4.4. Fragment and adaptor-tagged library preparation (II)

Furthermore, the adaptor-tagged gDNA libraries were repaired and amplified by PCR. Reagents were mixed according to Table 2.12. 40μL of the pre-capture PCR reaction mix was added to each 10μL of purified gDNA library and samples were placed into MyCycler^{TM} thermal cycler (BIO-RAD) with the conditions discriminated in Table 2.13.

Table 2.12. Reagents used for pre-capture PCR reaction mix

Reagents	Reaction Volume (μL)
Nuclease-free water	25
Herculase II 5x Reaction Buffer (Agilent Technologies)	10
100mM dNTP Mix (25mM each dNTP) (Agilent Technologies)	0.5
DMSO (Agilent Technologies)	2.5
SureSelect QXT Primer Mix (Agilent Technologies)	1
Herculase II Fusion DNA Polymerase (Agilent Technologies)	1

Table 2.13. Thermal cycler conditions for pre-capture amplification

Cycle step	Temp. (°C)	Time	Cycles
Step1	68	2min	1
Step2	98	2min	1
Step3	98	30sec	8
	57	30sec	
	72	1min	
Step4	72	5min	1
Step5	4	Hold	1

After amplification, gDNA libraries were purified using AMPure XP beads (Beckman Coulter) as described above in section 2.3.4.3.

The quantity and quality of the adaptor-tagged gDNA libraries was assess using two methods. DNA was quantified in a Qubit® 4 Fluorometer (Invitrogen) as already described, with a dilution of 1:5. Also, quality and quantity of DNA was assessed using an Agilent TapeStation and D1000 Screen Tape (Agilent Technologies) following the instructions in the instrument manual user. The peak of DNA fragment size should be positioned between 245bp to 325bp.

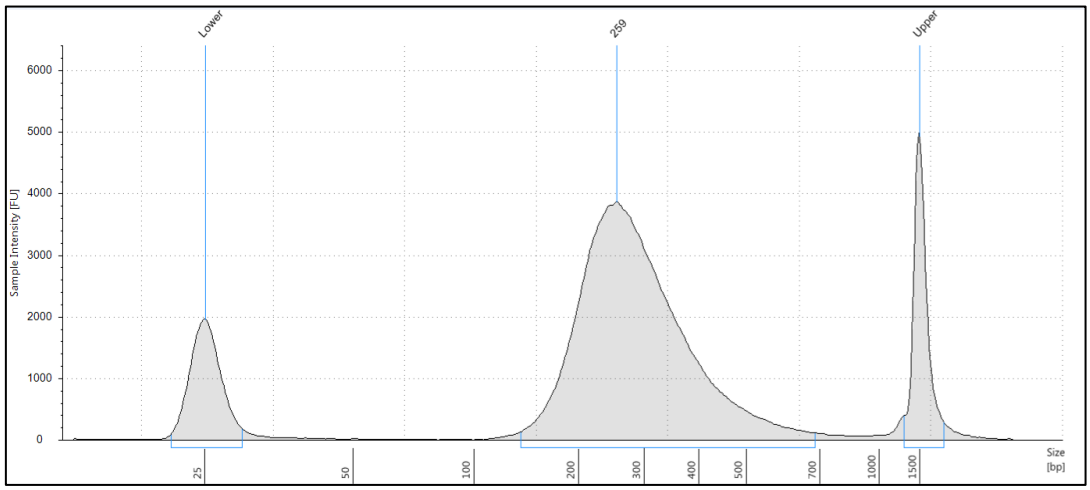

Figure 2.3. Representative sample electropherogram showing pre-capture analysis of amplified library DNA using the 2200 TapeStation with D1000 Screen Tape.

Libraries were properly labeled and stored at 4°C for short term or at -20°C for longer term storage.

2.3.4.5. Hybridization and Capture

In order to prepared he gDNA libraries for the hybridization reaction, approximately 500 to 750ng of each gDNA library in 12μL of volume was mixed with 5μL of SureSelect QXT Fast Blocker Mix (Agilent Technologies) and hybridization reactions were placed into MyCycler™ thermal cycler (BIO-RAD) following conditions discriminated in Table 2.14.

Table 2.14. Thermal cycler conditions for hybridization*

Cycle step	Temp. (°C)	Time	Cycles
Step1	95	5min	1
Step4	65	10min	1
Step3	65	1min**	1
Step4	65 37	1min 3sec	8
Step5	65	Hold	1

* Set up the thermocycler for the final reaction volume, 30μL

**Thermocycler was paused here

On step 3, 13μL of capture library hybridization mix, which reagents are described on Table 2.15, was added to each hybridization reaction, and thermal cycler program was resumed to allow hybridization of the prepared DNA samples.

Table 2.15. Reagents for preparation of capture library hybridization mix

Reagents	Reaction Volume (μL)
25% RNase Block solution*	2
Capture Library	2
SureSelect QXT Fast Hybridization Buffer (Agilent Technologies)	6
Nuclease-free water	3

* 0.5μL of SureSelect RNase Block (Agilent Technologies) + 1.5μL Nuclease-free water

The hybridized DNA was captured using Dynabeads™ MyOne™ Streptavidin T1 (Invitrogen), previously washed in a total of three washes with SureSelect Binding Buffer (Agilent Technologies) using the DynaMag™-2 magnetic stand (Invitrogene) and resuspended in 200μL of the same buffer. Hybridization samples (30μL) were mixed with the streptavidin-coated magnetic beads for 30 minutes and beads were collected from the suspension using a magnetic separator. Then, the beads were

initially washed with SureSelect Wash Buffer 1 and then with pre-warmed SureSelect Wash Buffer 2 (65°C) for a total of four washes. After removing the supernatant from the final wash, 23μL of nuclease-free water was added to each sample.

2.3.4.6. Indexing

The 23μL of bead suspension was added to 25μL of PCR reaction mix described on Table 2.16. Also, to add index tags to the captured libraries, 1μL of each appropriate dual index primer (P7 i1 to i12 and P5 i13 to i20) was added to each reaction. Tubes were placed into MyCycler™ thermal cycler (BIO-RAD) according with the conditions discriminated in Table 2.17.

Table 2.16. Reagents for preparation of post-capture PCR reaction mix

Reagents	Reaction Vol. (μL)
Nuclease-free water	13.5
Herculase II 5x Reaction Buffer (Agilent Technologies)	10
100mM dNTP Mix (25mM each dNTP) (Agilent Technologies)	0.5
Herculase II Fusion DNA Polymerase (Agilent Technologies)	1

Table 2.17. Thermal cycler condition for post-capture PCR

Cycle step	Temp. (°C)	Time	Cycles
Step1	98	2min	1
Step2	98	30sec	14
	58	30sec	
	72	1min	
Step3	72	5min	1
Step4	4	Hold	1

When the PCR amplification was completed, the supernatant was removed using the DynaMag™-96 side magnetic stand (Invitrogene) and the streptavidin-coated beads were discarded.

The amplified captured libraries were purified using AMPure XP beads (Beckman Coulter) as already described in section 2.3.4.3.

The quantity and quality of the capture libraries was assess using an Agilent TapeStation and High Sensitivity D1000 Screen Tape (Agilent Technologies) following

the instructions of the instrument manual user. The peak of DNA fragment size should be positioned between 325bp and 450bp, and the concentration of each library was given by the area under the entire peak on the electropherogram.

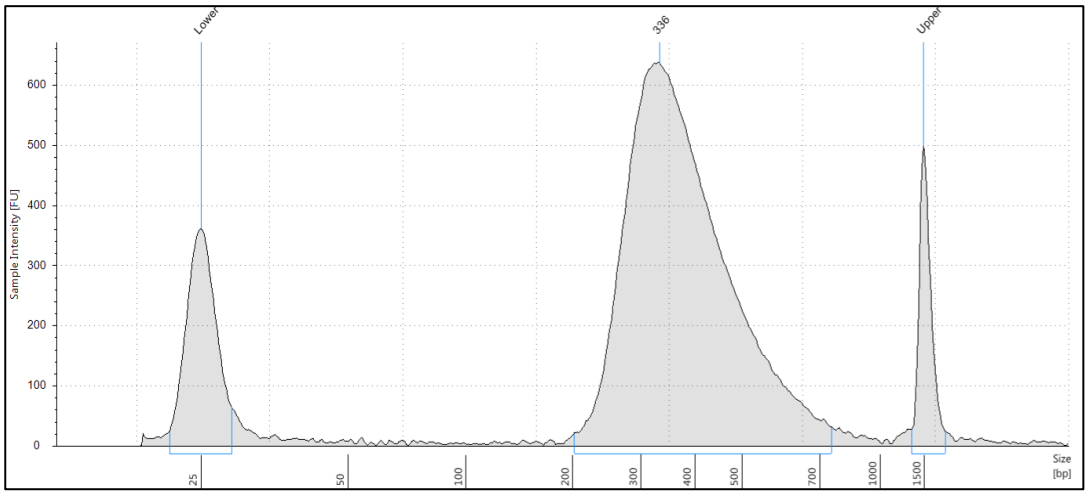

Figure 2.4. Representative electropherogram showing post-capture analysis of amplified indexed library DNA using the 2200 TapeStation with High Sensitivity D1000 Screen Tape

Each index-tagged library was also quantified by qPCR using the KAPA Library Quant Kit for Illumina (Roche) following the manufacture instructions.

Libraries were properly labeled and stored at -20°C for longer term storage.

2.3.4.7. Multiplexed sequencing

Libraries were combined in order to get equimolar amounts of each index-tagged sample in the pool samples, using the formula

$$\text{Volume of Index} = \frac{V(f) \times C(f)}{\# \times C(i)}$$

to determine the amount of each library to use, where $V(f)$ is the final desired volume of the pool sample, $C(f)$ is the desired final concentration of all the DNA in the pool, # is the number of indexes, and $C(i)$ is the initial concentration of each indexed sample.

Preparation of sequencing samples was done following MiSeq® System Denature and Dilute Libraries Guide for a MiSeq® v2 Reagent Kit of 300 Cycles.

Samples were sequenced on MiSeq™ Illumina® Sequencer following MiSeq® System Guide instructions.

2.3.4.8. Bioinformatic Analysis and Sequence Variants Interpretation

Sequence read files were exported in FASTQ format and processed using the SureCall v4.0 software (Agilent) to align the sequences to the human reference genome sequence hg19 with Burrows-Wheeler aligner (BWA) and variant call. Analysis was conducted for a virtual customized gene panel of known cSVD causative genes: *NOTCH3* (NM_000435.2), *HTRA1* (NM_002775.4), *CTSA* (NM_000308.3), *COL4A1* (NM_001845.5), *COL4A2* (NM_001846.3), *TREX1* (NM_033629.6), and *GLA* (NM_000169.2); and for patients with particular aggressive phenotype, known dementia related genes were also included: *PSEN1* (NM_000021.4), *PSEN2* (NM_000447.3), *APP* (NM_000484.4), *APOE* (NM_000041.4), *SORL1* (NM_003105.6), *CHMP2B* (NM_014043.4), *FUS* (NM_004960.4), *GRN* (NM_002087.4), *MAPT* (NM_005910.5), *SQSTM1* (NM_003900.4), and *TBK1* (NM_013254.3). Coverage assessment and mapping visualization was performed using the Integrative Genomics Viewer (IGV) and interpretation of found variants was performed using an in-house multistep process workflow to assess variants pathogenicity, based on population, variant and disease databases and *in silico* tools, following the recommendations of the ACMG and the Association of Molecular Pathology (Richards et al., 2015), as described previously in section 2.3.3.8.

All identified variants of uncertain significance, probable pathogenic and/or pathogenic were further confirmed on a second PCR amplification with subsequent Sanger sequencing and discriminated in the genetic report.

2.3.5. Neurofilament quantification

Neurofilaments were quantified in serum samples using SiMoA™ NF-light ®Advantage Kit (Quanterix) which complies single molecule array (SiMoA) bead technology, a digital ultrasensitive immunoassay that can detect proteins in blood at very low concentrations. Briefly, a 2-step immunoassay was performed with incubation of the antibody coated magnetic microbeads with the samples and a biotinylated detector antibody, resulting in the formation of an immune-complex between these components. After washing,

streptavidin-β-galactosidase was mixed with the samples, binding to the biotinylated detector antibody. After several washes and stabilization, the plate was transferred to Quanterix SR-X™ Ultra-Sensitive Biomarker Detection System. Beads were resuspended in a resorufin-β-D-galactopyranoside substrate solution and transferred to the SiMoA Disc. This disc has 300,000 femtoliter-sized microwells and these wells can accommodate only one bead each. Microwells were sealed and fluorescent signal in each well was counted, resulting in a digital signal that correspond to the presence or absence of single enzyme molecules, which allows the extreme sensitivity of this technique. Results were then exported and analyzed.

2.4. Statistical Analysis

All statistical analyses were performed using IBM SPSS Statistics v1.0.0.1461 software. Normality was determined using Shapiro-Wilk test and Chi-Square test of independence was used to analyze categorical variables.

Mann-Whitney U test was applied to assess statistical difference between mean values of two independent groups with non-parametric distributions. Results were presented in boxplots.

Furthermore, Spearman rank correlation was used as a measure of the association between variables with non-parametric distributions. Results were presented in scatter plots to visualize the association between two variables.

3. Results

This study was divided in two main tasks, starting with the (I) genetic and clinical characterization of our CADASIL patients' cohort, followed by the (II) evaluation of the potential of sNF-L values in the prognosis of CADASIL patients.

3.1. Genetic and Clinical Characterization

3.1.1. Study Population (I)

Therefore, in order to perform the first task, a total of 70 individuals with clinical features and/or family history of CADASIL were genetic studied with Sanger and/or NGS assays, and a total of 53 *NOTCH3* mutation carriers were identified. Of those, 20 were referred index cases from different and unrelated families and 33 were family relatives. Twelve out of the 20 index cases were female (60%) and eight of 20 were male (40%), with a mean age value of 58.2 $\pm$ 8.7 (range between 40 and 73). Additionally, of the 50 studied family members, 24 were female (48%) and 26 were male (52%), with a mean age value of 46.7 $\pm$ 14.7 (range between 20 and 76).

3.1.2. Molecular Analysis

The genetic analysis revealed 12 different heterozygous mutations in the *NOTCH3* gene, in which eight were missense cysteine altering mutations (p.R110C, p.R153C, p.G420C, p.R427C, p.C446F, p.R558C, p.R607C, p.C1099Y), three were missense cysteine sparing mutations (p.S497L, p.S978R, p.V1952M) and one was a nonsense mutation (p.R1893*), all illustrated in Figures 3.1 to 3.3 and described in Table 3.1. Of note, all the missense mutations were previously reported in the literature associated with CADASIL.

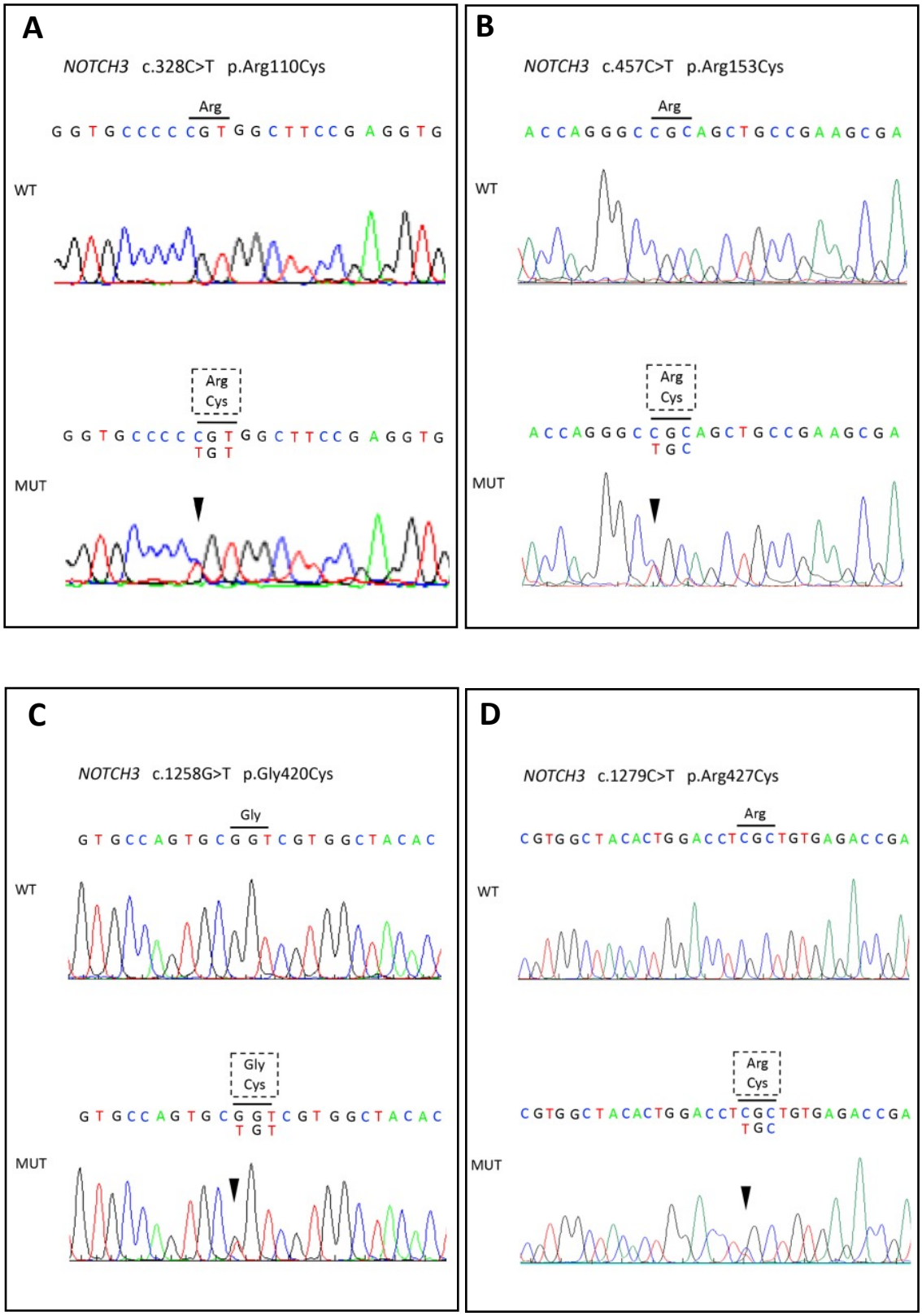

Figure 3.1. Electropherograms of missense cysteine altering variants identified on *NOTCH3* gene (I). (A) Heterozygous p.R110C variant in the exon 3, found in index case 1 (B) Heterozygous p.R153C variant in the exon 4, found in index cases 2 and 3 (C) Heterozygous p.G420C variant in the exon 8, found in index cases 4, 5, 6, 7 and 8 (D) Heterozygous p.R427C variant in the exon 8, found in index case 9. Each corresponding amino acid substitution is depicted within a limited reading frame.

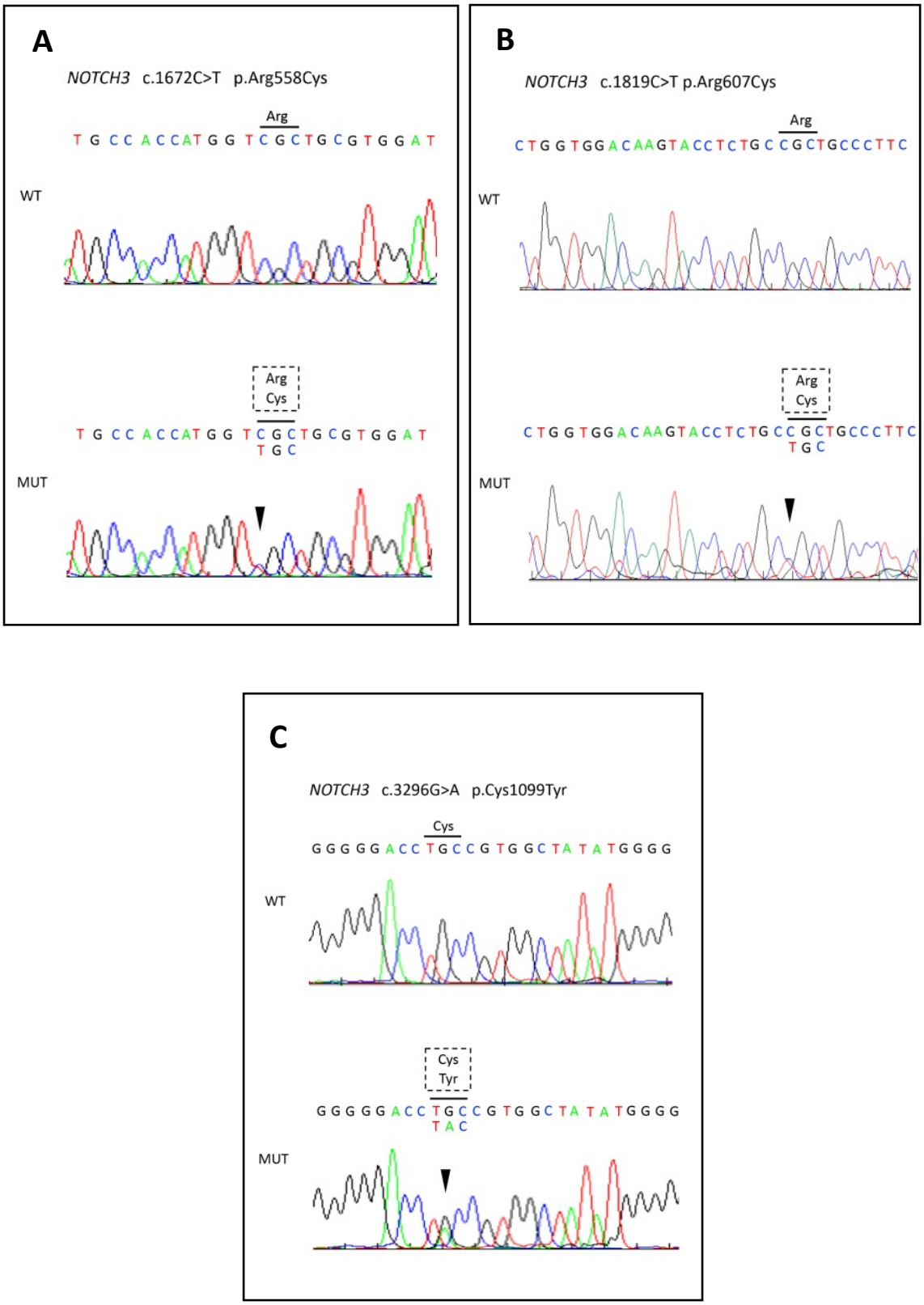

Figure 3.2. Electropherograms of more missense cysteine altering variants identified on *NOTCH3* gene (II). (A) Heterozygous p.R558C variant in the exon 11, found in index cases 12, 13, 14 and 15 (C) Heterozygous p.R607C variant in the exon 11, found in index case 16 (D) Heterozygous p.C1099Y variant in the exon 20, found in index case 18. Each corresponding amino acid substitution is depicted within a limited reading frame.

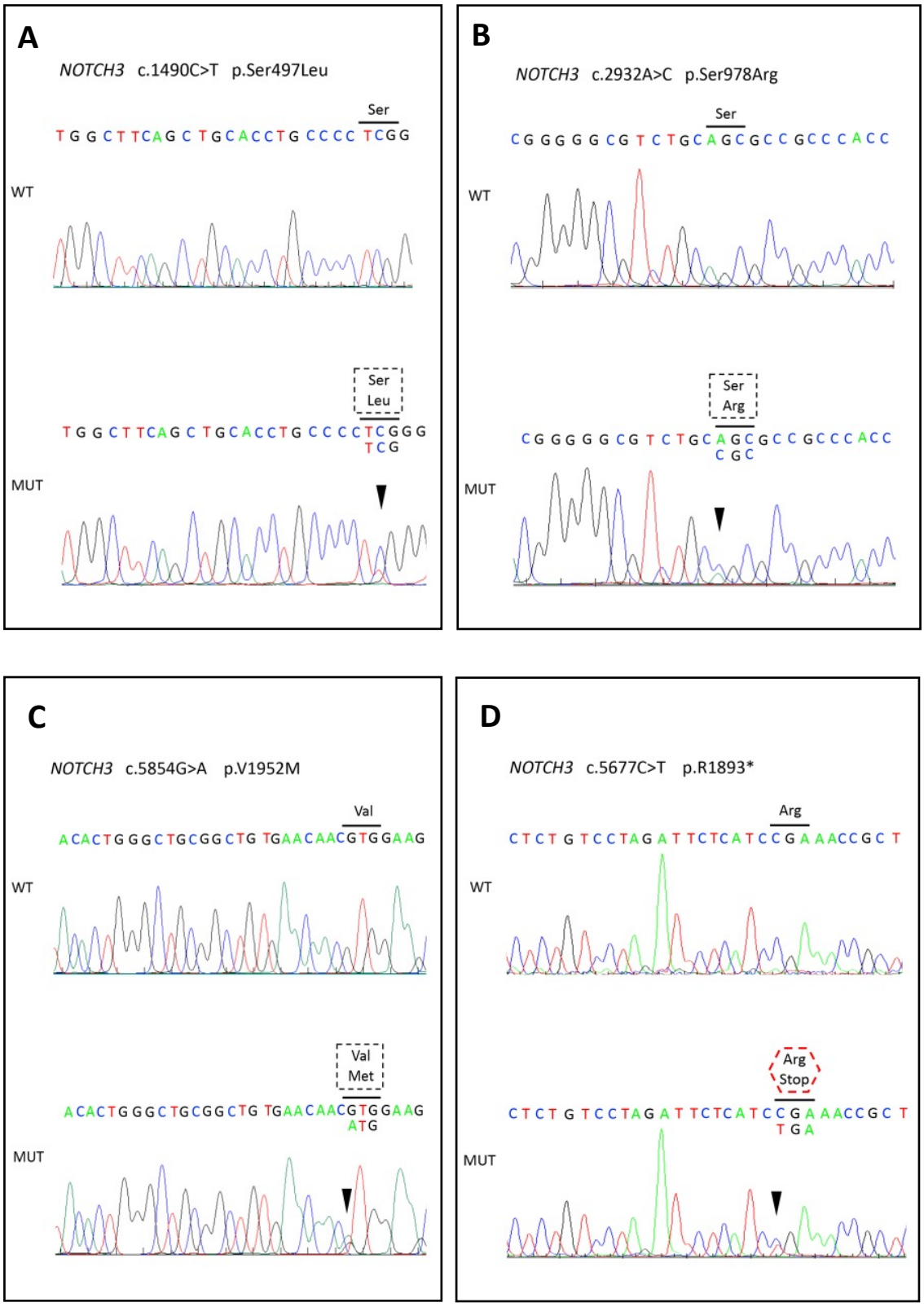

Figure 3.3. Electropherograms of missense cysteine sparing (A-C) and nonsense (D) variants identified on *NOTCH3* gene. (A) Heterozygous p.S497L variant in the exon 9, found in index case 11 (B) Heterozygous p.S978R variant in the exon 18, found in index 17 (C) Heterozygous p.V1952M variant in the exon 32, found in index cases 20 (D) Heterozygous p.R1893* variant in the exon 31, found in index case 19. Each corresponding amino acid substitution is depicted within a limited reading frame.

Table 3.1. *NOTCH3* gene variants found in the 20 index cases identified in our CADASIL patients' cohort

Index case	Nucleotide Change	Amino Acid Chage	Exon	EGFr	References
1	c.328C>T	p.R110C	3	2	Joutel et al., 1997
2,3	c.457C>T	p.R153C	4	3	Joutel et al., 1997
4-8	c.1258G>T	p.G420C	8	10	Joutel et al., 2001
9	c.1279C>T	p.R427C	8	10	Hewamadduma et al., 2010
10	c.1337G>T	p.C446F	8	11	Lesnik Oberstein, 2003
11	c.1490C>T	p.S497L	9	12	Abramycheva et al., 2015
12-15	c.1672C>T	p.R558C	11	14	Joutel et al., 1997
16	c.1819C>T	p.R607C	11	15	Escary et al., 2000
17	c.2932A>C	p.S978R	18	25	Ferreira et al., 2007; Muiño et al., 2017
18	c.3296G>A	p.C1099Y	20	28	Ferreira et al., 2007
19	c.5677C>T	p.R1893*	31	NA	Smith et al., 2013
20	c.5854G>A	p.V1952M	32	NA	Sassi et al., 2018

Key: EGFr, epidermal growth factor-like repeat; NA, not applicable.

Interestingly, when analyzing our 53 mutation carriers, the majority of the individuals harbored a mutation in exon 11 (n=23, 43.4%), followed by exon 8 (n=10, 18.9%), exon 20 (n=6, 11.3%), exon 31 (n=5, 9.4%), exon 4 (n=3, 5.7%) or exon 18 (n=3, 5.7%) (Figure 3.4A). Exons 3, 9, and 32 were only affected in one individual each. Moreover, the most common mutations found in our cohort were p.R558C, p.G420C, p.C1099Y, and p.R1893*, reported in index cases 20, 7, 6, and 5 respectively (Figure 3.4C and Table 3.1).

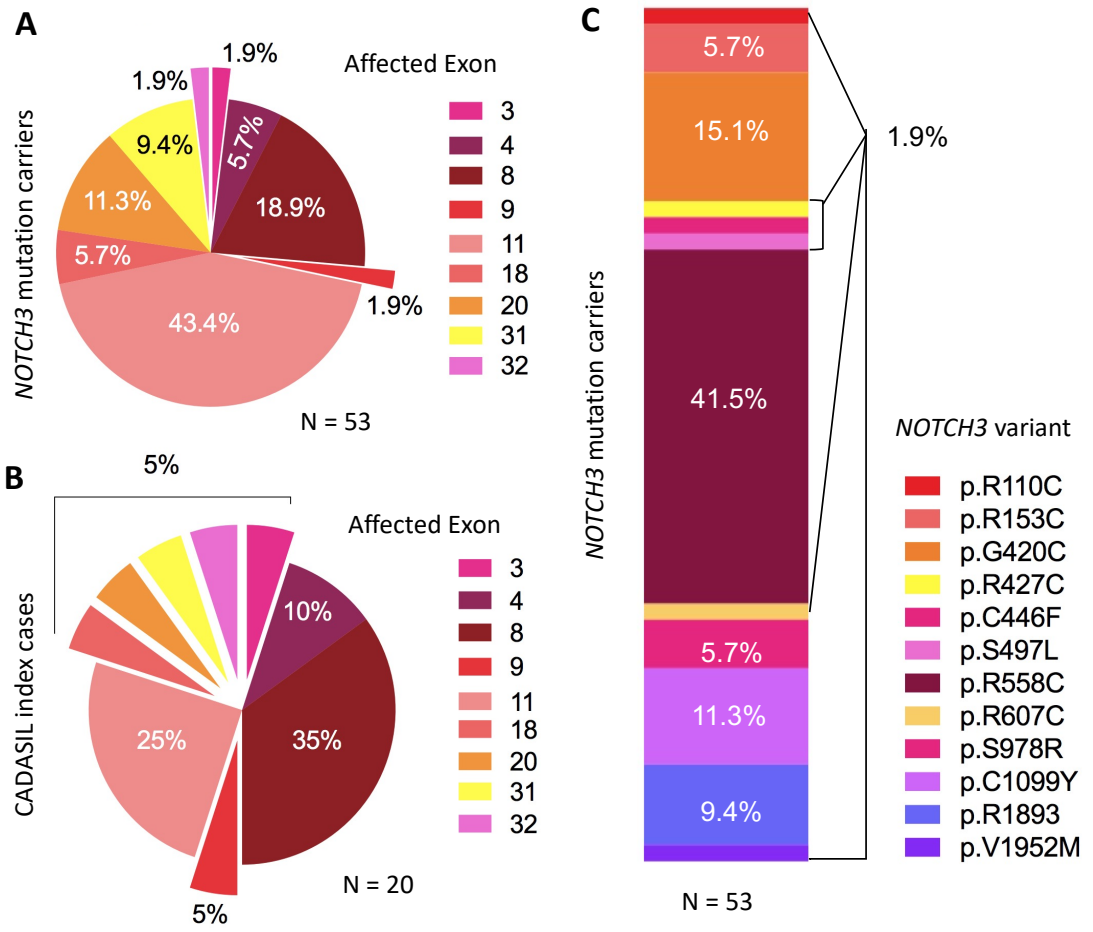

Figure 3.4. *NOTCH3* gene variants distribution and frequency. Pie chart showing the frequency of *NOTCH3* variants per affected exon in: mutation carriers (n = 53) of our CADASIL patients' cohort (A) and the identified CADASIL index cases (n = 20; B). (C) Vertical slice chart showing the frequency of each *NOTCH3* variant found in the mutation carriers (n = 53) of our CADASIL patients' cohort.

The majority of identified *NOTCH3* variants, ten out of twelve, affected the EGFr encoding sequences (83.3%; Figure 3.5), located in the NECD. Seven out of the 20 index cases (35%) harbored a mutation affecting Delta/Jagged ligand binding site, EGFr 10 or 11. Additionally, most index cases had a mutation affecting EGFr 7-34 (83.3%), while only 16.7% of cases harbored a mutation affecting EGFr 1-6. To denote that two mutations in the ICD encoding sequences (p.R1893* and p.V1952M) were also found.

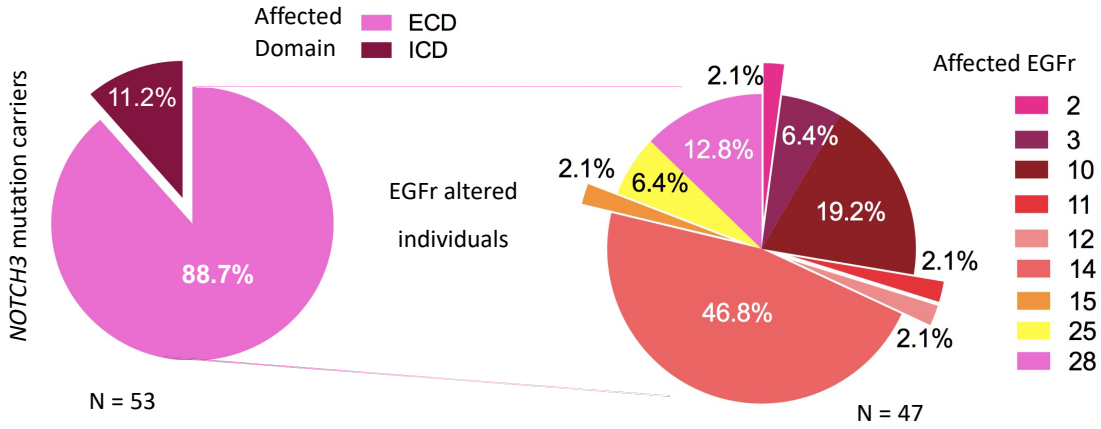

Figure 3.5. Notch3 affected domain and *NOTCH3* affected EGFr encoding sequence frequencies. Pie chart on the left showing the frequencies of affected Notch3 receptor domains found in the *NOTCH3* mutation carriers (n = 53). Pie chart on the right showing the frequencies of affected EGFr encoding sequences found in the EGFr altered individuals (n = 47). ECD, extracellular domain; ICD, intracellular domain; EGFr, epidermal growth factor-like repeat.

The majority of mutations identified (n=8) in the present study were missense mutations predicted to result in gain or loss of a cysteine residue of one of the EGFr of the receptor. These distinctive EGFr cysteine altering Notch3 variants are considered specific to CADASIL and confirmative of a diagnosis. However, in the present study, three index cases were found to carry missense cysteine sparing mutations (p.S497L, p.S978R, and p.V1952M), and one family harbored a nonsense mutation (p.R1893*). All 20 index cases were heterozygous for the *NOTCH3* mutation identified. Of the 33 *NOTCH3* mutation carriers, 30 were heterozygous carriers and only 3 were homozygous carriers, all of them relatives of index case 12, and thereby harboring variant p.R558C in exon 11 in homozygosity (Table 3.1).

Further, 34 common polymorphic variants were found in the coding region of known cSVD related genes (*COL4A1, COL4A2, CTSA, GLA, HTRA1, NOTCH3,* and *TREX1*) of our cohort (Table 3.2). Of those, 24 were synonymous and 6 were non-synonymous, all described in dbSNP and predicted to be benign.

Table 3.2. Polymorphic variants in cSVD related genes identified in the index cases using NGS

Gene	Amino Acid Change	dbSNP	MAF
COL4A1 (NM_001845.5)	p.V7L	rs9515185	0.42
	p.A144	rs532625	0.47
	p.T555P	rs536174	< 0.01
	p.P605	rs61749897	0.10
	p.P710	rs16975492	0.31
	p.G1061	rs874204	0.32
	p.R1063	rs874203	0.32
	p.Q1334H	rs3742207	0.29
	p.A1490	rs1133219	0.31
	p.S1600	rs650724	0.13
COL4A2 (NM_001846.3)	p.T99	rs4238272	0.06
	p.P336	rs4103	0.48
	p.P1268	rs439831	0.06
	p.G1269	rs409858	0.06
	p.T1361	rs438758	0.02
	p.A1363	rs4773199	0.19
	p.F1430	rs4771683	0.06
	p.P1505	rs445348	0.25
	p.A1539	rs391859	0.10
CTSA (NM_000308.3)	p.L37-	rs1241378191	< 0.01
HTRA1 (NM_002775.4)	p.A34	rs1049331	0.29
	p.G36	rs2293870	0.29
	p.I251	rs17624021	0.02
	p.D450	rs374675648	< 0.01
NOTCH3 (NM_000435.2)	p.T101	rs3815188	0.22
	p.A202	rs1043994	0.14
	p.C846	rs1043996	0.48
	p.P914	rs1043997	0.26
	p.A1020P	rs35769976	0.11
	p.P1521	rs1044006	0.13
	p.A2223V	rs1044009	0.7
TREX1 (NM_033629.6)	p.G9	rs908382062	< 0.01
	p.Y177	rs11797	0.31
	p.L304	rs3135945	0.04

Key: MAF, minor allele frequency.

3.1.3. Bioinformatic Analysis

When classifying and reporting variants, databases and published literature can be useful for gathering information. Therefore, population databases, which provide variants frequency in general population, *in silico* tools, disease databases and variant databases should be consulted.

As mentioned above, variants frequency in the general population is an important criterion to ascertain variants clinical significance. Therefore, *NOTCH3* variants frequency were assessed using three different population databases, ExAC, 1000G, and gnomAD (Table 3.3). All variants had a minor allele frequency (MAF) ≤ 1%.

Table 3.3. *NOTCH3* gene minor allele frequency

NOTCH3 variant	ExAC	1000G	gnomAD
p.R110C	0.000009	-	0.000
p.R153C	-	-	-
p.G420C	-	-	-
p.R427C	-	-	-
p.C446F	-	-	-
p.S497L	0.012338	0.007388	0.006707
p.R558C	0.0000412	-	0.00004957
p.R607C	0.000009	-	0.0000244
p.S978R	0.000461	0.000399	0.0002586
p.C1099Y	-	-	-
p.R1893*	0.000008	-	0.000004021
p.V1952M	0.008494	0.004992	0.008156

Key: ExAC, exome aggregation consortium database; 1000G, 1000 genomes; gnomAD, genome aggregation database.

In addition, several *in silico* predictive tools, based on different algorithms, such as SIFT, PolyPhen, CADD, Mutation Taster, MUTPred and FATHM-MLK, were used to predict the impact of the missense changes identified on the structure and function of Notch3 receptor (Table 3.4). All cysteine altering variants had at least four out of 6 *in silico* tools predicting a receptor function alteration. Regarding the missense cysteine sparing variants p.S497L, p.S978R and p.V1952M, they were deemed to

affect protein structure according to three out of five, two out of six, and five out of five *in silico* tools, respectively. To denote that all variants had a CADD score ≥ 15.

Table 3.4. *In silico* analysis of the *NOTCH3* gene variants

			In silico analysis					
			SIFT[1]	PolyPhen-2[2]	CADD[3]	Mutation Taster[4]	MUTpred[5]	FATHM-MLK[6]
NOTCH3 Gene	Cysteine altering variants	p.R110C	Tolerated	Possibly damaging	23	Disease causing	Medium risk	Damaging
		p.R153C	Deleterious	Possibly damaging	28	Disease causing	Medium risk	Damaging
		p.G420C	Tolerated	Probably damaging	25	Disease causing	High risk	Neutral
		p.R427C	Deleterious	Probably damaging	31	Disease causing	Pathogenic	Damaging
		p.C446F	Deleterious	Probably damaging	26	Disease causing	Very high risk	Damaging
		p.R558C	Deleterious	Possibly damaging	28	Disease causing	High risk	Damaging
		p.R607C	Tolerated	Possibly damaging	24	Disease causing	High risk	Damaging
		p.C1099Y	Deleterious	Probably damaging	26	Disease causing	Very high risk	Damaging
	Cysteine sparing variants	p.S497L	Tolerated	Benign	24	Disease causing	Unknown	Damaging
		p.S978R	Tolerated	Benign	19	Polymorphism	High risk	Neutral
		p.V1952M	Deleterious	Probably damaging	26	Disease causing	Unknown	Damaging

Key: SIFT, Sorting Intolerant From Tolerant; PolyPhen-2. Polymorphism Phenotyping 2; CADD, Combined Annotation Dependent Depletion; MUTpred, mutation predictor; FATHM-MLK, Functional Analysis through Hidden Markov Models; NA, not applicable; [1]Kummar et al., 2009; [2]Adzhubei et al., 2010; [3]Rentzsch et al., 2019; [4]Schwarz et al., 2010; [5]Pejaver et al., 2017; [6]Shihab et al., 2015.

Further analysis using ClinVar and HGMD disease databases, which primarily contain variants found in patients with disease and assessment of the variants' pathogenicity, was also performed and the results are presented in Table 3.5. Varsome and UMD-Predictor variant databases were also consulted. All cysteine altering variants were predicted to be pathogenic or likely pathogenic in all databases. The pathogenic nature of the missense cysteine sparing variants among the different databases was controversial in some cases, which will be discussed in detailed in the section 4, and the nonsense variant was predicted to be pathogenic in all databases.

Table 3.5. *NOTCH3* gene variants classification in disease and variant databases

			Disease databases		Variant databases	
		dbSNP	ClinVar	HGMD	Varsome	UMD-Predictor
NOTCH3 Gene	Cysteine altering variants	p.R110C	rs775836288	P	CM971056 DM	Pathogenic	Pathogenic
		p.R153C	rs797045014	P	CM971060 DM	Pathogenic	Pathogenic
		p.G420C	rs1323608032	P/LP	CM23657 DM	Likely Pathogenic	Pathogenic
		p.R427C	rs1599391536	Not provided	CM108354 DM	Likely Pathogenic	Pathogenic
		p.C446F	rs1568360410	P	CM035649 DM	Likely Pathogenic	Pathogenic
		p.R558C	rs75068032	P	CM961046 DM	Likely Pathogenic	Pathogenic
		p.R607C	rs777751303	P/LP	CM003019 DM	Likely Pathogenic	Pathogenic
		p.C1099Y	rs1555727841	P	HM0709 DM	Uncertain Significance	Pathogenic
	Cysteine sparing variants	p.S497L	rs114207045	B/LB	CM119547 DM?	Benign	Probably Pathogenic
		p.S978R	rs141956294	LB/US	HM0711 DM	Likely Benign	Polymorphism
		p.R1893*	rs535683988	-	CM136159 DM?	Pathogenic	Pathogenic
		p.V1952M	rs115582213	B/LB	CM186057 DM?	Benign	Probable polymorphism

Key: HGMD, human gene mutation database; P, pathogenic; LP, likely pathogenic; B, benign; LB, likely benign; US, uncertain significance; DM, disease causing mutation; DM?, disease causing mutation?.

3.1.4. Clinical features

Clinical records of our 20 referred CADASIL index cases were reviewed and clinical features are summarized in Table 3.6. Mean age onset was 48.3 ± 10.8 years, ranging between 27 and 68. Among the main features, the most prevalent was migraine affecting 65% of cases, with only two cases showing migraine with aura (index cases 7 and 11). Furthermore, 60% of index cases had cerebrovascular events as stroke and/or TIA, with a mean age onset of 50.9 ± 12.4 years. Psychiatric disturbances as depression and anxiety were also found, affecting 40 and 30% of index cases, respectively, with three cases showing both disturbances (index case 6, 15, and 18). Some patients presented other symptoms as gait disturbances (index case 6), anterior ischemic optic neuropathy (index case 1) and seizures (index case 14).

Table 3.6. Clinical features of the 20 referred CADASIL index cases

Index Case	Sex	Onset age, years	*NOTCH3* variant		Age at first stroke, years	Migrane	Psychiatric disturbances	Risk factos	Other manifestations
			Exon	Amino Acid Chage					
1	F	27	3	p.R110C	27	+	-	-	AOIN
2	F	30	4	p.R153C	45	+	DP	OB	-
3	M	32	4	p.R153C	32	+	-	AL, HTN	-
4	M	49	8	p.G420C	49	-	-	AL, DL, HTN	-
5	M	57	8	p.G420C	57	-	-	DM, HTN	-
6	F	48	8	p.G420C	-	+	DP	DL, HTN	GTD
7	F	50	8	p.G420C	50	+[a]	-	S	-
8	F	46	8	p.G420C	46	+	-	-	-
9	F	45	8	p.R427C	-	+	-	S	-
10	F	59	8	p.C446F	60	-	DP	-	-
11	F	40	9	p.S497L	-	+[a]	ANX	-	-
12	M	-	11	p.R558C	-	-	ANX	DL, HTN, pS	-
13	F	45	11	p.R558C	62	+	DP	-	-
14	M	68	11	p.R558C	72	+	-	-	SZ
15	M	49	11	p.R558C	-	+	ANX, DP	pS	-
16	F	-	11	p.R607C	-	-	DP	DL	-
17	F	59	18	p.S978R	-	+	ANX	HTN, OB	-
18	M	54	20	p.C1099Y	-	-	ANX, DP	-	-
19	F	48	31	p.R1893*	48	+	DP	DL, HTN	-
20	M	63	32	p.V1952M	63	-	-	HTN	-

Key: F, female; M, male; ANX, anxiety; DP, depression; AL, alcoholism; DL, dyslipidemia; HTN, hypertension; OB, obesity; pS, past smoking; S, smoking; AOIN, anterior ischemic optic neuropathy; GTD, gait disturbances; SZ, seizures; [a] migraine with aura

Risk factors were available for all index cases. Eight out of our 20 index cases presented hypertension (40%) and five had dyslipidemia (25%). Two out of 20 had alcoholism, other two had obesity. Additionally, three patients were active smoker while two past smokers. Also, there was on case with diabetes (index case 5).

Moreover, evaluation of the overall cognitive status revealed cognitive impairment in about 45% of our index cases (Table 3.7), with severe cognitive decline in index cases 4 and 6. Further, brain MRI exams of patients were obtained and Fazekas scale, which range the WMH from 1 to 3 (1 = small punctate lesions, 2 = several punctate and/or small confluent lesions, 3 = confluent and diffuse lesions), was applied. Neuroimaging examination results are presented in Table 3.7. The majority of patients (42.1%) presented a severe MRI burden, with a confluent and diffuse lesions pattern on MRI (Grade 3 on Fazekas scale). Index cases 1, 2, 9, 12, 15, 16 and 18 had a several punctate and/or small confluent lesions pattern on MRI (Grade 2), with only index case 11 presenting a light MRI burden, corresponding to a small

punctate lesions pattern on the MRI exam (Grade 1). To denote, index cases 12 and 16 were at-risk asymptomatic patients due their lack of clinical features beyond a positive MRI exam.

Table 3.7. Neuropsychological and neuroimaging features of the 20 referred CADASIL index cases

Index Case	*NOTCH3* variant		Cognitive decline	MRI burden (Fazekas scale)
	Exon	Amino Acid Chage		
1	3	p.R110C	-	2
2	4	p.R153C	-	2
3	4	p.R153C	-	3
4	8	p.G420C	+	3
5	8	p.G420C	+	3
6	8	p.G420C	+	3
7	8	p.G420C	-	3
8	8	p.G420C	-	3
9	8	p.R427C	-	2
10	8	p.C446F	+	3
11	9	p.S497L	-	1
12	11	p.R558C	-	2
13	11	p.R558C	+	3
14	11	p.R558C	+	3
15	11	p.R558C	+	2
16	11	p.R607C	-	2
17	18	p.S978R	-	N/A
18	20	p.C1099Y	+	2
19	31	p.R1893*	-	3
20	32	p.V1952M	+	3

Key: MRI, magnetic resonance imaging; N/A, not applicable.

3.1.5. Severe Clinical Cases

As already mentioned, CADASIL is characterized by a large phenotypic variability where some cases present a more severe phenotype, characterized by an early-onset stroke, gait disturbances, dementia and/or severe emotional dysregulation together with a severe white matter burden on MRI.

Among the CADASIL patients referred for the molecular analysis (section 3.1.2), the ones who presented a particular aggressive phenotype were further evaluated in order to rule out the presence of other genetic factors which might modulate their phenotype. Index cases 1-6, 10, 13, 14, 18, and 19 were all pointed as aggressive phenotypes due to their white matter burden on MRI and at least one of the following

features: cognitive impairment (cases 4, 5, 6, 10, 13, 14, and 20), severe emotional dysregulation (cases 2, 5, 6, 10, and 18), gait disturbances (case 6), and an early on stroke age (cases 1 and 3). Due to their particular aggressive cognitive impairment, index cases 6 and 20 were genetic studied for known genes commonly associated with dementia phenotype (*APOE, APP, CHMP2B, FUS, GRN, MAPT, PSEN1, PSEN2, SORL1, SQSTM1,* and *TBK1*) using Sanger and/or NGS assays. Besides the previously reported *NOTCH3* variants identified by Sanger sequencing, the NGS analysis of index case 6 revealed a heterozygous frameshift mutation in *SQSTM1* gene, p.S275Ffs*17 (Figure 3.6 and Table 3.8).

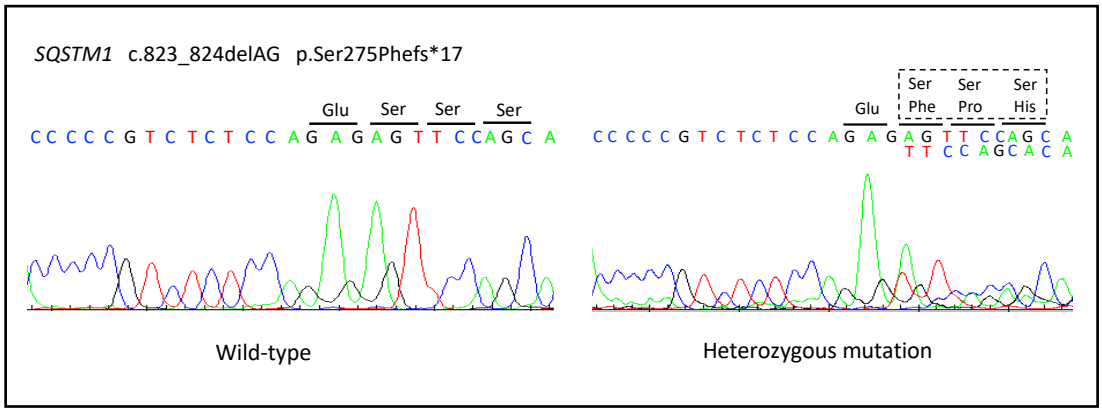

Figure 3.6. Electropherograms illustrating a heterozygous c.823_824 delAG pathogenic variant in the exon 6 of *SQSTM1* gene, with a limited reading frame depicting the corresponding amino acid substitutions p.S275Ffs*17.

Table 3.8. *SQSTM1* frameshift identified variant using NGS

Gene	Nucleotide Change	Amino Acid Chage	Exon	References
SQSTM1 NM_003900.5	c.823_824delAG	p.S275Ffs*17	6	Zúñiga-Ramírez et al., 2019

This pathogenic variant, located in exon 6, is predicted to create a premature stop codon and to cause loss of normal protein function either through protein truncation or nonsense mediated mRNA decay (Table 3.9). In addition, it is not observed in large population cohorts as 1000G and ExAC. To denote, this variant is located within the first PEST domain (region from amino acids 266 to 294) of the gene, which is responsible for signaling peptide for rapid protein degradation.

Table 3.9. Classification of *SQSTM1* frameshift identified variant in disease and variant databases

SQSTM1 variant	dbSNP	Disease databases		Variant databases	
		ClinVar	HGMD	Varsome	UMD-Predictor
p.S275Ffs*17	rs1273214757	P	CD190843 DM	Pathogenic	NA

Key: HGMD, human gene mutation database; P, pathogenic; DM, disease causing mutation; NA, not applicable.

Index case 6 is a 62 years old female, currently presenting emotional dysregulation with significant perceived depressive symptoms and reported previous suicidal attempts, and dementia and gait disturbances that started at the age of 48 (Table 3.6). Neuropsychological examination revealed severe cognitive impairment (MoCA=8; MMSE=11) and brain MRI disclosed the presence of severe white matter burden (Table 3.7). Family history revealed that her mother, who had a history of migraine, and also motor and cognitive impairment, committed suicide by the age of 52. We also identified a 41 years old brother, who had an early-onset stroke (at age of 39), migraine with aura and depression since his 30s, high levels of anxiety, mild cognitive impairment (MoCA=22; MMSE=26) and also presented severe white matter burden on MRI. Further screening and molecular analysis of her brother revealed the co-occurrence of the same pathogenic variants found in index case 6, both in heterozygosity. To denote, the p.S275Ffs*17 variant was not found in any other studied CADASIL case.

Further, 25 common polymorphic variants were identified in the coding region of known dementia phenotype related genes (*APOE, APP, CHMP2B, FUS, GRN, MAPT, PSEN1, PSEN2, SORL1, SQSTM1,* and *TBK1*) of our cohort (Table 3.10). Of those, 19 were synonymous and 6 were non-synonymous, all described in dbSNP and predicted to be benign.

Table 3.10. Polymorphic variants in dementia related genes identified in the index cases using NGS

Gene	Amino Acid Change	dbSNP	MAF
APP (NM_000484.4)	p.A344T	rs201045185	< 0.01
CHMP2B (NM_014043.4)	p.T104	rs11540913	0.18
FUS (NM_004960.3)	p.G49	rs741810	0.28
	p.Y97	rs1052352	0.47
GRN (NM_002087.3)	p.R418Q	rs63751100	< 0.01
MAPT (NM_005910.5)	p.P176	rs1052551	0.09
	p.A227	rs1052553	0.09
	p.N255	rs17652121	0.09
PSEN2 (NM_000447.2)	p.A23	rs11405	0.26
	p.G37D	rs1231154581	< 0.01
	p.N43	rs143227762	< 0.01
	p.H87	rs1046240	0.44
SORL1 (NM_003105.5)	p.H269	rs12364988	0.44
	p.A551	rs636588	0.01
	p.Q1074E	rs1699107	0.98
	p.S1187	rs2070045	0.34
	p.N1246	rs1699102	0.41
	p.A1584	rs3824968	0.40
	p.V1967I	rs1792120	0.02
SQSTM1 (NM_003900.5)	p.D292	rs4935	0.31
	p.G302	rs11548642	0.02
	p.R312	rs4797	0.41
	p.E319K	rs61748794	0.02
	p.V346	rs150470670	< 0.01
TBK1 (NM_013254.4)	p.I326	rs7486100	0.35

Key: MAF, minor allele frequency.

3.2. Evaluation of the prognostic value of sNF-L levels

3.2.1. Study Population (II)

In order to perform the second proposed task, sNF-L levels were assessed using ultrasensitive immunoassay SiMoA technology in a total of 68 individuals. Of those, 37 *NOTCH3* mutation carriers were previously identified and characterized in the first task (sections 3.1) and the remaining 31 were healthy control individuals. The demographical characteristics of the study population, as well as the included controls were collected and are shown in Table 3.11.

Table 3.11. Demographical characteristics of NF-L study population

Features	Controls	CADASIL	*p* Value
N =	31	37	
Age (years; mean ± SD)	48.1 ± 17.7	51.9 ± 13.2	0.411
Gender (% female)	61.3%	51.4%	0.420

Key: SD, standard deviation.

Nineteen out of the 37 *NOTCH3* mutation carriers were female (51.4%) and eighteen of 37 were male (48.6%), with a mean age value of 51.9 $\pm$ 13.2 (range between 26 and 75). Additionally, of the 31 control individuals 19 were female (61.3%) and 12 were male (38.7%), with a mean age value of 48.1 $\pm$ 17.7 (range between 25 and 78). Both gender (p = 0.411) and age (p = 0.420) did not show significant differences between CADASIL patients and control individuals.

3.2.2. sNF-L levels assessment in CADASIL patients

The sNF-L levels assessment using ultrasensitive immunoassay technology revealed mean sNF-L value of 17.55 $\pm$ 29.06 pg/mL in CADASIL patients and a mean sNF-L value of 8.33 $\pm$ 5.16 pg/mL in control individuals. Although the difference between the mean value of the two groups is not significant (p = 0.103), we can observe that sNF-L levels in CADASIL patients are more disperse and vary within a wider range (from 3.33 to 163.28 pg/mL; Figure 3.7A). In addition, some patients had much higher levels of sNF-L than others, like index case 20 (163.28 pg/mL) and index case 6 brother (85.26 pg/mL). Following, in order to explore the relation between sNF-L levels in our

study groups and variables as gender and age, a correlation analysis was performed (Figure 3.7B and 3.8).

Regarding gender, there were no significant differences between males and females in both CADASIL patients (p = 0.564) and control individuals (p = 0.372), although with an overall tendency for higher sNF-L levels in male when compared with females (Figure 3.7B). Further, in relation to age, Figure 3.8A shows a stronger correlation between sNF-L levels and this variant in control individuals (ρ = 0.853; p < 0.001) than in *NOTCH3* mutation carriers (ρ = 0.536; p = 0.001) (Figure 3.8B).

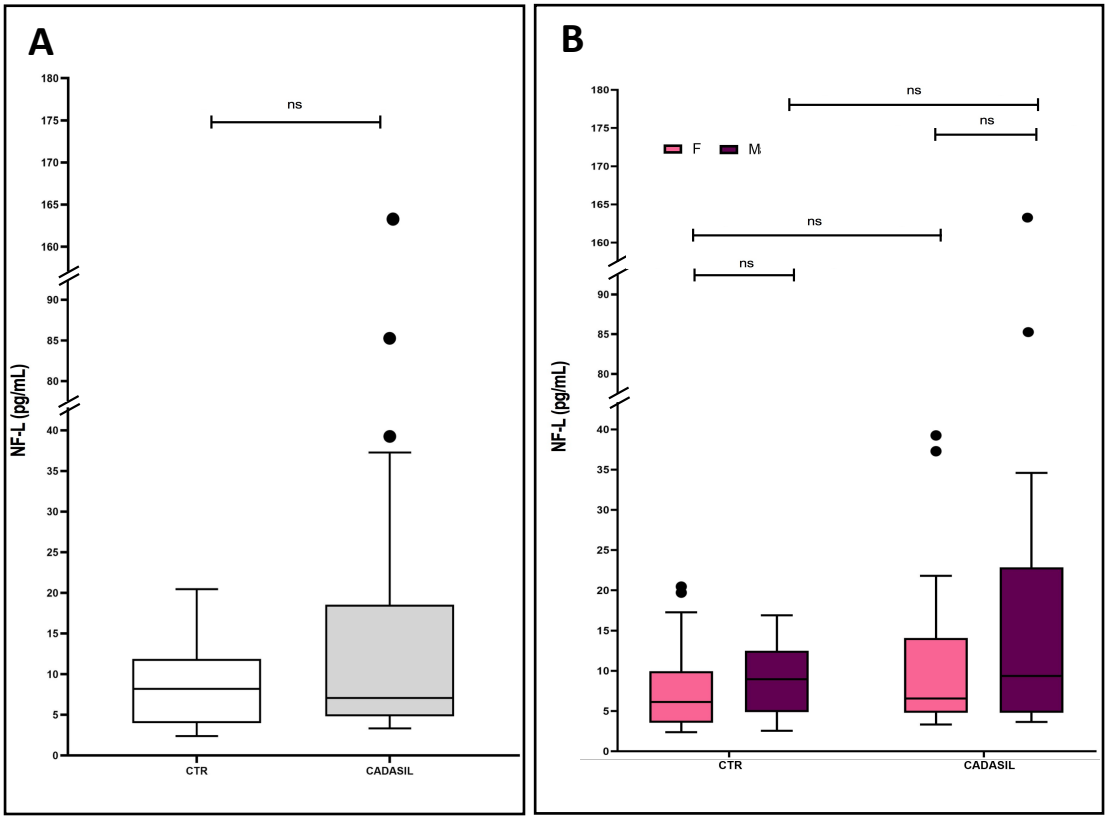

Figure 3.7. Neurofilament serum levels in CADASIL patients. Box plot showing the lower (Q1) quartile, median and the upper (Q3) quartile are depicted. Observations outside the 9-91 percentile range are plotted as outliers. (A) Comparison of sNF-L levels between CADASIL patients (n = 37) and controls (n =31). (Test of Homogeneity Variance; ns, non significant) (B) Comparison between sNF-L levels of female (n = 19) and male (n = 18) CADASIL patients and female (n = 19) and male (n = 12) controls. (Mann-Whitney U test; ns, non significant) CTR, controls; F, female; M, male.

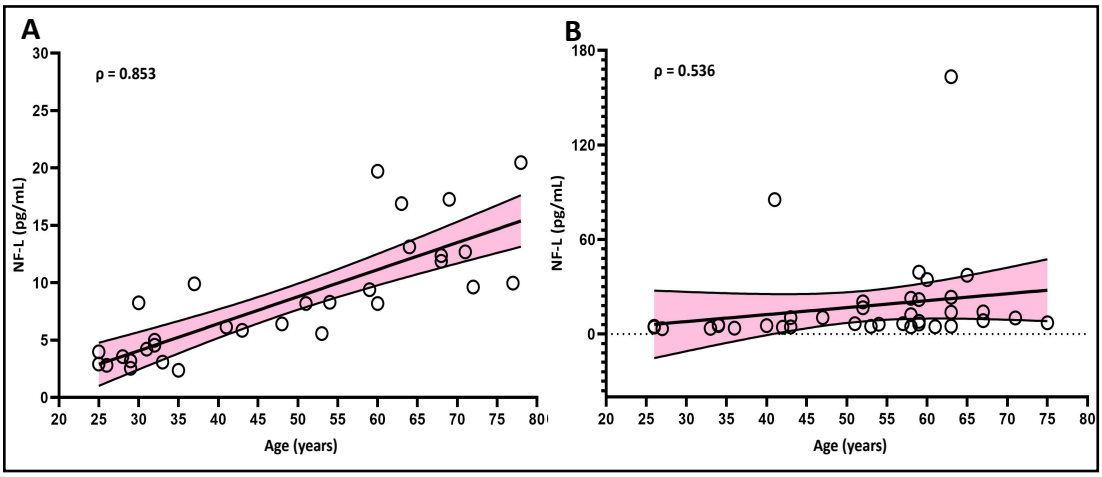

Figure 3.8. Correlation between neurofilament light chain serum (sNF-L) levels and age. Spearman correlation between sNF-L levels and age of controls (A) and CADASIL patients (B). Scatter plots showing the values obtain (points), the regression line and the confidence interval set to 0.95 in the grey area around. ρ, Rho.

3.2.3. sNF-L levels relation with disease onset in CADASIL patients

Due to the high variability of sNF-L values found in our CADASIL patients, we hypothesize that this variability might correlate with disease onset. Therefore, this group was divided in symptomatic (n = 31) and asymptomatic (n = 6) individuals, and differences between these two groups were analyzed (Figure 3.9). As shown, there is a significant difference (p = 0.022) between sNF-L levels of symptomatic (19.78 ± 30.78 pg/mL) and asymptomatic (6.04 ± 3.56 pg/mL) individuals, with higher levels on symptomatic ones. Taking this into account, we analyzed the differences between sNF-L levels of symptomatic patients and controls. Although near, there are still no significant differences between patients and controls sNF-L levels (p = 0.071).

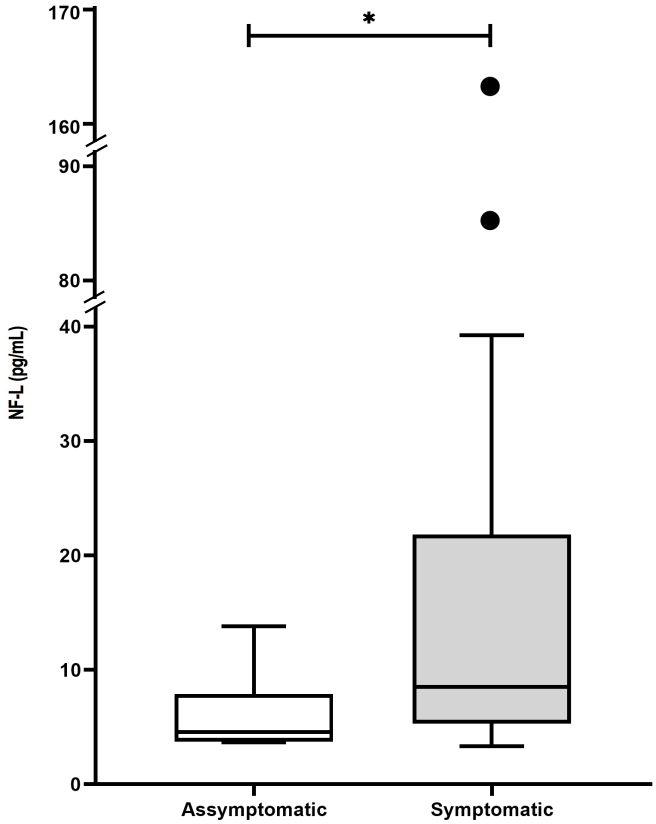

Figure 3.9. Neurofilament serum levels relation with disease onset. Comparison of sNF-L levels between asymptomatic *NOTCH3* mutation carriers (n = 6) and symptomatic ones (n = 31). Box plot showing the lower (Q1) quartile, median and the upper (Q3) quartile are depicted. Observations outside the 9-91 percentile range are plotted as outliers. (Mann-Whitney U test; *, $p < 0.050$)

3.2.4. sNF-L levels relation with WML load and cognitive impairment in CADASIL patients

In line with the results presented in the previous section (3.2.3), further analyzes were only performed in symptomatic individuals. Due to the small samples size symptomatic patients with available Fazekas scale grade were divided in patients with light/mild WML burden (grades 1 and 2; n = 8; mean values 19.28 $\pm$ 27.29 pg/mL) and patients with severe WML burden (grade 3; n = 14; mean values 25.80 $\pm$ 40.97 pg/mL), and statistical analysis was performed (Figure 3.10). Tests revealed no significant differences (p = 0.616) between groups.

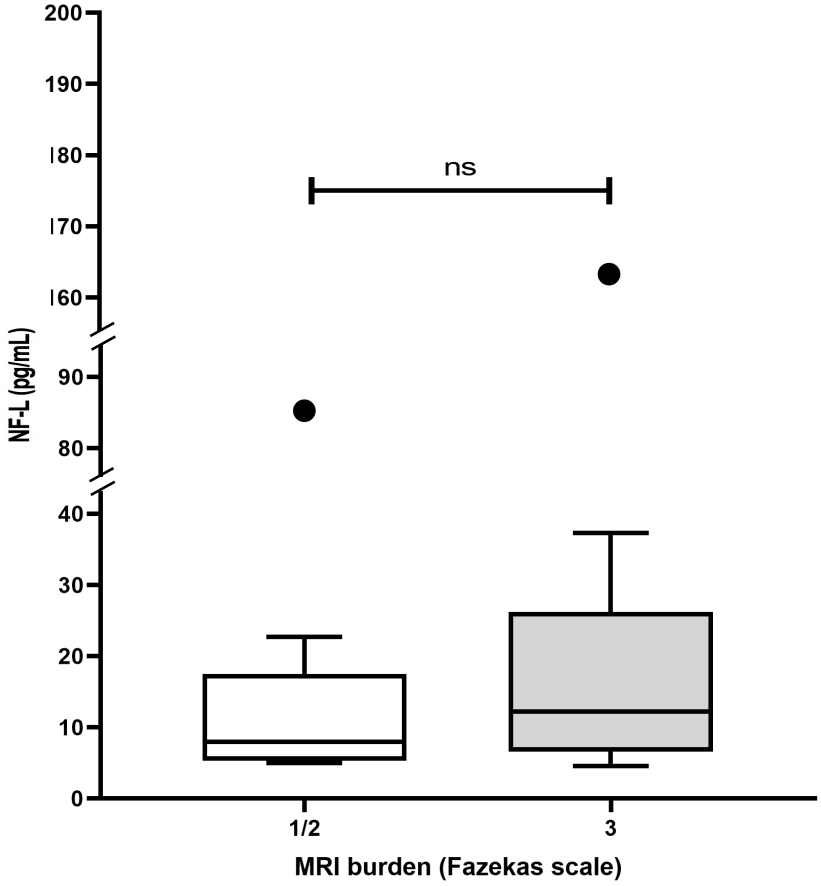

Figure 3.10. Neurofilament serum levels relation with WML load. Comparison between sNF-L levels of symptomatic CADASIL patients with light/mild WML burden (grade 1 and 2; n = 8) and severe WML burden (grade 3; n = 14) at Fazekas scale. Box plot showing the lower (Q1) quartile, median and the upper (Q3) quartile are depicted. Observations outside the 9-91 percentile range are plotted as outliers. (Mann-Whitney U test; ns, non significant)

On the other hand, statistical tests revealed a significant difference (p = 0.020) between sNF-L values of CADASIL symptomatic individuals with (n = 11; mean value 36.78 $\pm$ 45.17 pg/mL) and without cognitive impairment (n = 15; mean value 11.79 $\pm$ 11.20 pg/mL), with higher levels of sNF-L observed in patients' group with cognitive decline (Figure 3.11).

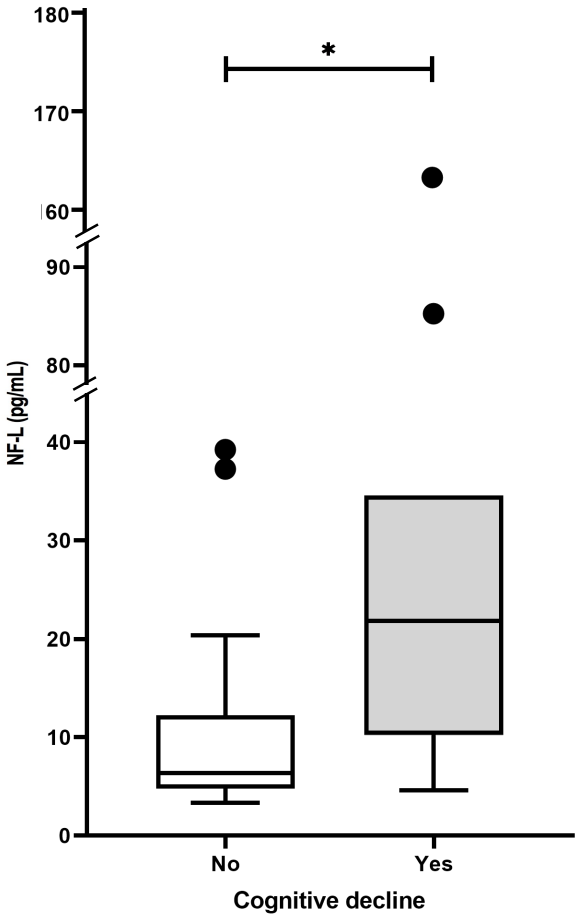

Figure 3.11. Neurofilament serum levels relation with cognitive impairment. Comparison of sNF-L levels between symptomatic CADASIL patients with (n = 11) and without cognitive impairment (n = 15). Box plot showing the lower (Q1) quartile, median and the upper (Q3) quartile are depicted. Observations outside the 9-91 percentile range are plotted as outliers. (Mann-Whitney U test; *, $p < 0.050$)

3.2.5. sNF-L levels relation with disease severity in CADASIL patients

In order to assess sNF-L levels value predicting disease severity we compared the sNF-L levels of symptomatic patients with a clinical phenotype considered as severe (n = 11; mean value 36.78 $\pm$ 47.38 pg/mL) and with a mild phenotype (n = 19; mean value 10.64 $\pm$ 10.90 pg/mL). Analysis of the differences between the two groups revealed significant higher values on severe cases (p = 0.006; Figure 3.12).

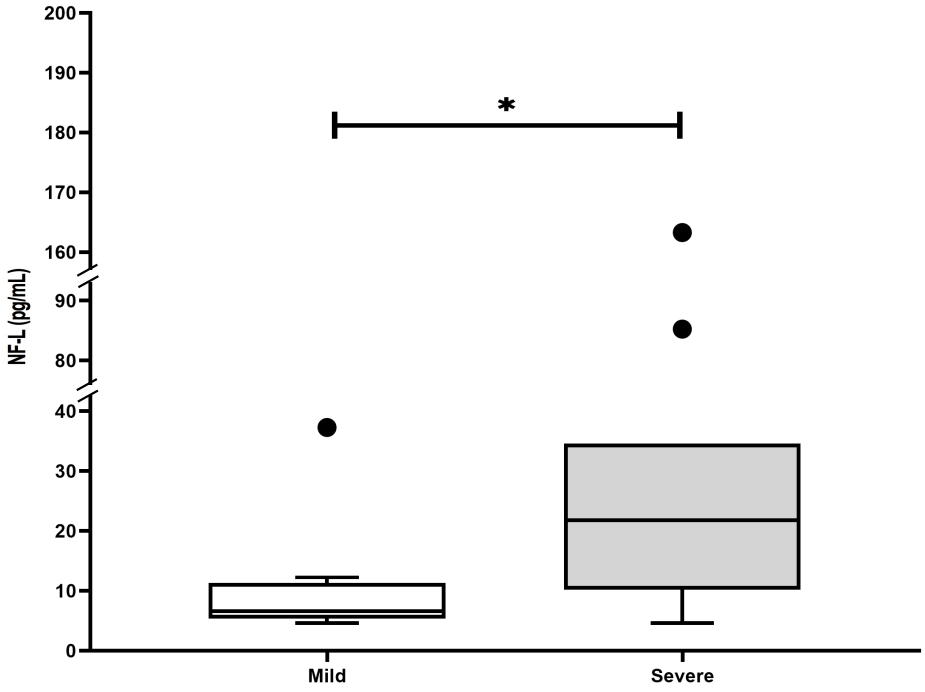

Figure 3.12. Neurofilament serum levels relation clinical severity. Comparison of sNF-L levels between symptomatic CADASIL patients with a mild phenotype (n = 19) and patients with severe phenotype (n = 11). Box plot showing the lower (Q1) quartile, median and the upper (Q3) quartile are depicted. Observations outside the 9-91 percentile range are plotted as outliers. (Mann-Whitney U test; *, $p < 0.050$)

In accordance with chapter 1, we also analyzed the differences between symptomatic CADASIL patients harboring a variant affecting EGFr 1-6 (n = 4; mean value 11.16 $\pm$ 4.72 pg/mL) vs EGFr 7-34 (n = 25; mean value 15.95 $\pm$ 18.12 pg/mL). However, no significant differences were identified (p = 0.784).

4. Discussion

Since the discovery of *NOTCH3* gene mutations as the underlaying cause of CADASIL in 1996, therapeutic strategies remained very limited with no disease modifying treatment found to date. Treatment of cSVD's patients usually focuses on symptomatic management, and as a consequence, preventive care regiments are sometimes inconsistence and some cases might be mistreated. Also, it is important to highlight that CADASIL is a progressive and fatal disease. Therefore, efforts aimed at understanding the pathogenesis of this inheritable disorder as well as an early and accurate diagnosis are crucial for a more efficient patient preventive care. Additionally, in current days, diagnosis can provide challenges, particularly with the increasing use of NGS techniques which allowed a substantial increase in sequencing content and thereby in variants identification. Thus, it has been crucial to develop tools or pipelines to determine whether found variants are disease-causing variants. In line with this, in this study, we characterized the genetic profile of a total of 53 *NOTCH3* mutation carriers that have been identified in our CADASIL patients' cohort and further assessed the value of sNF-L concentrations as a prognostic marker in CADASIL.

Herein, in a total of 53 *NOTCH3* mutation carriers (20 referred CADASIL index cases), genetic analysis revealed 12 different heterozygous mutations: eight were missense cysteine altering variants (p.R110C, p.R153C, p.G420C, p.R427C, p.C446F, p.R558C, p.R607C, p.C1099Y), three were missense cysteine sparing variants (p.S497L, p.S978R, p.V1952M) and one was a nonsense variant (p.R1893*), all previously reported in the literature. According to our results, the most affected exons in our cohort are exons 8, 11, 20, and 31, which differs from the reported previously in the literature, once the exons 4, 11, 18, and 19 are the ones described as the most affected in the Portuguese population (Guimarães et al., 2010). Moreover, the most common mutations found in our cohort were p.R558C, p.G420C, p.C1099Y, and p.R1893*, with some cases of homozygosity harboring the first variant. Curiously, these findings are not in line with the literature that describes the p.R544C as the most frequent homozygous mutation associated with CADASIL (Mizuno et al., 2020). It is also reported worldwide that the

majority of the mutations associated with CADASIL affects one of the 34 EGFr on the ECD of the *NOTCH3* receptor, which is in agreement to what we found in our cohort with 83,3% of the variants localized in this region. Additionally, in line with recent publications, the most identified variants affected the EGFr 7-34 (Rutten et al., 2016, 2019).

As mentioned in section 1.4.3, the vast majority of reported variants associated with CADASIL phenotype are missense cysteine altering variants that result in alterations of a cysteine encoding triplet and are reported to be associated with GOM deposits due to defective NECD accumulation in the vascular wall, probably consequence of a reduction of clearance efficiency. This accumulation is toxic for the VSMCs and in time, leads to cellular stress with formation of ROS which ultimately result in activation of apoptotic pathways and VSMCs death, constituting the disease-mechanism most commonly accepted. Accordingly, in this study, we have identified a total of eight different missense cysteine altering variants (p.R110C, p.R153C, p.G420C, p.R427C, p.C446F, p.R558C, p.R607C, p.C1099Y) in our CADASIL patients' cohort corresponding to the majority of found variants. Moreover, the *in silico* analysis corroborates with the prediction of an alteration on the structure and function of the receptor caused by these variants (Table 3.3) and all variant and disease databases classify them as disease-causing variants (Table 3.4).

Regarding missense cysteine sparing variants, as mentioned previously, literature presents contradictory cases in terms of clinical significance and, therefore, each case should be evaluated carefully (Rutten et al., 2014). Some studies found cysteine sparing variants associated with GOM and in those cases pathogenic mechanism behind seems to be similar with the one described above (Scheid et al., 2008). However, the molecular mechanism behind missense cysteine sparing variants that are not associated with GOM is still poorly understood. In this study, we have identified missense cysteine sparing variants p.S497L, p.S978R, and p.V1952M but unfortunately the evaluation of the skin biopsy of these individuals have not been performed. However, the first cysteine sparing variant concerning the substitution of the serine residue at position 497 to leucine in Notch3 receptor was first reported by Joutel et al. as a polymorphism once it is found in co-occurrence with other known pathogenic *NOTCH3* mutations (Joutel et al., 1997; Lim et al., 2015). In contrast, other studies indicate that this variant can result in significant

changes of Notch3 secondary structure (Schmidt et al., 2011; Vlachakis et al., 2014). Curiously, this controversy continues as recent studies point this variant as a polymorphism once more, while our analysis, integrating the results from disease databases, *in silico* studies and the clinical context of index case 11, seem to support a pathogenic role in the disease (Abramycheva et al., 2015; Maksemous et al., 2016). Unfortunately, segregation studies have not been possible to conducted yet. Furthermore, Ferreira et al. reported p.S978R variant as disease causing and later *in silico* studies, done by Vlachakis et al., shown that the same variant should lead to loss of Notch3 receptor ß-sheet structure (Ferreira et al., 2007; Vlachakis et al., 2014). Although our *in silico* analysis indicates that this variant should be consider benign, our segregation studies, disease databases, variant databases, and the clinical context of the index case 17, as well as the positive family history, supports a pathogenic nature of this variant. Finally, once more, results in disease databases, variant databases and *in silico* analysis for p.V1952M variant are contradictory. Despite the fact that this variant was found in CADASIL patients and in controls too, p.V1952M variant has been reported to be correlated to severe WML and ischemic stroke (Fernández et al., 2015; Freudenberger et al., 2012; Ross et al., 2013; Schmidt et al., 2011). Although most studies report this variant as a rare polymorphism, even more recent ones, in the present study, the clinical findings in index case 20 seem to support a possible pathogenic role of this variant in the disease (Sassi et al., 2018). Unfortunately, segregation studies have not yet been possible to conducted. To denote, this variant affects the ANKr 5 of the NICD which, as mentioned in section 1.4.2, after cleavage, is responsible for the activation of the *NOTCH3* downstream genes.

Interestingly, the nonsense variants are rarely found in *NOTCH3* gene and the ones reported thus far in literature are considered as hypomorphic mutations, not generating GOM deposits, and with a controversial role in CADASIL (Erro et al., 2014; Greisengger et al., 2020; Gripp et al., 2015; Moccia et al., 2014; Parmeggiani et al., 2000; Pippucci et al., 2015; Rutten et al., 2013; Yoon et al., 2015). Rutten et al. reported p.R103* variant in two brothers aged 50 and 55, with brain MRI and skin biopsy not suggestive of CADASIL (Rutten et al., 2013). However, more recent studies have identified the same variant in members of a family with CADASIL phenotype, even in the absence of GOM deposits (Erro et al., 2014; Moccia et al., 2014). Also, Moccia et al. suggested that the

two clinical unaffected siblings previously reported by Rutten et al. could still develop the disease because of the atypical age onset found associated on their proband, which manifested the first symptoms only at the age of 72. Yoon et al. found p.S567* variant in the *NOTCH3* gene of a patient with subcortical vascular cognitive impairment, although not directly associated with CADASIL (Yoon et al., 2015). Furthermore, some studies have shown other diseases to be associated with nonsense *NOTCH3* variants. Pippucci et al. identified the p.C966* *NOTCH3* variant in homozygosity in a patient previously diagnosed with Sneddon syndrome, a rare disorder that affects small and medium blood vessels and that is characterized by recurrent strokes and livedo reticularis (Parmeggiani et al., 2000; Pippucci et al. 2015). More recently, Greisengger et al. have reported two siblings with childhood-onset stroke also diagnosed with Sneddon syndrome, who harbored p.R735* *NOTCH3* variant in homozygosity too (Greisengger et al., 2020). Taking all into account, authors suggested that bi-allelic loss-of-function mutations in *NOTCH3* might also cause familial Sneddon syndrome. Interestingly, Gripp et al. identified nonsense *NOTCH3* variants p.K2083*, p.Y2221* and p.Y2244*, all affecting the PEST domain (exon 33) of Notch3 receptor, a region found in many short-lived proteins and that acts as a signal peptide for rapid protein degradation, to be associated with lateral meningocele syndrome, also known as Lehman syndrome, which is a rare skeletal disorder with facial anomalies and meningocele-related neurologic dysfunction (Gripp et al., 2015). Moreover, authors suggest a dominant gain-of-function effect due to the variants' location rather than typical haploinsufficiency resulting from nonsense mediated decay usually associated with nonsense *NOTCH3* variants. Curiously, in this study, we have identified an index case harboring the p.R1893* nonsense variant which has been previously reported in the literature in the germline of a patient diagnosed with colorectal cancer (CCR) and in a patient with metastatic CCR, although it has never been associated with CADASIL phenotype (Ross et al., 2018; Smith et al., 2013). This variant generates a premature stop codon predicted to cause loss of normal protein function either through protein truncation or nonsense mediated mRNA decay. In the present study, variant and disease databases analysis support a damaging effect of this variant (Table 3.4). Additionally, segregation studies, family history and clinical findings also support a variant pathogenic nature. To denote, p.R1893* nonsense variant affects one of the ANKr encoding sequences and thereby is predicted to affect

the NICD function. Also, this variant results in the absence of the PEST domain, probably impairing NICD degradation in the mutant VSMCs leading, eventually, to a toxic accumulation of NICD in the cytoplasm which result in cellular stress with formation of ROS, ultimately leading to activation of apoptotic pathways and cellular death. Further screening of the coding region of known cSVD related genes also revealed a total of 34 common variants, all reported in literature and databases as polymorphisms.

Clinical records of the 20 referred index cases (mean age onset of 48.3 years) revealed that the most prevalent clinical features identified in our patients were migraine and cerebrovascular events as stroke or TIA, up to than 65% of index cases as expected (Table 3.6). In accordance with literature, the mean age at first stroke of our patients was 50.9 years (Chabriat et al., 2009). Curiously, psychiatric disorders, which Valenti et al. reported to affect up to 41% of CADASIL patients, were found in around 40% of our index cases, with depression being the most frequent reported mood disturbance, as expected (Valenti et al., 2008). Moreover, although studies point cognitive decline as the second most frequent manifestation of CADASIL, our results show only 45% of patients presenting cognitive impairment (Chabriat and Bousser, 2007). In accordance with the literature, the vast majority of index cases presented a high WML load on brain MRI, illustrated by a confluent and diffuse lesion pattern (Grade 3 on Fazekas scale) on MRI (Table 3.7). To denote that some uncommon features were also identified as gait disturbance in index case 6, anterior ischemic optic neuropathy in index case 1, and seizures in index case 14.

However, as described in section 3.1.5, a large phenotypic variability is observed in CADASIL, and thereby we could identify some index cases with a more severe clinical presentation like index cases 1-6, 10, 13, 14, 18, and 20. Accordingly to Rutten et al., CADASIL patients carrying variants affecting EGFr 1-6 should present a more severe phenotype (Rutten et al., 2016, 2019). Curiously, despite all identified index cases with a pathogenic variant affecting EGFr 1-6 were considered as presenting a severe phenotype, our results show many other severe cases with harboring a pathogenic variant affecting EGFr 7-34. Further molecular analysis of dementia related genes in index cases 6 and 20 revealed the co-occurrence of previously identified *NOTCH3* variant and a frameshift variant (p.S275Ffs*17) in exon 6 of *SQSTM1* gene in index case 6. When investigating this case, we found a sibling who shared the aggressive phenotype

identified in the index case, characterized by early-onset stroke, gait disturbances and/or dementia, severe emotional dysregulation, dysexecutive syndrome together with severe white matter burden on brain MRI. Thereby, index case 6 brother was also tested and was found to carry the same pathogenic variants in heterozygosity too.

The p.S275Ffs*17 frameshift variant is located within the first PEST domain of the *SQSTM1* gene, which acts as a signal peptide for rapid protein degradation as mentioned before (Geetha et al., 2002). Also, it predicts to create a premature stop codon and to cause loss of normal protein function either through protein truncation or nonsense mediated mRNA decay. Recently, Zúñiga-Ramírez et al. reported this *SQSTM1* pathogenic variant in homozygosity in two siblings from a Jordan consanguineous family with dystonia, ataxia and gaze palsy and mild cognitive symptoms (Zúñiga-Ramírez et al., 2019). It is known that *SQSTM1* (Sequestosome 1) gene encodes the multifunctional protein p62 that contains several domains, including the ubiquitin-binding domain (UBA), that targets misfolded, aggregates and/or ubiquitinated proteins for degradation via autophagy (Bjørkøy et al., 2006; Hewitt et al., 2017; Pankiv et al., 2007; Wooten et al., 2008), and/or the ubiquitin-proteasome system (Babu et al., 2005; Seibenhener et al., 2004). And, although mutations in this gene were initially identified as a cause of Paget disease of bone (PDB) (Laurin et al., 2002), they were also reported in frontotemporal lobar degeneration (FTLD) and ALS (Le Ber et al., 2013; Rubino et al., 2012) as well as other neurodegenerative diseases (Kuusisto et al., 2002; Ma et al., 2019; Nakaso et al., 2004). Curiously, despite this being the first CADASIL family reported with double heterozygous pathogenic variants in both *NOTCH3* and *SQSTM1* genes, the functional interaction of these two genes encoded proteins has been already demonstrated in CADASIL (Hanemaaijer et al., 2018; Hase et al., 2018). Growing evidence suggests that autophagy is enhanced following cerebral ischemia and is stimulated in response to *in vivo* or *in vitro* instigated energy deficits, hypoxia, ER stress and oxidative stress (Rami et al., 2008; Xu et al., 2012). Three common studied proteins involved in autophagy are LC3 (microtubule associated protein 1, light chain 3), Beclin-1 and p62. This later protein promotes autophagy degradation by directly binding to LC3 through a LC3 interacting region (LIR) (Pankiv et al., 2007). Combined with its ability to bind ubiquitinated proteins at the UBA domain, p62 serves as an autophagy receptor in the clearance of unwanted protein molecules and aggregates (Ma et al., 2019; Puissant

et al., 2012). In CADASIL patients, one of the major pathological hallmarks is the loss of VSMCs in arteries/arterioles and it has been demonstrated that an autophagy dysfunction or an insufficient autophagy in stress conditions is the cause of astrocytes apoptosis in the deep white matter of CADASIL patients (Hase et al., 2018). Furthermore, an accumulation of autophagy markers including, LC3, p62 and Caspase-3 in GFAP-positive clasmatodendritic cells has been observed, arguing an autophagy blockade, which has been implicated in a range of neurological pathologies and could result in the loss of cell viability (Menzies et al., 2017). Previous studies have shown that mutant Notch3 is more prone to form aggregates than wild type and that these aggregates are resistant to degradation, ultimately impairing cell proliferation (Takahashi et al., 2010). Additionally, insufficient autophagy has been linked to lower proliferation rate of VSMCs (Panahi et al., 2018). Indeed, studies using cerebral VSMCs from CADASIL patients carrying p.R133C mutation have shown a dysfunction in the autophagy-lysosomal pathway, as a consequence of accumulation of intracellular mutated Notch3 (Hanemaaijer et al., 2018). Taken together, it seems that there is a functional interaction between p62 and Notch3 receptor and that the co-occurrence of these two pathogenic variants might affect the functional interaction of those two proteins.

Furthermore, no more pathogenic variants were found in dementia related genes of any study case. Molecular analysis also revealed a total of 25 common variants in dementia related genes, all predicted to be benign in databases and literature.

At the assessment of the potential value of sNF-L concentrations in CADASIL prognosis, which is generally considered a biomarker of axonal damage, sNF-L values showed no significant differences between *NOTCH3* mutation carriers and controls, which is not in line with recent publications (Duering et al., 2018; Gravesteijn et al., 2019). Studies show higher levels of sNF-L in both sporadic cSVD patients and CADASIL patients, compared to the levels of a control group. Several hypothesis can explain the apparent absence of differences between these two groups: 1) the wide range of sNF-L values that was obtained in our *NOTCH3* mutation carriers (from 3.33 to 163.28 pg/mL) indicates high inter-individual variability and a spread-out distribution, thereby this group was extremely heterogeneous, making it harder to reach statistical significant difference; 2) the high variability of disease stages among the *NOTCH3* mutation carriers group; 3) sample size might not be big enough to reach statistical significance. Therefore,

although no statistically significant differences between sNF-L levels were found, we cannot exclude that this marker might have a role in predicting disease progression. To denote that, as mention in chapter 1, previous studies in CADASIL patients have associated high sNF-L levels with a decrease in survival, higher MRI burden, and a decline in cognitive and executive functions (Duering et al., 2018; Gravesteijn et al., 2019).

Studies have shown that no gender effect on sNF-L levels has been found and that a positive association between age and sNF-L levels has been well established (Khalil et al., 2020). Accordingly, we found no gender effect on sNF-L levels of both *NOTCH3* mutation carriers and controls (Figure 3.7). Additionally, our results showed correlation of sNF-L levels with age in both groups, although stronger in the control one (Figure 3.8). Thus, there was a need to perform age-adjusted analyses by cohort stratification, adding another layer of complexity to these studies.

Due to the high variability of sNF-L content in the *NOTCH3* mutation carriers, we hypothesize that this variability might correlate with disease onset. Therefore, we divided the group as symptomatic and asymptomatic individuals and statistical analysis revealed a significantly higher sNF-L value ($p = 0.022$) in symptomatic patients, similar to previous observations in FTD patients' vs presymptomatic carriers (Meeter et al., 2016). These findings suggest that sNF-L levels might be a good marker to predict disease onset.

An extremely important parameter evaluated in CADASIL patients relates to the assessment of WML burden through brain MRI scans. In the present study, lesion severity was assessed by the Fazekas scale (Fazekas et al., 1987), a highly accepted method used even in recent publications (Dobrynina et al., 2020; Ferguson et al., 2018; Marek et al., 2019). However, our results showed no significant difference between the mean values of sNF-L levels of patients with a light/mild WML burden and patients with a severe WML burden. However, it is important to highlight the small size of the patients presenting light/mild WML burden ($n = 8$) that might affect the statistical power of the applied test.

Moreover, studies have shown a correlation between cognitive impairment and sNF-L levels. Accordingly, we divided our symptomatic CADASIL patients in two groups, patients with cognitive impairment and normal ones, and our analysis revealed significant difference between the sNF-L levels of both groups, with higher levels in

patients with cognitive impairment which is in line to the reported in the literature (Duering et al., 2018; Gravesteijn et al., 2019).

In order to assess sNF-L levels value to predict disease severity, we compared the sNF-L levels of patients with a severe phenotype and patients with a mild phenotype, and results showed a significant difference ($p = 0.006$) between the two groups, with higher levels on severe cases. Therefore, sNF-L levels might represent a disease severity marker.

Curiously, although Rutten et al. suggested that patients harboring EGFr 1-6 affecting variants were associated with a more severe phenotype, when comparing mean sNF-L levels of symptomatic patients harboring a variant affecting EGFr 1-6 vs EGFr 7-34, no significant differences ($p = 0.784$) were observed (Rutten et al., 2016, 2019). However, the small size of EGFr 1-6 affected patients might lower the statistical power of these results.

5. Conclusion and Future Perspectives

Taken together, in the matter of the genetic and clinical characterization of our CADASIL patients' cohort, our results suggest that sequencing of the entire coding region of the *NOTCH3* gene is relevant for an early and accurate diagnosis of CADASIL patients. In addition, it unveiled the mutation spectrum of the affected individuals of center region of Portugal. Furthermore, the identification of the co-occurrence of *NOTCH3* and *SQSTM1* pathogenic variants in two siblings with a more aggressive CADASIL phenotype, indicates that the expansion of genetic analysis to other genes associated with patients' clinical phenotype should take place, using NGS-customized gene panel assay, towards a better genetic counseling and patient management. It is also important to highlight that our study enlarged the pathogenic *NOTCH3* mutation spectrum, with the identification of the p.R1893* nonsense pathogenic variant. To date, the exact mechanisms underlying CADASIL are far from being understood and evidences suggest that multiple pathogenic mechanisms might underlie the disease. Accordingly, our findings contribute to the debate of alternative pathogenic mechanisms behind CADASIL that are not related with the formation of toxic GOM deposits, as the case of cysteine sparing variants or the nonsense variant that we have identified in this study. Furthermore, we hypothesize that variants impairing NICD interaction with RBP-Jk repressor protein or the co-activator MAML through alteration of ANKr or the RAM domain encoding sequences might represent one alternative mechanism of the disease. The lack of interaction represses transcription and expression of Notch3 effector genes, ultimately with cellular homeostasis and VSMCs proliferation being affected, resulting in activation of apoptotic pathways and cell death. Moreover, we also hypothesize that variants that lead to the absence or affect the PEST domain, might affect the NICD degradation system, leading to a cytoplasmatic accumulation of altered NICD, which result in cellular stress with formation of ROS and once more ultimately resulting in activation of apoptotic pathways and VSMCs death. However, the biological mechanisms hindering mutant proteins degradation are still poorly understood and

therefore, studies to unravel those mechanisms are relevant. Regarding the evaluation of the potential prognostic value of sNF-L values in CADASIL patients, we found a correlation between high levels of sNF-L and disease onset, patients' cognitive impairment and disease severity. We believe that, the lack of significance obtained with all the other evaluated parameters might result from the progressive development of clinical features, characteristic of CADASIL. Therefore, future studies with more CADASIL patients might be helpful to have a better notion of the true prognostic value of this marker. Nevertheless, results also suggest that sNF-L levels might be a significant marker for disease onset, which may also indicate a potential ability of sNF-L levels to monitor therapeutic efficiency in CADASIL patients. Results suggest that this marker may be a significant indicator of disease severity too. To denote that recent studies have shown correlation of other biomarkers, such as TNF-α and TGF-β1, with WML load and cognitive impairment in cSVD patients (Dobrynina et al., 2020). In line with this, it might also be interesting in the future to evaluate the prognostic value of these markers in our cohort of CADASIL patients.

Bibliography

ABOU AL-SHAAR, H., QADI, N., Al-Hamed, M. H., MEYER, B. F., BOHLEGA, S. (2016). Phenotypic comparison of individuals with homozygous or heterozygous mutation of NOTCH3 in a large CADASIL family. *J Neurol Sci.* 367, 239-243. doi: 10.1016/j.jns.2016.05.061

ABRAMYCHEVA, N., STEPANOVA, M., KALASHNIKOVA, L., ZAKHAROVA, M., MAXIMOVA, M., TANASHYAN, M., […], ILLARIOSHKIN, S. (2015). New mutations in the Notch3 gene in patients with cerebral autosomal dominant arteriopathy with subcortical infarcts and leucoencephalopathy (CADASIL). *J Neurol Sci*. 349(1-2), 196-201. doi: 10.1016/j.jns.2015.01.018

ADZHUBEI, I. A., SCHMIDT, S., PESHKIN, L., RAMENSKY, V. E., GERASIMOVA, A., BORK, P., […], SUNYAEV, S. R. (2010). A method and server for predicting damaging missense mutations. *Nat Methods*. 7, 248-249. doi: 10.1038/nmeth0410-248

ANDRE, C. (2010). CADASIL: pathogenesis, clinical and radiological findings and treatment. *Arq Neuropsiquiatr*. 68(2), 287-299. doi: 10.1590/s0004-242x2010000200026

BABU, J. R., GEETHA, T., WOOTEN, M. W. (2005). Sequestosome 1/p62 shuttles polyubiquitinated tau for proteasomal degradation. *J Neurochem*. 94(1), 192-203. doi: 10.1111/j.1471-4159.2005.03181.x

BELLAVIA, D., CHECQUOLO, S., CAMPESE, A. F., FELLI, M. P., GULINO, A., SCREPANTI, I. (2008). Notch3: from subtle structural differences to functional diversity. *Oncogene*. 27(38), 5092-5098. doi: 10.1038/onc.2008.230

BJØRKØY, G., LAMARK, T., JOHANSEN, T. (2006). p62/SQSTM1: a missing link between protein aggregates and the autophagy machinery. *Autophagy.* 2(2), 138-139. doi: 10.4161/auto.2.2.2405

BUGIANI, M., KEVELAM, S., BAKELS, H. S., WAISFISZ, Q., CEUTERICK-DE GROOTE, C., NIESSEN, H. W. M., [...] VAN DER KNAAP, M. S. (2016). Cathepsin A–related arteriopathy with strokes and leukoencephalopathy (CARASAL). *American Academy of Neurology*, 87(17), 1777-1786. doi: 10.1212/WNL.0000000000003251

CHABRIAT, H., BOUSSER, M. G. (2007). Neuropsychiatric manifestations in CADASIL. *Dialogues Clin Neurosci*. 9(2), 199-208.

CHABRIAT, H., JOUTEL, A., DICHGANS, M., TOURNIER-LASSERVE, E., BOUSSER, M. G. (2009). Cadasil. *Lancet Neurol*. 8(7), 643-653. doi: 10.1016/S1474-4422(09)70127-9

CHABRIAT, H., LEVY, C., TAILLIA, H., IBA-ZIZEN, M. T., VAHEDI, K., JOUTEL, A., […], BOUSSER, M. G. (1998). Patterns of MRI lesions in CADASIL. *Neurology*. 51(2), 452-457. doi: 10.1212/wnl.51.2.452

CHABRIAT, H., PAPPATA, S., POUPON, C., CLARK, C. A., VAHEDI, K., POUPON., F, […], BOUSSER, M. G. (1999). Clinical severity in CADASIL related to ultrastructural damage in white matter: in vivo study with diffusion tensor MRI. *Stroke*. 30(12), 2637-2643. doi: 10.1161/01.str.30.12.2637

CHABRIAT, H., VAHEDI, K., IBA-ZIZEN, M. T., JOUTEL, A., NIBBIO, A., NAGY, T. G., […], LYON-CAEN, O. (1995). Clinical spectrum of CADASIL: a study of 7 families. Cerebral autosomal dominant arteriopathy with subcortical infarcts and leukoencephalopathy. *Lancet*. 346(8980), 934-939. doi: 10.1016/s0140-6736(95)91557-5

CIPOLLA, M. J. (2009). *The Cerebral Circulation*. Chapter 2, Anatomy and Ultrastructure. Morgan & Claypool Life Sciences. San Rafael (CA).

COUPLAND, K., LENDAHL, U., KARLSTRÖM, H. (2018). Role of NOTCH3 Mutations in the Cerebral Small Vessel Disease Cerebral Autosomal Dominant Arteriopathy With Subcortical Infarcts and Leukoencephalopathy. *Stroke*. 49(11), 2793-2800. doi: 10.1161/STROKEAHA.118.021560

CUTTING, G. R., KAZAKIAN, H. H., ANTONARAKIS, S. E., KILLEN, P. D., YAMADA, Y., FRANCOMANO, C. A. (1988). Macrorestriction Mapping of COL4A1 and COL4A2 Collagen Genes on Human Chromosome 13q34. *Genomics*. 3(3), 256-263. doi: 10.1016/0888-7543(88)90086-9

DI DONATO, I., BIANCHI, S., DE STEFANO, N., DICHGANS, M., DOTTI, M. T., DUERING, M., […], FEDERICO, A. (2017). Cerebral Autosomal Dominant Arteriopathy with Subcortical Infarcts and Leukoencephalopathy (CADASIL) as a model of small vessel disease: update on clinical, diagnostic, and management aspects. *BMC Med.* 15(41). https://doi.org/10.1186/s12916-017-0778-8

DICHGANS, M. (2009). Cognition in CADASIL. *Stroke*. 40(3), S45-S47. doi: 10.1161/STROKEAHA.108.534412

DICHGANS, M., MAYER, M., UTTNER, I., BRÜNING, R., MÜLLER-HÖCKER, J., RUNGGER, G., […], GASSER, T. (1998). The phenotypic spectrum of CADASIL: clinical findings in 102 cases. *Ann Neurol*. 44(5), 731-739. doi: 10.1002/ana.410440506

DOBRYNINA, L. A., ZABITOVE, M. R., SHABALINA, A. A., KREMNEVA, E. I., AKHMETZYANOV, B. M., GADZHIEVA, Z. S., [...], KROTENKOVA, M. V. (2020). MRI Types of Cerebral Small Vessel Disease and Circulating Markers of Vascular Wall Damage. *Diagnostics.* 10, 354. doi:10.3390/diagnostics10060354

DONG, H., DING, H., YOUNG, K., BLAIVAS, M., CHRISTENSEN, P. J., WANG, M. M. (2013). Advanced intimal hyperplasia without luminal narrowing of leptomeningeal arteries in CADASIL. *Stroke*. 44(5), 1456-1458. doi: 10.1161/STROKEAHA.111.000721

DUERING, M., KARPINSKA, A., ROSNER, S., HOPFNER, F., ZECHMEISTER, M., PETERS, N., […], OPHERK, C. (2011). Co-aggregate formation of CADASIL-mutant NOTCH3: a single-particle analysis. *Hum Mol Genet*. 20(16), 3256-3265. doi: 10.1093/hmg/ddr237

DUNN, P. J., MAKSEMOUS, N., SMITH, R. A., SUTHERLAND, H. G., HAUPT, L. M., GRIFFITHS, L. R. (2020). Investigating diagnostic sequencing techniques for CADASIL diagnosis. *Hum Genomics*. 14(2). doi: 10.1186/s40246-019-0255-x

ENG, C. M., DESNICK, R. J. (1994). Molecular Basis of Fabry Disease: Mutations and Polymorphisms in the Human α-Galactosidase A Gene. *Human Mutation*. 3(2), 103-111. doi: 10.1002/humu.1380030204

ERRO, R., LEES, A. J., MOCCIA, M., PICILLO, M., PENCO, S., MOSCA, L., […], BARONE, P., (2014). Progressive parkinsonism, balance difficulties, and supranuclear gaze palsy. *JAMA Neurol*. 71(1), 104-107. doi: 10.1001/jamaneurol.2013.5149

ESCARY, J. L., CÉCILLON, M., MACIAZEK, J., LATHROP, M., TOURNIER-LASSERVE, E., JOUTEL, A. (2000). Evaluation of DHPLC analysis in mutational scanning of Notch3, a gene with a high G-C content. *Hum Mutat.* 16(6), 518–526. doi: 10.1002/1098-1004(200012)16:63. 0.CO;2-Q

FAZEKAS, F., CHAWLUK, J. B., ALAVI, A., HURTIG, H. I., ZIMMERMAN, R. A. (1987). MR Signal Abnormalities at 1.5 T in Alzheimer's Dementia and Normal Aging deficiency. *American Journal of Roentgenology*. 149(2), 351–356. doi: 10.2214/ajr.149.2.351

FERGUSON, K. J., CVORO, V., MACLULLICH, A., SHENKIN, S. D., SANDERCOCK, P., SAKKA, E., WARDLAW, J. M. (2018). Visual Rating Scales of White Matter Hyperintensities and Atrophy: Comparison of Computed Tomography and Magnetic Resonance Imaging. *J Stroke Cerebrovasc Dis*. 27(7), 1815–1821. doi: 10.1016/j.jstrokecerebrovasdis.2018.02.028

FERNÁNDEZ, A., GÓMEZ, J., ALONSO, B., IGLESIAS, S., COTO, E. (2015). A Next-Generation Sequencing of the NOTCH3 and HTRA1 Genes in CADASIL Patients. *J Mol Neurosci*. 56(3), 613-616. doi: 10.1007/s12031-015-0560-3

FERREIRA, S., FONTOURA, P., GUERREIRO, R., OLIVEIRA, J. P. (2007). Novel human pathological mutations. Gene symbol: NOTCH3. Disease: cerebral autosomal dominant arteriopathy with subcortical infarcts and leucoencephalopathy (CADASIL). *Hum Genet*. 121(5),649-650.

FREUDENBERGER, P., SCHMIDT, R., SCHMIDT, H. (2012). Genetics of age-related white matter lesions from linkage to genome wide association studies. *J Neurol Sci.* 322(1-2), 82-86. doi: 10.1016/j.jns.2012.06.016

GATTRINGER, T., PINTER, D., ENZINGER C., SEIFERT-HELD, T., KNEIHSL, M., FANDLER, S., […], KHALIL, M. (2017). Serum neurofilament light is sensitive to active cerebral small vessel disease. *Neurology*. 89(20), 2108–2114. doi: 10.1212/HNL.0000000000004645

GEETHA, T., WOOTEN, M. W. (2002). Structure and functional properties of the ubiquitin binding protein p62. *FEBS Lett*. 512(1-3), 19-24. doi: 10.1016/s0014-5793(02)02286-x

GIAU, V. V., BAGYINSZKY, E., YOUN, Y. C., AN, S. S. A., KIM, S. Y. (2019). Genetic Factors of Cerebral Small Vessel Disease and Their Potential Clinical Outcome. *Int J Mol Sci*. 20(17), 4298. doi: 10.3390/ijms20174298

GRAND, M. G., KAINE, J., FULLING, K., ATKINSON, J., DOWTON, S. B., FARBER, M., [...] RICE, K. (1988) Cerebroretinal Vasculopathy: A New Hereditary Syndrome. *Ophthalmology*. 95(5), 649-659. doi: 10.1016/s0161-6420(88)33131-3

GRAVESTEIJN, G., RUTTEN, J. W., VERBERK, I. M. W., BÖHRINGER, S., LIEM, M. K., VAN DER GROND, J., […], LESNIK OBERSTEIN, S. A. J. (2018). Serum Neurofilament light correlates with CADASIL disease severity and survival. *Ann Clin Transl Neurol*. 6(1), 46-56. doi: 10.1002/acn3.678

GREISENEGGER, E. K., LLUFRIU, S., CHAMORRO, A., CERVERA, A., JIMENEZ-ESCRIG, A., RAPPERSBERGER, K., […], ZIMPRICH, A. (2020). A NOTCH3 homozygous nonsense mutation in familial Sneddon syndrome with pediatric stroke. *J Neurol*. doi: 10.1007/s00415-020-10081-5

GRIPP, K. W., ROBBINS, K. M., SOBREIRA, N. L., WITMER, P. D., BIRD, L. M., AVELA, K., […], SOL-CHURCH, K. (2015). Truncating mutations in the last exon of NOTCH3 cause lateral meningocele syndrome. *Am J Med Genet A*. 167A(2), 271-281. doi: 10.1002/ajmg.a.36863

GUIMARÃES, J., AZEVEDO, E. (2010). Causas Genéticas de Acidente Vascular Cerebral Isquémico. *ArquiMed*. 24(1), 23-28

HACK, R., RUTTEN, J., LESNIK OBERSTEIN, S. A. J. (2019). CADASIL. *GeneReviews*.

HANEMAAIJER, E. S., PANAHI, M., SWADDIWUDHIPONG, N., TIKKA, S., WINBLAD, B., VIITANEN, M., […], BEHBAHANI, H. (2018). Autophagy-lysosomal defect in human CADASIL vascular smooth muscle cells. *Eur J Cell Biol*. 97(8), 557-567. doi: 10.1016/j.ejcb.2018.10.001

HARA, K., SHIGA, A., FUKUTAKE, T., NOZAKI, H., MIYASHITA, A., YOKOSEKI, A., [...], OSAMU-ONODERA, M. D. (2009). Association of HTRA1 mutations and familial ischemic cerebral small-vessel disease. *The New England Journal of Medicine*. 360, 1729-1739. doi: 10.1056/NEJMoa0801560

HASE, Y., CHEN, A., BATES, L. L., CRAGGS, L. J. L., YAMAMOTO, Y., GEMMELL, E., […], KALARIA, R. N. (2018). Severe white matter astrocytopathy in CADASIL. *Brain Pathol*. 28(6), 832-843. doi: 10.1111/bpa.12621

HEWAMADDUMA, C., HARKNESS, K. A., CHADHA, D. K., DALTON, A., MCDERMOTT, C. J. (2010). POG09 – CADASIL in a mother and son due to a novel mutation of the *NOTCH-3* gene *Journal of Neurology, Neurosurgery & Psychiatry*. 81(11), e50. doi: 10.1136/jnnp.2010.226340.131

HEWITT, G., KOROLCHUK, V. I. (2017). Repair, Reuse, Recycle: The Expanding Role of Autophagy in Genome Maintenance. *Trends Cell Biol*. 27(5), 340-351. doi: 10.1016/j.tcb.2016.11.011

IHALAINEN, S., SOLIYMANI, R., IIVANAINEN, E., Mykkänen, K., Sainio, A., Pöyhönen, M., […], Baumann, M. (2007). Proteome analysis of cultivated vascular smooth muscle cells from a CADASIL patient. *Mol Med*. 13(5-6), 305-314. doi: 10.2119/2016-00069.Ihalainen

JEN, J., COHEN, A. H., YUE, Q., STOUT, J. T., VINTERS, H. V., NELSON, S., BALOH, R. W. (1997). Hereditary endotheliopathy with retinopathy, nephropathy, and stroke (HERNS). *Neurology*. 49(5), 1322-1330. doi:10.1212/WNL.49. 5.1322

JONSSON, M., ZETTERBERG, H., VAN STRAATEN, E., LIND, K., SYVERSEN, A., EDMAN, K., […], WALLIN, A. (2010). Cerebrospinal fluid biomarkers of white matter lesions - cross-sectional results from the LADIS study. *European Journal of Neurology*. 17(3), 377-382. doi: 10.1111/j.1468-1331.2009.02808.x

JOUTEL, A. (2010). Pathogenesis of CADASIL. *BioEssays*. 33(1), 73–80. doi:10.1002/bies.201000093

JOUTEL, A., ANDREUX, F., GAULIS, S., DOMENGA, V., CECILLON, M., BATTAIL, N., […], TOURNIER-LASSERVE, E. (2000). The ectodomain of the Notch3 receptor accumulates within the

cerebrovasculature of CADASIL patients. *J Clin Invest.* 105(5), 597-605. doi: 10.1172/JCI8047

JOUTEL, A., CORPECHOT, C., DUCROS, A., VAHEDI, K., CHABRIAT, H., MOUTON, P., […], TOURNIER-LASSERVE, E. (1996). Notch3 mutations in CADASIL, a hereditary adult-onset condition causing stroke and dementia. *Nature*. 383(6602), 707-710. doi: 10.1038/383707a0

JOUTEL, A., FAVROLE, P., LABAUGE, P., CHABRIAT, H., LESCOAT, C., ANDREUX, F., […], TOURNIER-LASSERVE, E. (2001). Skin biopsy immunostaining with a Notch3 monoclonal antibody for CADASIL diagnosis. *Lancet.* 358(9298), 2049-2051. doi:10.1016/S0140-6736(01)07142-2

JOUTEL, A., MONET, M., DOMENGA, V., RIANT, F., TOURNIER-LASSERVE, E. (2004). Pathogenic mutations associated with cerebral autosomal dominant arteriopathy with subcortical infarcts and leukoencephalopathy differently affect Jagged1 binding and Notch3 activity via the RBP/JK signaling Pathway. *Am J Hum Genet*. 74(2), 338-347. doi: 10.1086/381506

JOUTEL, A., MONET-LEPRÊTRE, M., GOSELE, C., BARON-MENGUY, C., HAMMES, A., SCHMIDT, S., […], HUBNER, N. (2010). Cerebrovascular dysfunction and microcirculation rarefaction precede white matter lesions in a mouse genetic model of cerebral ischemic small vessel disease. *J Clin Invest*. 120(2), 433-445. doi: 10.1172/JCI39733

JOUTEL, A., VAHEDI, K., CORPECHOT, C., TROESCH, A., CHABRIAT, H., VAYSSIÈRE, C., […], TOURNIER-LASSERVE, E. (1997). Strong clustering and stereotyped nature of Notch3 mutations in CADASIL patients. *Lancet*. 350(9090), 1511-1515. doi: 10.1016/S0140-6736(97)08083-5

KALIMO, H., VIITANEN, M., AMBERLA, K., JUVONEN, V., MARTTILA, R., PÖYHÖNEN, M., […], WINBLAD, B. (1999). CADASIL: hereditary disease of arteries causing brain infarcts and dementia. *Neuropathol Appl Neurobiol*. 25(4), 257-265. doi: 10.1046/j.1365-2990.1999.00198.x

KHALIL, M., PIRPAMER, L., HOFER, E., VOORTMAN, M. M., BARRO, C., LEPPERT, D., […], KUHLE, J. (2020). Serum neurofilament light levels in normal aging and their association with morphologic brain changes. *Nat Commun*. 11(1), 812. doi: 10.1038/s41467-020-14612-6

KHOSHNOODI, J., PEDCHENKO, V., HUDSON, B. (2016). Mammalian Collagen IV. *Microsc Res Tech*. 71(5), 357-370. doi:10.1002/jemt.20564

KUMAR, P., HENIKOFF, S., NG, P. C. (2009). Predicting the effects of coding non-synonymous variants on protein function using the SIFT algorithm. *Nat Protoc*. 4(7), 1073-1081. doi: 10.1038/nprot.2009.86

KUO, D. S., LABELLE-DUMAIS, C., GOULD, D. B. (2012). COL4A1 and COL4A2 mutations and disease: insights into pathogenic mechanisms and potential therapeutic targets. *Human Molecular Genetics*. 21(1), 97-110. doi:10.1093/hmg/dds346

KUUSISTO, E., SALMINEN, A., ALAFUZOFF, I. (2002). Early accumulation of p62 in neurofibrillary tangles in Alzheimer's disease: possible role in tangle formation. *Neuropathol Appl Neurobiol*. 28(3), 228-237. doi: 10.1046/j.1365-2990.2002.00394.x

LAURIN, N., BROWN, J. P., MORISSETTE, J., RAYMOND, V. (2002). Recurrent mutation of the gene encoding sequestosome 1 (SQSTM1/p62) in Paget disease of bone. *Am J Hum Genet*. 70(6), 1582-1588. doi: 10.1086/340731

LE BER, I., CAMUZAT, A., GUERREIRO, R., BOUYA-AHMED, K., BRAS, J., NICOLAS, G., […], BRICE, A. French Clinical and Genetic Research Network on FTD/FTD-ALS. SQSTM1 mutations in French patients with frontotemporal dementia or frontotemporal dementia with amyotrophic lateral sclerosis. *JAMA Neurol.* 70(11), 1403-1410. doi: 10.1001/jamaneurol.2013.3849

LESNIK OBERSTEIN, S. A. (2003). Diagnostic strategies in CADASIL. *Neurology.* 60(12), 2020.

LEWANDOWSKA, E., DZIEWULSKA, D., PARYS, M., PASENNIK, E. (2011). Ultrastructure of granular osmiophilic material deposits (GOM) in arterioles of CADASIL patients. *Folia Neuropathol.* 49(3), 174-180.

LIM, K. S., TAN, A. H., LIM, C. S., CHUA, K. H., LEE, P. C., RAMLI, N., […], NG, C. C. (2015). R54C Mutation of NOTCH3 Gene in the First Rungus Family with CADASIL. *PLoS One.* 10(8), e0135470. doi: 10.1371/journal.pone.0135470

LORENZI, T., RAGNO, M., PAOLINELLI, F., CASTELLUCCI, C., SCARPELLI, M., MORRONI, M. (2017). CADASIL: Ultrastructural insights into the morphology of granular osmiophilic material. *Brain Behav*. 7(3), e00624. doi: 10.1002/brb3.624

LU, C. H., MACDONALD-WALLIS, C., GRAY, E., PEARCE, N., PETZOLD, A., NORGREN, N., […], MALASPINA, A. (2015). Neurofilament light chain: A prognostic biomarker in amyotrophic lateral sclerosis. *Neurology.* 84(22), 2247-2257. doi: 10.1212/WNL.0000000000001642

LUO, Z., MU, L., ZHENG, Y., SHEN, W., LI, J., XU, L., […], ZHOU, Y. (2020). NUMB enhances Notch signaling by repressing ubiquitination of NOTCH1 intracellular domain. *Journal of Molecular Cell Biology*. 12(5), 345-358. doi:10.1093/jmcb/mjz088

MA, S., ATTARWALA, I. Y., XIE, X. Q. SQSTM1/p62: A Potential Target for Neurodegenerative Disease. *ACS Chem Neurosci.* 10(5), 2094-2114. doi: 10.1021/acschemneuro.8b00516

MAKSEMOUS, N., SMITH, R. A., HAUPT, L. M., GRIFFITHS, L. R. (2016). Targeted next generation sequencing identifies novel NOTCH3 gene mutations in CADASIL diagnostics patients. *Hum Genomics.* 10(1), 38. doi: 10.1186/s40246-016-0093-z

MANCUSO, M., ARNOLD, M., BERSANO, A., BURLINA, A., CHABRIAT, H. DEBETTE, S., […], MARKUS, H. S. (2020). Monogenic cerebral small-vessel diseases: diagnosis and therapy. Consensus recommendations of the European Academy of Neurology. *Eur J Neurol*. 27(6), 909-927. doi:10.1111/ene.14183

MAREK, M., HORYNIECKI, M., KARPE, J., ADAMCZYK-SOWA, M., WALECKI, J., KLUCZEWSKA, E. (2019). Relationship between stroke severity, extensity of leukoaraiosis, and brain atrophy in patients with ischaemic stroke. *Polish journal of radiology.* 84, e80–e85. doi:10.5114/pjr.2019.82917

MARKUS, H. S., MARTIN, R. J., SIMPSON, M. A., DONG, Y. B., ALI, N., CROSBY, A. H., POWELL, J. F. (2002). Diagnostic strategies in CADASIL. *Neurology*. 59(8), 1134-1138. doi:10.1212/wnl.59.8.1134

MARTINS, J., SERINO, J., MARTINS, J. (2014). PO9 - CADASIL com Apresentação Oftalmológica. *Sinapse.* 14(2), 101.

MEETER, L. H., DOPPER, E. G., JISKOOT, L. C., SANCHEZ-VALLE, R., GRAFF, C., BENUSSI, L., […], VAN SWIETEN, J. C. (2016). Neurofilament light chain: a biomarker for genetic frontotemporal dementia. *Ann Clin Transl Neurol*. 3(8), 623-636. doi: 10.1002/acn3.325

MENZIES, F. M., FLEMING, A., CARICASOLE, A., BENTO, C. F., ANDREWS, S. P., ASHKENAZI, A., […], RUBINSZTEIN, D. C. Autophagy and Neurodegeneration: Pathogenic Mechanisms and Therapeutic Opportunities. *Neuron*. 93(5), 1015-1034. doi: 10.1016/j.neuron.2017.01.022

MIRANDA, M., DICHGANS, M., SLACHEVSKY, A., URBINA, F., MENA, I., VENEGAS, P., GALVEZ, M. (2006). CADASIL presenting with a movement disorder: a clinical study of a Chilean kindred. *Mov Disord.* 21(7), 1008-1012. doi: 10.1002/mds.20879

MIZUNO, T., MIZUTA, I., WATANABE-HOSOMI, A., MUKAI, M., KOIZUMI, T. (2020). Clinical and Genetic Aspects of CADASIL. *Front Aging Neurosci*. 12, 91. doi:10.3389/fnagi.2020.00091

MIZUNO, T., MURANISHI, M., TORUGUN, T., TANGO, H., NAGAKANE, Y., KUDEKEN, T., […], NAKAGAWA, M. (2008). Two Japanese CADASIL families exhibiting Notch3 mutation R75P not involving cysteine residue. *Intern Med*. 23, 2067–2072. doi: 10.2169/internalmedicine.47.1391

MOCCIA, M., MOSCA, L., ERRO, R., CERVASIO, M., ALLOCCA, R., VITALE, C., […], PENCO, S. (2015). Hypomorphic NOTCH3 mutation in an Italian family with CADASIL features. *Neurobiol Aging*. 36(1), 547.e5-547.e11. doi: 10.1016/j.neurobiolaging.2014.08.021

MONET-LEPRÊTRE, M., HADDAD, I., BARON-MENGUY, C., FOUILLOT-PANCHAL, M., RIANI, M., DOMENGA-DENIER, V., […], JOUTEL, A. (2013). Abnormal recruitment of extracellular matrix proteins by excess Notch3 ECD: a new pathomechanism in CADASIL. *Brain.* 136(Pt6), 1830-1845. doi: 10.1093/brain/awt092

MORRONI, M., MARZIONI, D., RAGNO, M., DI, B. P., CARTECHINI, E., PIANESE, L., […], SCARPELLI, M. (2013). Role of electron microscopy in the diagnosis of cadasil syndrome: a study of 32 patients. *PLoS One*. 8, e65482. doi: 10.1371/journal.pone.0065482

MUIÑO, E., GALLEGO-FABREGA, C., CULLELL, N., CARRERA, C., TORRES, N., KRUPINSKI, J., […], FERNÁNDEZ-CADENAS, I. (2017). Systematic Review of Cysteine-Sparing NOTCH3 Missense Mutations in Patients with Clinical Suspicion of CADASIL. *Int J Mol Sci.* 18(9), 1964. doi: 10.3390/ijms18091964

NAKASO, K., YOSHIMOTO, Y., NAKANO, T., TAKESHIMA, T., FUKUHARA, Y., YASUI, K., […], NAKASHIMA, K. (2004). Transcriptional activation of p62/A170/ZIP during the formation of the aggregates: possible mechanisms and the role in Lewy body formation in Parkinson's disease. *Brain Res*. 1012(1-2), 42-51. doi: 10.1016/j.brainres.2004.03.029

NOZAKI, H., NISHIZAWA, M., ONODERA, O. (2014). Features of Cerebral Autosomal Recessive Arteriopathy With Subcortical Infarcts and Leukoencephalopathy. *Stroke*. 45, 3447–3453. doi:10.1161/STROKEAHA.114.004236

OPHERK, C., DUERING, M., PETERS, N., KARPINSKA, A., ROSNER, S., SCHNEIDER, E., […], DICHGANS, M. (2009). CADASIL mutations enhance spontaneous multimerization of NOTCH3. *Human Molecular Genetics*. 18(15), 2761–2767. doi: 10.1093/hmg/ddp211

OPHERK, C., PETERS, N., HERZOG, J., LUEDTKE, R., DICHGANS, M. (2004). Long-term prognosis and causes of death in CADASIL: a retrospective study in 411 patients. *Brain.* 127(Pt11), 2533-2539. doi: 10.1093/brain/awh282

OPHOFF, R. A., DEYOUNG, J., SERVICE, S. K., JOOSSE, M., CAFFO, N. A., SANDKUIJL, L. A., [...], FRANTS, R. R. (2001). Hereditary Vascular Retinopathy, Cerebroretinal Vasculopathy, and Hereditary Endotheliopathy with Retinopathy, Nephropathy, and Stroke Map to a Single Locus on Chromosome 3p21.1-p21.3. *Am J Hum Genet*. 69(2), 447–453. doi:10.1086/321975

OPITZ, J. M., STILES, F. C., WISE, D., RACE, R. R., SANGER, R., VON GEMMINGEN, G. R., [...], DE GROOT, W. P. (1965). The Genetics of Angiokeratoma Corporis Diffusum (Fabry's Disease) and Its Linkage Relations with the Xg Locus. *Am J Hum Genet*. 4(4), 325-342.

PANAHI, M., YOUSEFI MESRI, N., SAMUELSSON, E. B., COUPLAND, K. G., FORSELL, C., GRAFF, C., […], BEHBAHANI, H. (2018). Differences in proliferation rate between CADASIL and control vascular smooth muscle cells are related to increased T Fβ expression. *J Cell Mol Med.* 22(6), 3016-3024. doi: 10.1111/jcmm.13534

PANKIV, S., CLAUSEN, T. H., LAMARK, T., BRECH, A., BRUUN, J. A., OUTZEN, H., […], JOHANSEN, T. (2007). p62/SQSTM1 binds directly to Atg8/LC3 to facilitate degradation of ubiquitinated protein aggregates by autophagy. *J Biol Chem.* 282(33), 24131-24145. doi: 10.1074/jbc.M702824200

PANTONI, L. (2010). Cerebral small vessel disease: from pathogenesis and clinical characteristics to therapeutic challenges. *Lancet Neurol*. 9(7), 689-701. doi: 10.1016/S1474-4422(10)70104-6

PARMEGGIANI, A., POSAR, A., DE GIORGI, L. B., SANGIORGI, S., MOCHI, M., MONARI, L., […], ROSSI, P. G. (2000). Sneddon syndrome, arylsulfatase A pseudodeficiency and impairment of cerebral white matter. *Brain Dev*. 22(6), 390-393. doi: 10.1016/s0387-7604(00)00157-1

PEJAVER, V., URRESTI, J., LUGO-MARTINEZ, J., PAGEL, K. A., LIN, G. N., NAM, H., […], RADIVOJAC, P. (2017). MutPred2: inferring the molecular and phenotypic impact of amino acid variants. *bioRxiv*. doi: 10.1101/134981.

PIPPUCCI, T., MARESCA, A., MAGINI, P., CENACCHI, G., DONADIO, V., PALOMBO, F., […], SERI, M. (2015). Homozygous NOTCH3 null mutation and impaired NOTCH3 signaling in recessive early-onset arteriopathy and cavitating leukoencephalopathy. *EMBO Mol Med*. 7(6), 848-858. doi: 10.15252/emmm.201404399

PUISSANT, A., FENOUILLE, N., AUBERGER, P. (2012). When autophagy meets cancer through p62/SQSTM1. *Am J Cancer Res*. 2(4), 397-413. doi: 10.1111/bpa.12621

RAMI, A., LANGHAGEN, A., STEIGER, S. (2008). Focal cerebral ischemia induces upregulation of Beclin 1 and autophagy-like cell death. *Neurobiol Dis*. 29(1), 132-141. doi: 10.1016/j.nbd.2007.08.005

RENTZSCH, P., WITTEN, D., COOPER, G. M., SHENDURE, J., KIRCHER, M. (2019). CADD: predicting the deleteriousness of variants throughout the human genome. *Nucleic Acids Res*. 47(D1), D886-D894. doi: 10.1093/nar/gky1016

RICHARDS, A., VAN DEN MAAGDENBERG, A. M. J. M., JEN, J. C., KAVANAGH, D., BERTRAM, P., SPITZER, D., [...] ATKINSON, J. P. (2007). C-terminal truncations in human 3'-5' DNA exonuclease TREX1 cause autosomal dominant retinal vasculopathy with cerebral leukodystrophy. *Nature Genetics*. 39(9), 1068-1070. doi: 10.1038/ng2082

RICHARDS, S., AZIZ, N., BALE, S., BICK, D., DAS, S., GASTIER-FOSTER, J., […], REHM, H. L. (2015) ACMG Laboratory Quality Assurance Committee. Standards and guidelines for the interpretation of sequence variants: a joint consensus recommendation of the American College of Medical Genetics and Genomics and the Association for Molecular Pathology. *Genet Med.* 17(5), 405-424. doi: 10.1038/gim.2015.30

ROHRER, J. D., WOOLLACOTT, I. O. C., DICK, K. M., BROTHERHOOD, E., GORDON, E., FELLOWS, A., […], ZETTERBERG, H. (2016). Serum neurofilament light chain protein is a measure of disease intensity in frontotemporal dementia. *Neurology*. 87(13), 1329-1336. doi: 10.1212/WNL.0000000000003154

ROSS, J. S., FAKIH, M., ALI, S. M., ELVIN, J. A., SCHROCK, A. B., SUH, J., […], GAY, L. M. (2018). Targeting HER2 in colorectal cancer: The landscape of amplification and short variant mutations in ERBB2 and ERBB3. *Cancer.* 124(7), 1358-1373. doi: 10.1002/cncr.31125

ROSS, O. A., SOTO-ORTOLAZA, A. I., HECKMAN, M. G., VERBEECK, C., SERIE, D. J., RAYAPROLU, S., […], MESCHIA, J. F. (2013). NOTCH3 variants and risk of ischemic stroke. *PLoS One*. 8(9), e75035. doi: 10.1371/journal.pone.0075035

RUBINO, E., RAINERO, I., CHIÒ, A., ROGAEVA, E., GALIMBERTI, D., FENOGLIO, P., […], PINESSI, L. (2012). SQSTM1 mutations in frontotemporal lobar degeneration and amyotrophic lateral sclerosis. *Neurology*. 79(15), 1556-1562. doi: 10.1212/WNL.0b013e31826e25df

RUTTEN, J. W., BOON, E. M., LIEM, M. K., DAUWERSE, J. G., PONT, M. J., VOLLEBREGT, E., […], LESNIK OBERSTEIN, S. A. (2013). Hypomorphic NOTCH3 alleles do not cause CADASIL in humans. *Hum Mutat.* 34(11), 1486-1489. doi: 10.1002/humu.22432

RUTTEN, J. W., DAUWERSE, H. G., GRAVESTEIJN, G., VAN BELZEN, M. J., VAN DER GROND, J., POLKE, J. M., […], LESNIK OBERSTEIN, S. A. (2016). Archetypal NOTCH3 mutations frequent in public exome: implications for CADASIL. *Ann Clin Transl Neurol.* 3(11), 844-853. doi: 10.1002/acn3.344

RUTTEN, J. W., HAAN, J., TERWINDT, G. M., VAN DUINEN, S. G., BOON, E. M., LESNIK OBERSTEIN, S. A. (2014). Interpretation of NOTCH3 mutations in the diagnosis of CADASIL. *Expert Rev Mol Diagn*. 14(5), 593-603. doi: 10.1586/14737159.2014.922880

RUTTEN, J. W., VAN EIJSDEN, B. J., DUERING, M., JOUVENT, E., OPHERK, C., PANTONI, L., […], LESNIK OBERSTEIN, S. A. J. (2019). The effect of NOTCH3 pathogenic variant position on CADASIL disease severity: NOTCH3 EGFr 1-6 pathogenic variant are associated with a more severe phenotype and lower survival compared with EGFr 7-34 pathogenic variant. *Genet Med*. 21(3), 676-682. doi: 10.1038/s41436-018-0088-3

SANGER, F., NICKLEN, S., COULSON, A. R. (1977). DNA sequencing with chain-terminating inhibitors. *Proc Natl Acad Sci U S A.* 74(12), 5463-5467. doi: 10.1073/pnas.74.12.5463

SASSI, C., NALLS, M. A., RIDGE, P. G., GIBBS, J. R., LUPTON, M. K., TROAKES, C., […], HARDY, J. (2018). Mendelian adult-onset leukodystrophy genes in Alzheimer's disease: critical influence of CSF1R and NOTCH3. *Neurobiol Aging*. 66, 179.e17-179.e29. doi: 10.1016/j.neurobiolaging.2018.01.015

SCHEID, R., HEINRITZ, W., LEYHE, T., THAL, D. R., SCHOBER, R., STRENGE, S., […], FROSTER, U. G. (2008). Cysteine-sparing notch3 mutations: cadasil or cadasil variants? *Neurology*. 71(10), 774-776. doi: 10.1212/01.wnl.0000324928.44694.f7

SCHMIDT, H., ZEGINIGG, M., WILTGEN, M., FREUDENBERGER, P., PETROVIC, K., CAVALIERI, M., […], SCHMIDT, R. (2011). Genetic variants of the NOTCH3 gene in the elderly and magnetic resonance imaging correlates of age-related cerebral small vessel disease. *Brain.* 134(Pt11), 3384-3397. doi: 10.1093/brain/awr252

SCHWARZ, J. M., RÖDELSPERGER, C., SCHUELKE, M., SEELOW, D. (2010). MutationTaster evaluates disease-causing potential of sequence alterations. *Nat Methods*. 7(8), 575-576. doi: 10.1038/nmeth0810-575

SEIBENHENER, M. L., BABU, J. R., GEETHA, T., WONG, H. C., KRISHNA, N. R., WOOTEN, M. W. (2004). Sequestosome 1/p62 is a polyubiquitin chain binding protein involved in

ubiquitin proteasome degradation. *Mol Cell Biol*. 24(18), 8055-8068. doi: 10.1128/MCB.24.18.8055-8068.2004

SHI, Y., LI, S., LI, W., ZHANG, C., GUO, L., PAN, Y., […], ZHANG, Z. (2018). MRI Lesion Load of Cerebral Small Vessel Disease and Cognitive Impairment in Patients With CADASIL. *Front Neurol.* 9, 862. doi: 10.3389/fneur.2018.00862

SHIHAB, H. A., GOUGH, J., COOPER, D. N., STENSON, P. D., BARKER, G. L., EDWARDS, K. J., […], GAUNT, T. R. (2012). Predicting the functional, molecular, and phenotypic consequences of amino acid substitutions using hidden Markov models. *Hum Mutat*. 34(1), 57-65. doi: 10.1002/humu.22225

SJÖGREN, M., BLOMBERG, M., JONSSON, M., WAHLUND, L. O., EDMAN, A., LIND, K., […], WALLIN, A. (2001). Neurofilament Protein in Cerebrospinal Fluid: A Marker of White Matter Changes. *Journal of Neuroscience Research*. 66(3), 510-516. doi: 10.1002/jnr.1242

SKEHAN, S. J., HUTCHINSON, M., MACERLAINE, D. P. (1995). Cerebral autosomal dominant arteriopathy with subcortical infarcts and leucoencephalopathy: MR findings. *AJNR Am J Neuroradiol*. 16(10), 2115-2119.

SMITH, C. G., NAVEN, M., HARRIS, R., COLLEY, J., WEST, H., LI, N., […], CHEADLE, J. P. (2013). Exome resequencing identifies potential tumor-suppressor genes that predispose to colorectal cancer. *Hum Mutat*. 34(7), 1026-1034. doi: 10.1002/humu.22333

SOONG, B. W., LIAO, Y. C., TU, P. H., TSAI, P. C., LEE, I. H., CHUNG, C. P., LEE, Y. C. (2013). A homozygous NOTCH3 mutation p.R544C and a heterozygous TREX1 variant p.C99MfsX3 in a family with hereditary small vessel disease of the brain. *J Chin Med Assoc.* 76(6), 319-324. doi: 10.1016/j.jcma.2013.03.002

SOURANDER, P., WALINDER, J. (1977). Hereditary multi-infarct dementia. Morphological and clinical studies of a new disease. *Acta Neuropathol (Berl).* 39(3), 247-254. doi: 10.1007/BF00691704

STORIMANS, C. W., VAN SCHOONEVELD, M. J., OOSTERHUIS, J. A., BOS, P. J. (1991). A new autosomal dominant vascular retinopathy syndrome. *Eur J Ophthalmolog.*, 1(2), 73–78.

TAKAHASHI, K., ADACHI, K., YOSHIZAKI, K., KUNIMOTO, S., KALARIA, R. N., WATANABE, A. (2010). Mutations in NOTCH3 cause the formation and retention of aggregates in the endoplasmic reticulum, leading to impaired cell proliferation. *Hum Mol Genet.* 19(1), 79-89. doi: 10.1093/hmg/ddp468

THELIN, E. P., ZEILER, F. A., ERCOLE, A., MONDELLO, S., BÜKI, A., BELLANDER, B., […], NELSON, D. W. (2017). Serial sampling of serum protein biomarkers for monitoring human traumatic brain injury dynamics: a systematic review. *Front Neurol*. 8, 300. doi: 10.3389/fneur.2017.00300

TIKKA, S., MYKKÄNEN, K., RUCHOUX, M. M., BERGHOLM, R., JUNNA, M., PÖYHÖNEN, M., [...], KALIMO, H. (2009). Congruence between NOTCH3 mutations and GOM in 131 CADASIL patients. *Brain*. 132(Pt 4), 933-939. doi: 10.1093/brain/awn364

TOURNIER-LASSERVE, E., JOUTEL, A., MELKI, J., WEISSENBACH, J., LATHROP, G. M., CHABRIAT, H., […], BOUSSER, M. (1993). Cerebral autosomal dominant arteriopathy with subcortical infarcts and leukoencephalopathy maps to chromosome 19q12. *Nat Genet*. 3(3), 256-259. doi: 10.1038/ng0393-256

TUOMINEN, S., JUVONEN, V., AMBERLA, K., JOLMA, T., RINNE, J. O., TUISKU, S., […], KALIMO, H. (2001). Phenotype of a homozygous CADASIL patient in comparison to 9 age-matched heterozygous patients with the same R133C Notch3 mutation. *Stroke*. 32(8), 1767-1774. doi: 10.1161/01.str.32.8.1767

UNGARO, C., MAZZEI, R., CONFORTI, F. L., SPROVIERI, T., SERVILLO, P., LIGUORI, M., […], QUATTRONE, A. (2009). Cadasil: Extended polymorphisms and mutational analysis of the NOTCH3 gene. *J Neurosci Res.* 87(5), 1162–1167. doi: 10.1002/jnr.21935

VAHEDI, K., CHABRIAT, H., LEVY, C., JOUTEL, A., TOURNIER-LASSERVE, E., BOUSSER, M. G. (2004). Migraine with aura and brain magnetic resonance imaging abnormalities in patients with CADASIL. *Arch Neurol*. 61(8), 1237-40. doi: 10.1001/archneur.61.8.1237

VALENTI, R., POGGESI, A., PESCINI, F., INZITARI, D., PANTONI, L. (2008). Psychiatric disturbances in CADASIL: a brief review. *Acta Neurol Scand*. 118(5), 291-295. doi: 10.1111/j.1600-0404.2008.01015.x

VAN AGTMAEL, T., SCHLOTZER-SCHREHARDT, U., MCKIE, L., BROWNSTEIN, D. G., LEE, A. W., CROSS, S. H., [...], JACKSON, I. J. (2005). Dominant mutations of Col4a1 result in basement membrane defects which lead to anterior segment dysgenesis and glomerulopathy. *Human Molecular Genetics*. 14(21), 3161–3168. doi:10.1093/hmg/ddi348

VAN BOGAERT, L. (1955). Encéphalopathie sous-corticale progressive (Binswanger) à évolution rapide chez deux soeurs. *Med Hellen*. 24, 961-972.

VERIN, M., ROLLAND, Y., LANDGRAF, F., CHABRIAT, H., BOMPAIS, B., MICHEL, A., […], LEMAITRE, M. H. (1995). New phenotype of the cerebral autosomal dominant arteriopathy mapped to chromosome 19: migraine as the prominent clinical feature. *J Neurol Neurosurg Psychiatry*. 59(6), 579-85. doi: 10.1136/jnnp.59.6.579

VISWANATHAN, A., GODIN, O., JOUVENT, E., O'SULLIVAN, M., GSCHWENDTNER, A., PETERS, N., […], CHABRIAT, H. (2010). Impact of MRI markers in subcortical vascular dementia: a multi-modal analysis in CADASIL. *Neurobiol Aging*. 31(9), 1629-36. doi: 10.1016/j.neurobiolaging.2008.09.001

VLACHAKIS, D., TSANIRAS, S. C., IOANNIDOU, K., PAPAGEORGIOU, L., BAUMANN, M., KOSSIDA, S. (2014). A series of Notch3 mutations in CADASIL; insights from 3D molecular modelling and evolutionary analyses. *J Mol Biochem*. 3(3), 134.

WANG, T., BARON, M., TRUMP, D. (2008). An overview of Notch3 function in vascular smooth muscle cells. *Prog Biophys Mol Biol*. 96(1-3), 499-509. doi: 10.1016/j.pbiomolbio.2007.07.006

WEGNER, F., STRECKER, K., SCHWARZ, J., WAGNER, A., HEINRITZ, W., SOMMERER, F., […], SABRI, O. (2007). Vascular parkinsonism in a CADASIL case with an intact nigrostriatal dopaminergic system. *J Neurol*. 254(12), 1743-1745. doi: 10.1007/s00415-007-0529-4

WOOTEN, M. W., GEETHA, T., BABU, J. R., SEIBENHENER, M. L., PENG, J., COX, N., […], MOSCAT, J. (2008). Essential role of sequestosome 1/p62 in regulating accumulation of Lys63-ubiquitinated proteins. *J Biol Chem*. 283(11), 6783-6789. doi: 10.1074/jbc.M709496200

XU, F., GU, J. H., QIN, Z. H. (2012). Neuronal autophagy in cerebral ischemia. *Neurosci Bull.* 28(5), 658-666. doi: 10.1007/s12264-012-1268-9

YOON, C. W., KIM, Y. E., SEO, S. W., KI, C. S., CHOI, S. H., KIM, J. W., NA, D. L. (2015). NOTCH3 variants in patients with subcortical vascular cognitive impairment: a comparison with typical CADASIL patients. *Neurobiol Aging*. 36(8), 2443.e1-2443.e7. doi: 10.1016/j.neurobiolaging.2015.04.009

ZARATE, Y. A., HOPKIN, R. J. (2008). Lysosomal Storage Disease 3: Fabry's disease. *Lancet*. 372(9647), 1427–1435. doi:10.1016/S0140- 6736(08)61589-5

ZÚÑIGA-RAMÍREZ, C., DE OLIVEIRA, L. M., KRAMIS-HOLLANDS, M., ALGARNI, M., SOTO-ESCAGEDA, A., SÁENZ-FARRET, M., […], FASANO, A. (2019). Beyond dystonia and ataxia: Expanding the phenotype of SQSTM1 mutations. *Parkinsonism Relat Disord.* 62, 192-195. doi: 10.1016/j.parkreldis.2018.12.031